Design Of Piezoelectric Oscillometry, Accuracy In Tracking Time-Varying Impedance And Implications On The Frequency Dependence Of Resistance

by

Hamed Hanafi

Submitted in partial fulfilment of the requirements
for the degree of Doctor of Philosophy

at

Dalhousie University
Halifax, Nova Scotia
September 2015

To mom, dad, Hesam and baba Alamdari

TABLE OF CONTENTS

List of Tables

List of Figures

ABSTRACT

Oscillometry (OS) is commonly performed by actuators that are heavy and bulky. In this thesis I designed and simulated a new single frequency OS system. This novel design used a piezoelectric bimorph actuator on resonance. To predict the performance, a dynamic model was simulated that included realistic respiratory impedance loads, and realistic recorded breathing noise. Model performance was also validated in a scaled prototype device. We found that while breathing noise substantially lowered SNR, the model could produce sufficient pressure and flows for acceptable SNR and accuracy. Together the results of the simulations and the scaled prototype indicated that this design is a feasible approach to develop an accurate lightweight, portable, single-frequency OS device.

Tracking the within-breath impedance of the lung has gained attention among researchers because it is believed that it contains important information regarding the health of the lung. However, to date, there are very few studies that address the accuracy of estimating time-varying impedance. In this thesis we analytically and computationally developed a time-frequency transfer function that demonstrated increasing error with increasing breathing rate. Then we evaluated the accuracy of using short-time Fourier transform (STFT) methods in tracking time-varying impedance in simulations of a sample population (children). As expected however, these errors were much higher than noise-free simulations. Results indicated that current methods can track the impedance versus time reasonably accurately, but at high breathing rates, errors may be unacceptable.

It is established that resistance exhibits a pronounced frequency dependence that is increased in obstructive disease. Similarly, and thought to be unrelated, variations in reactance are also increased in COPD. By analyzing the equation of motion in the time-domain with time-varying resistance and elastance we found and proved that variations in elastance surprisingly influence the frequency dependence of resistance. This relationship was demonstrated again by the same time-frequency transfer function presented previously. Although this effect was small in the OS frequency range it was substantial at breathing frequencies. This is important as it provides a novel mechanism for frequency dependence of resistance, indistinguishable from OS methods alone, in addition to tissue viscoelasticity and heterogeneity of the lung.

List Of Abbreviations Used

cmH_2O	centimeter of water
COPD	chronic obstructive pulmonary disease
E_{rs}	elastance of the respiratory system
E	model elastance
E_L	elastance of the lung
f	frequency
FEV_1	forced expiratory volume in one second
FFT	fast Fourier transform
FOT	forced oscillation technique
FRC	functional residual capacity
G	Constant phase model's tissue damping
H	Constant phase model's tissue elastance
$h(\tau)$	linear system impulse response
$H(f)$	linear system transfer function
$H(f,t)$	linear system time-frequency transfer function
Zrs	Lung impedance
I	inertance of the respiratory system
kg	kilogram
K1	Rohrer coefficient 1
K2	Rohrer coefficient 2
L	liter
OS	Oscillometry
OVW	optimal ventilator waveform
P	pressure
P_{ao}	airway opening pressure
P_{pl}	pleural pressure
PEEP	positive end expiratory pressure
R_{aw}	airway resistance
R_L	model lung impedance

R_{rs}	resistance of the respiratory system
R_u	Rohrer resistance
R5-R20	R_{rs} at 5 Hz minus R_{rs} at 20 Hz
s	second or seconds
SD	standard deviation
SNR	signal to noise ratio
TV	tidal volume
Q	flow
X_L	model lung reactance
X_{rs}	model reactance of the respiratory system
Z_a	impedance model non-terminal airway branch
Z_c	closed system impedance (FOT)
Z_{in}	input impedance of the respiratory system
Z_{CP}	constant phase model impedance
Z_L	model lung impedance
Z_{rs}	impedance of the respiratory system
α	Constant phase model's experimental power
α_p	Electromechanical coupling
η	hysteresivity
ω	angular frequency

Acknowledgements

Firstly, I would like to express my sincere gratitude to my thesis supervisor, Prof. G. N. Maksym, for his guidance and patience in teaching me a huge amount of knowledge that I was not familiar with before starting the PhD program. Indeed, your generous style of teaching, which is to explain concepts in a very sophisticated but at the same time simple level has inspired me to be a better teacher in future. I would like to thank very warmly Dr. Jeremy Brown, Dr. Andrew Milne and Dr. Dietrich Henzler for their support and insightful feedback on my work. I am very grateful of Dr. Kamal El-Sankary for once again giving me the pleasure of joining my supervisory team after mentoring me during my Masters studies. I am also grateful to Prof. J. H. T. Bates (University of Vermont) for his feedback on the findings of the last chapter of this thesis. I would also like to greatly appreciate the mentorship that Prof. David Roach generously provided during my studies. You are indeed an inspiring role model for me.

It is important to mention my dear friend, Lucas Posada who prototyped and validated the device concept presented in this thesis. I have learned a lot from your work ethic. I would like to thank several other people who contributed to my work at different stages including Swati Bhatawadekar for her selfless and sisterly help and advice during the last few years. You offered your MATLAB codes without any expectations, chatted when I needed it and took me to yoga classes. You are an inspiration to me. I have also been fortunate to have other wonderful lab mates and friends such as Ubong Peters and Del Leary. Ubong, our short and friendly meetings in the office were always refreshing.

Lastly, I would like to mention that without the unconditional love and support from my family, this would have been impossible. Mom, for your motherly and scientific advice, dad, for your strength and positivity that I could always rely on and Hesam for constantly reminding me that life has more important aspects than science or financial success. I can't be grateful enough to Mahshid Jan, Amir Khan, Khaleh Maryam, Mamani and all of you, my family, that offered your love and support. Last but not least I like to thank my dear friends in Halifax, my home, that supported me throughout the program including my friend, brother and mentor Dennis Venditti and dearests Monica Belliveau and Alida O'Connor.

Chapter 1: Introduction

This chapter presents the main aims of the thesis with a brief rationale for each aim before presenting the relevant literature in Chapter 2.

Oscillometry (OS) also known as the Forced oscillation technique (FOT) measures the respiratory system's mechanical impedance, Z_{rs}, that is, the impedance of airflow into the respiratory system, which is altered in diseases such as asthma or chronic obstructive pulmonary disease. This technique of probing lung's health is of interest because of its simplicity and ease of use, which is particularly helpful for assessing lung health in children and elderly. This is compared to the principle method of assessment of lung function, spirometry, as OS does not require much training and effort from the subject. However, OS is not yet widely used clinically, and thus perhaps has not yet reached its full potential. One issue is that the information potentially extracted from OS measurements possibly contains a great amount of knowledge linking lung function and its changes to lung structure and patterns of obstruction. Even after years of progress and development, improvements in methodology, signal processing techniques, including more recently techniques to track temporal changes in impedance precisely are still a work in progress. This thesis explores some factors such as accuracy in temporal tracking of impedance as well as the impact of assessing a temporally varying respiratory system with current signal processing methods.

Additionally, there has been movement to make commercial devices less expensive, and offer newer features such as portability that may improve progress towards greater clinical use. From the available OS devices in the market only the tremoFlo (Thorasys Inc., Montreal) is portable and operates as hand-held. Such a device requires advanced fabrication and motor technology to fulfill the requirements. However, the motor used in the device is expensive and fairly heavy. Therefore, together with a colleague, Lucas Posada, we embarked on developing a new compact and light with reduction in cost. To achieve this, in this thesis, I simulated a piezoelectric based, small oscillator device to guide the design of an optimal prototype device to measure lung

mechanics at a higher frequency not contaminated by breathing. This forms the first aim of this thesis and is presented in Chapter. 3.

Recently OS has been used to track temporal changes in impedance during breathing, as various indices from the impedance have been related to airflow limitation in COPD and have potential to distinguish different respiratory diseases. Estimating of time-varying mechanics of the respiratory system can be done either by time-domain approaches or by methods based on the short time Fourier transform (STFT), but little work has been done estimating their accuracy. Although the STFT is typically employed in the method developed to track Z_{rs} that is temporally changing, it nevertheless assumes stationarity at short time scales. As the second aim of this thesis, I analytically and computationally assessed the accuracy of the STFT method on tracking variation in Z_{rs}. Additionally I also developed, analytically, a time-frequency transfer function to use as an estimator of the error that occurs in estimating time varying Zrs. The analysis and results of this work is presented in Chapter 4.

In chapter 5, I further use this time-frequency transfer function, and also analytical analysis of both the single compartment and a double compartment model of the respiratory system to demonstrate that the errors arising from non-stationarity particularly in the variation of elastance of the respiratory system can contribute to frequency dependence observed from standard stationary frequency domain analyses. This is important as frequency dependence of impedance is used as an indication of disease severity using OS via standard forced oscillation and the optimal ventilation waveform (OVW).

Chapter 6 summarizes my thesis work by presenting the main results and original contributions to fields of lung modeling and lung mechanics accompanied by suggestions for future work.

Chapter 2: Review of Relevant Literature

This chapter provides a summary of the relevant literature to this dissertation. Topics reviewed include oscillometry (OS) and measurement of lung mechanics. This is followed by a review of the literature on frequency dependence of impedance, signal processing techniques to track time-varying respiratory mechanics and also a brief introduction of piezoelectric cantilever methodology as relevant to the development of an OS device oscillating motor.

2.1 Oscillometry (the Forced Oscillation Technique)

OS is a method for measurement of lung mechanics normally at frequencies not contaminated by breathing. OS is normally performed during tidal breathing and therefore is convenient for most patients specifically elderly and pediatrics compared to spirometry.

OS was originally introduced by Dubois et al. in 1956 [1] as a non-invasive method for assessment of respiratory mechanics, however, it has only gained considerable attention from a clinical point of view recently. Now, many comprehensive studies, both small and large have been done in healthy humans and in patients with a variety of respiratory pathologies [1-4, 7, 11, 15-17, 33, 46, 59, 62, 97, 105, 110-114, 118, 119, 122]. There also have been published recommendations and guidelines for clinical use [2]. In principle, OS evaluates the response of the respiratory system by probing it with predefined small oscillations of flow and pressure at specific frequencies. Although the technology of generating the oscillations can vary from one device to other, this method is usually applied at the mouth and the resulting pressure and flow are also measured at the same site or very close depending on the technology [3-6]. The most common technology for generating the oscillations is a loud speaker [7] which is often bulky and not portable.

To allow spontaneous breathing of fresh air during measurement, OS systems are open to atmosphere via either a bias tube or using a fixed mesh resistance. When a tube is used, the tube is designed to be of high impedance to oscillation frequencies and low impedance to breathing frequencies. This is achieved with a tube of sufficient length to present a high inertive path to the oscillations, but low resistive and inertive path for breathing. To avoid the accumulation of carbon dioxide, a continuous flow of fresh air is applied through the bias tube [2]. Other systems that use the mesh resistance are designed to have small intrinsic deadspace and airflow of fresh air is accomplished by the subject's breathing efforts [8]. Recently, Thorasys Inc. (Montreal), has developed a handheld, light and portable device that achieves its small size by replacing the usual loud speaker with a small mesh screen attached to an oscillating motor [9] (Figure 2.1).

Figure 2.1 TremoFlo (Thorasys) device with disposable anti-viral/anti bacterial filter affixed to the front.

Regardless of the source of the forced oscillations, the mechanical impedance of the respiratory system, Z_{rs}, is a complex quantity that is derived from the division of pressure by flow in the frequency domain:

$$Z_{rs}(\omega) = \frac{P\ (\omega)}{Q\ (\omega)} \tag{2.1}$$

where $Q\ (\omega)$ is the flow signal and $P\ (\omega)$ is the pressure signal at the angular frequency of ω, and $\omega = 2\pi f$ where f is the oscillation frequency. Normally filtering

and averaging from multiple windowed periods are employed to compute Z_{rs} as will be described in more detail in this thesis. Also equation (2.1) is applied for pressure and flow measured at the airway opening. Normally most devices measure pressure and flow at some distance from the airway opening and thus some compensation for the intervening impedance is required [8, 10]. Z_{rs} is a complex quantity with a real part: respiratory resistance (R_{rs}) largely due to airflow resistance of intrathoracic and extrathoracic airways, lung tissue and chest wall and an imaginary part: reactance (X_{rs}) arising from elastic properties of the lung and chest wall, and the inertia of the oscillating air:

$$Z_{rs}(\omega) = R_{rs}(\omega) + jX_{rs}(\omega) \tag{2.2}$$

R_{rs} and X_{rs} are often characterized by fitting models to the measured data. The most commonly used model is the single compartment model (Figure 2.2) where R_{rs} is assumed to be constant with frequency and $X_{rs} = \omega I_{rs} - \frac{E_{rs}}{\omega}$. E_{rs} and I_{rs} are idealized lumped elements that represent the elastance and inertance of the respiratory system respectively. At low frequencies such as below 5 Hz, E_{rs} is dominant and reflects tissue and chest wall stiffness. While I_{rs} is dominant at higher frequencies and represents the inertia of the respiratory system and largely accounts for the energy required to accelerate the gases in the respiratory system. The dominance of E_{rs} and I_{rs} switch at the resonance frequency where the elastic forces and inertial forces cancel each other, and where Z_{rs}becomes entirely resistive.

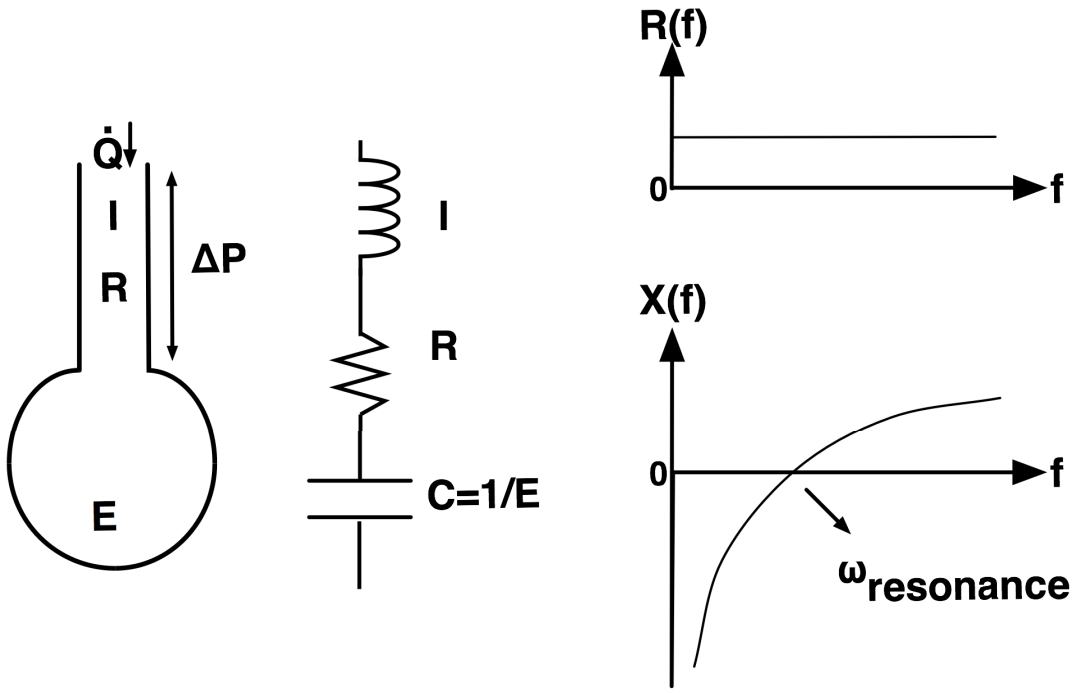

Figure 2.2 Single compartment lung model using idealized respiratory mechanical elements on the left, electrical analog in the center and frequency spectrum of resistance and reactance on the right.

2.2 Models That Incorporate Frequency Dependence

Although the single compartment model can account for a surprising amount of the pressure flow relationship of the respiratory system, particularly of the healthy lung, it lacks the ability to model an important phenomenon called the frequency dependence of resistance. This phenomenon arises from the fact that the resistance of the respiratory system is not constant at all frequencies. Frequency dependence in healthy adults occurs at very low frequencies below 0.04 Hz [11], however, in healthy children [12] or in animals [13, 14], it shifts to higher frequencies, and is thus dependent on lung size. Frequency dependence of resistance is increased in obstructive disease and can be observed to occur between 5 and 20 Hz [15, 16-19, 8, 20-22].

There exists two dominant mechanisms thought to give rise to the frequency dependence, one originating from the lung tissue viscoelasticity [23] which is present in health and may be increased in disease, and the other rooted in the regional differences in the lung that causes an uneven distribution of air flow. This is established to occur with obstruction in the branching airway tree, and leads to a distribution of time constants for ventilation and associated with a frequency dependent respiratory impedance [24-31].

Tissue Viscoelasticity and the Constant Phase Model

Tissue viscoelasticity describing a portion of the mechanics of the respiratory system was introduced by Mount [32] using multiple lumped idealized elements and was further developed by several other author's including Bates et al [33-35] using both parallel and series arrangements of the lumped elements. However, Mount's model or any of the lumped element models have difficulty reproducing the '1/f' behavior of resistance. Indeed, over a wide enough range of frequencies, the number of elements required to smoothly account for this behavior increases in order to follow a continuous distribution of time constants. An alternative to a distributed time constant and thus multiple lumped element model is the constant phase model that was introduced in the 1990s [36] constituting a single idealized Newtonian resistance for the airways in series with a frequency dependent tissue compartment (Figure 2.3). The airway compartment sometimes also includes an inertance that usually can be neglected at low frequencies. In the tissue compartment, G largely describes the resistive energy loss in tissue and H largely represents tissue stiffness. G would account entirely for viscous processes if the exponent α was equal to unity (and H would be elastic), but since the exponent is slightly less than unity, the behavior is more complex. The lung impedance equation (Z_{CP}) using the constant phase model is:

$$Z_{\mathrm{CP}} = R_L + \frac{\mathrm{G} - j\mathrm{H}}{\omega^{\alpha}} \tag{2.3}$$

where α, is a fairly constant value in the frequency spectrum and defined as $\alpha = \frac{2}{\pi}\tan^{-1}\frac{H}{G}$ [37]. Moreover, the ratio $\frac{G}{H}$ is known as hysteresivity (η) or the structural damping coefficient. The significance of the constant phase model is clearer when we realize that with this model, the entire mechanical behavior of the respiratory system is partitioned in two separate compartments with only three parameters. The model fits to impedance data below 20 Hz in animals [38-42] and humans [42, 43]. The constant phase model also fits to acute lung injury [44] and emphysema [45] and can track bronchoconstriction [41, 46], and the parameters are altered from healthy values in physiological meaningful ways.

Heterogeneity in Respiratory Models

Years before tissue viscoelasticity was attributed to frequency dependence, Otis et al. [26] utilized a simple parallel double compartment heterogeneous model to analytically demonstrate that frequency dependence can arise from the presence of different time constants in the lung. This is depicted in Figure 2.4 where time constant inequality due to differences in pathway resistance or differences in terminal compliances leads to non-uniform distribution of air flow and thus causes frequency dependence. The same concept was also explored by Mead [27] using a serial compartment model representing the airway opening and central airways in series with another compartment representing mechanics of the lung periphery. Mead postulated that the frequency dependence of compliance seen in obstructed patients arose from shunting of airflow in the compliant central airway wall while distal airways are severely constricted. Although Mead and Otis models can partly predict the frequency dependence, they can both be present in a combined model including parallel and series heterogeneous branches. In fact, models with multiple branches, as implied above in models with multiple lumped elements can better account for the observed frequency dependence.

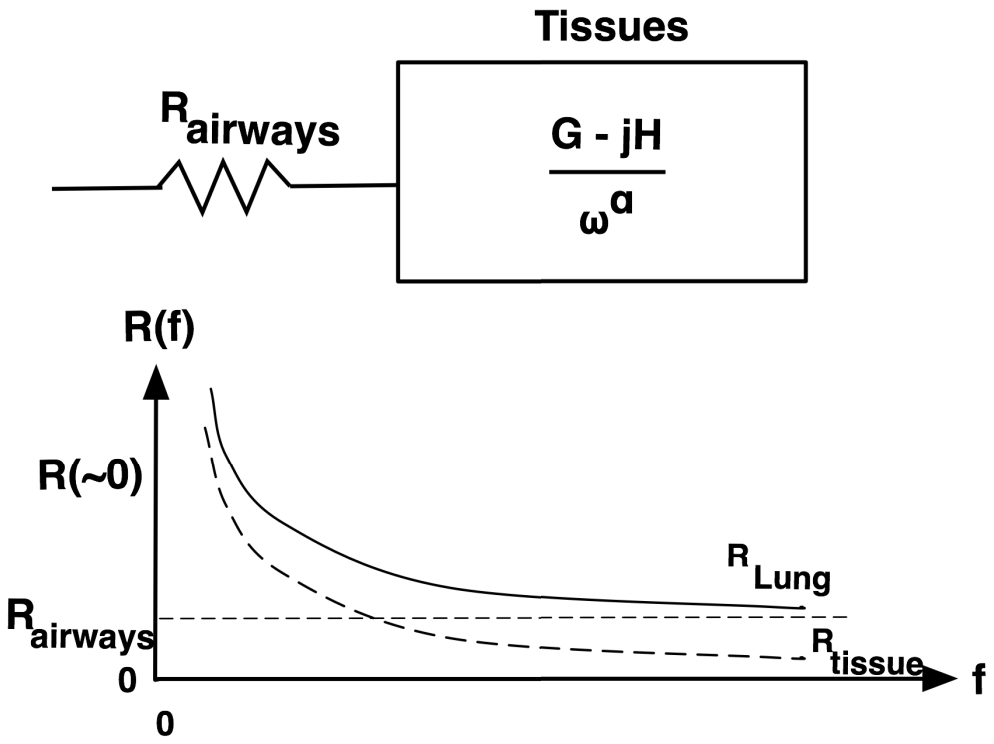

Figure 2.3 Top: The constant phase model consisting of airway resistance and tissue viscoelastic element. Bottom: Frequency spectrum of resistance of the lung with constant airway resistance and inversely frequency dependent tissue resistance ($R_{Lung} = R_{tissue} + R_{airways}$)

Combining Heterogeneous and Constant Phase Models

It is possible to have mixed models such as combining a heterogeneous model with multiple constant phase models. This concept has been explored in the literature and has also been shown to well describe the behavior of the lung with different pathologies [47-49]. Suki et al. [47] introduced the concept of using multiple branches of the structure shown in Figure 2.3 in parallel to introduce inhomogeneity to the model and separate it from tissue viscoelasticity. Kaczka et al. applied this concept to data collected from dogs [49] and found that at high levels of constriction induced by methacholine, the model accounted for the impedance from lungs with heterogeneous constriction better than the constant phase model in a single compartment configuration. While the constant phase model can describe frequency dependent resistance, it is structurally a homogenous

model, despite the fact that frequency dependence of resistance can arise from heterogeneity in airflow in the lung. Thus although heterogeneous models still do not provide specific information on where structural alterations occur [50], they can be more appropriate in describing lung pathology that often occurs in the lung with the development of obstruction in the multi-branch airway tree.

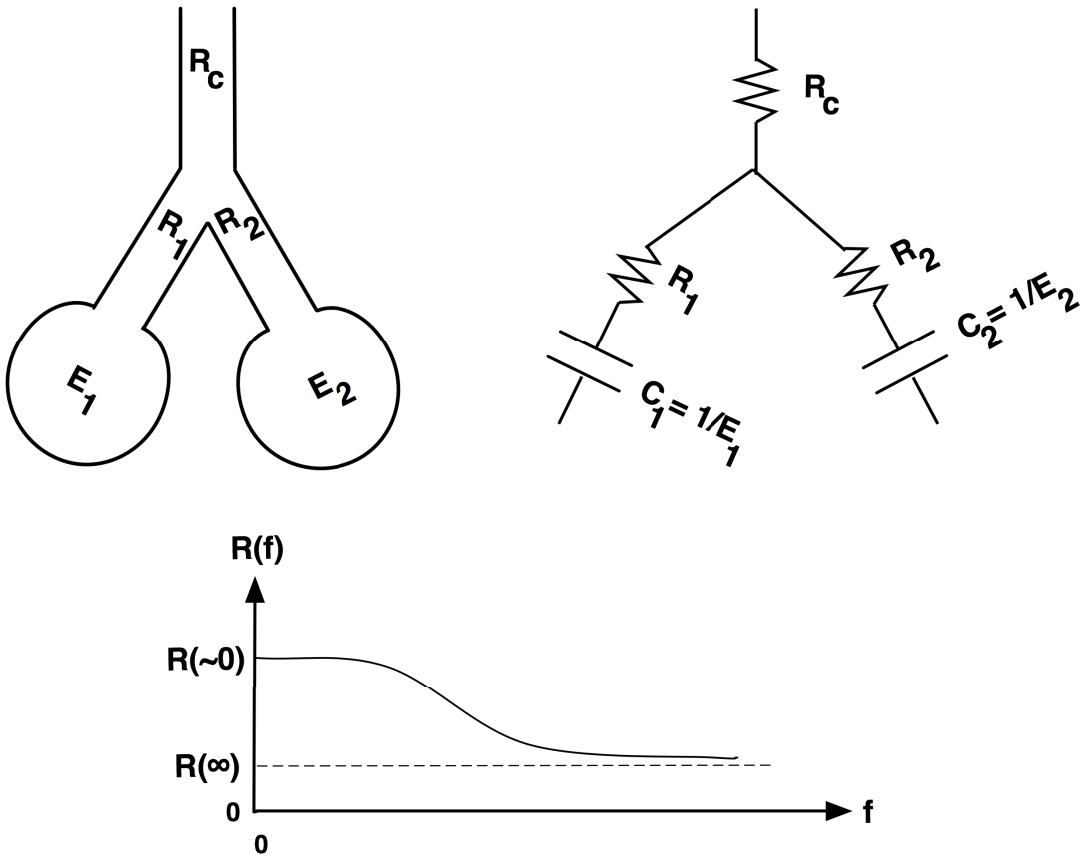

Figure 2.4. Double compartment model, schematic on top left, equivalent circuit top right and frequency spectrum of resistance on the bottom.

From the two mechanisms causing frequency dependence, tissue viscoelasticity likely provides the best explanation for respiratory mechanics in in healthy patients as their lungs are not as heterogeneous as in diseased populations, and indeed mechanical properties of measured tissue in vitro with inverse frequency dependence is remarkably similar [51, 52]. Although even in a healthy lung, the heterogeneous branching tree must contribute to some amount of frequency dependence of mechanics albeit likely at very low frequencies. However, heterogeneity becomes very pronounced in asthma and in

COPD and increases with the severity of these diseases. Therefore, although tissue viscoelasticity must still be present and account for some frequency dependence, heterogeneity in impedance pathways can easily account for the frequency dependence, particularly demonstrated in studies of Lutchen and colleagues using the OVW [28, 29, 53, 54], and even apparent in FOT frequency range between 5 and 20 Hz [16-19]. This has promoted the quantification of the frequency dependence of resistance, usually expressed as the resistance at 20 Hz subtracted from the resistance at 5 Hz, as a useful index of heterogeneity ascribed to small airways dysfunction, however, there is no quantitative direct link yet established between the index and the degree of heterogeneity within the lung.

Elastance has also been speculated as an index of heterogeneity as it represents lung volume de-recruitment caused by small airway narrowing, however, this has only been explored in animal studies [23, 24] and very recently using a computational model of human lung with different levels of asthma and therefore different levels of heterogeneity [50].

OS can be applied using multiple frequencies at once [55, 56] or at a single frequency. Multi-frequency OS systems permit the determination of the frequency dependence of the respiratory system useful for application of models and identification of distinct parameters as described above. These models can then be used to attribute the mechanics of different regions of the respiratory system to different parameters of the model depending on model structure while single frequency OS systems are more useful to monitor the time-course of the mechanics. Single frequency measurements are beginning to be used as they have been shown to be a useful tool for assessment of airflow limitation in COPD [57].

The current standard of calibration for FOT devices [2] suggests the use of reference impedance that is constant in all measured frequencies (i.e. resistive test loads), although it would be important to also include reactive loads to ensure accuracy in reproducing both terms of the complex impedance. After calibration, a maximum error of 10% has been recommended as acceptable performance for clinical measurement of respiratory impedance. This is important because researchers have shown systemic differences in estimation of impedance using different devices [2, 54]. However, although

tracking impedance over time is of recent interest, there does not yet exist any standard for the quantification and minimization of errors in tracking variable impedance versus time.

2.3 Signal Processing

After pressure and flow signals are collected, they must be processed to compute the respiratory impedance. Commonly, low frequency data contaminated by breathing is filtered out by using a high pass filter. This reduces the slowly varying breathing noise component from these signals that in the subsequent windowing would appear as a large dc drift. The breathing noise is particularly large during pressure and flow reversals. The high pass filtering helps reduce edge artifacts and spectral leakage that occurs from windowing commonly performed during the signal processing to identify impedance. The signal is usually windowed to short periods ranging from as low as 1/6 seconds for example for 6 Hz single frequency sinusoidal oscillations, to durations as long as 4 seconds. The signal is assumed to be sufficiently stationary after the filtering, and because of the short duration. The window duration is often chosen to have an integer number of cycles of oscillation in each window, as this also helps reduce edge artifacts. If this is not done, then it is essential to using Hanning or Hamming type windows that reduce the signal amplitude near the window edges, to help enforce periodicity. Often overlapping windows are used (i.e. 50% overlapping windows [59]) and sometimes the signal within the window is detrended. Calculating the ratio of the Fourier transformed pressure to Fourier transformed flow in each window and averaging the results from all windows provides an estimate of average impedance. To quantify the signal quality, and provide an indicator for the accuracy of the impedance the coherence is recommended to be greater than 0.9 [2].

However, in applications where we need to track changes in respiratory impedance over time, we cannot average the results from each of the windows. The impedance from each window provides the impedance at that time point. This approach is in fact akin to the short time Fourier transform (STFT) from time frequency analysis for

pressure and flow with overlapping windows, and computing impedance [59, 68, 61-64] (Figure 2.5)

Another approach to calculate impedance versus time is to use a time-domain recursive least-square (RLS) method [37, 58-62]. In either method, it is assumed that within each block of time, the system is stationary. Shifting each window in time allows estimates of the parameters to also vary temporally. In the RLS method, estimates of impedance are smoothed by applying a filtering function, usually a simple first order filter, sometimes described as a forgetting factor [58]. The output of the STFT may also be low-pass filtered but this is not commonly done.

For both techniques, the ability to track even rapid temporal changes improves if shorter windows are used, however, this increases the susceptibility to noise.

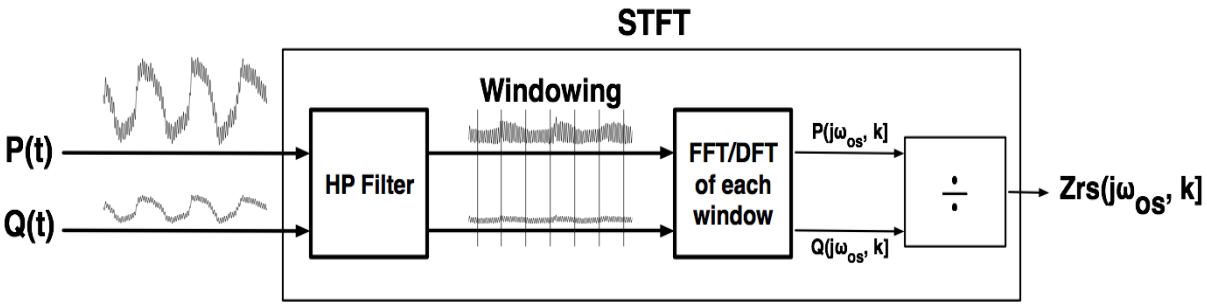

Figure 2.5 Schematic representation of the short-time Fourier transform

2.4 Linear Time-Varying Systems

Modeling a biological system is often associated with the assumption that elements in the model are not only linear, but also time-invariant (LTI), however, in reality most biological elements are time-varying and if they can be approximated as linear, they are linear time varying (LTV). The assumption of time invariance implies that model elements don't change over time and thus for inputs with stationary statistics, the output is also stationary.

If the goal is to track temporal variations in system properties, the decision to use a time-varying or time-invariant model depends on the rate at which the parameters of the

system are varying. If we model a time-invariant system by a static transfer function, the magnitude and phase of transfer function are fixed as a function of time. For example, if we have a filter consisting of a resistor and a capacitor, time invariance implies that the bandwidth does not changes as a function of time. Or in other words, the filter is only time-invariant if the values of the capacitor and the resistor do not change with time. The respiratory system is often modeled as linear single compartment system as a resistor and a capacitor (and sometimes an inductor) and can be assumed time-invariant over very short periods of time within the duration of a breath, or analysis is done over many breaths such that although the system is time varying it is assumed that the effects of time varying can be averaged out. However to be more accurate, the system actually varies with time during ordinary breathing. One way this occurs is because the lung changes dimensions during breathing, leading to airway dilation and narrowing as well as tissue stretching and relaxation during inhalation and exhalation respectively, leading to changes in its mechanical properties.

LTV systems can also be modeled analytically or numerically simulated in either the frequency domain or the time domain. In the time domain, an LTI system is described by an impulse response function at time τ, $h(\tau)$, to a unit input impulse applied at time $t = 0$. τ represents the difference between the time the impulse is applied and the time the impulse response is measured and is known as the elapsed time. The input-output relationship for a LTI system is given by convolution integral:

$$y(t) = \int_{-\infty}^{\infty} h(\tau)\, x(t-\tau)\, d\tau \tag{2.4}$$

where $x(t)$ and $y(t)$ are input and output of the system respectively. Taking the Fourier transform of the above equation yields the transfer function of the system in frequency domain:

$$Y(f) = X(f)H(f) \tag{2.5}$$

achieving $H(f)$ can yield the output $y(t)$ by taking the inverse transform of $Y(f)$:

$$y(t) = \int_{-\infty}^{\infty} Y(f)\, e^{-j\omega t}\, df = y(t) = \int_{-\infty}^{\infty} X(f)\, H(f) e^{-j\omega t}\, df \qquad (2.6)$$

The same principle of using an impulse response applies to the LTV systems in the time domain; however, the impulse response takes the form of $h(\tau, t)$ which describes a time-varying impulse response function. Since the system is not stationary (time-invariant), the impulse response varies from the time the impulse is applied $(t - \tau)$ and the time the response is measured (t). In an LTI system, the impulse response is strictly a function of τ represented by $h(\tau)$ while the impulse response of a time-varying system is a function of two variables. In other words, in an LTI system, $h(\tau, t_1) = h(\tau, t_2) = h(\tau,)$ but in an LTV system $h(\tau, t_1) \neq h(\tau, t_2)$. To elaborate further, Figure 2.6 depicts the comparison between impulse responses to a time-invariant system and a time-varying system.

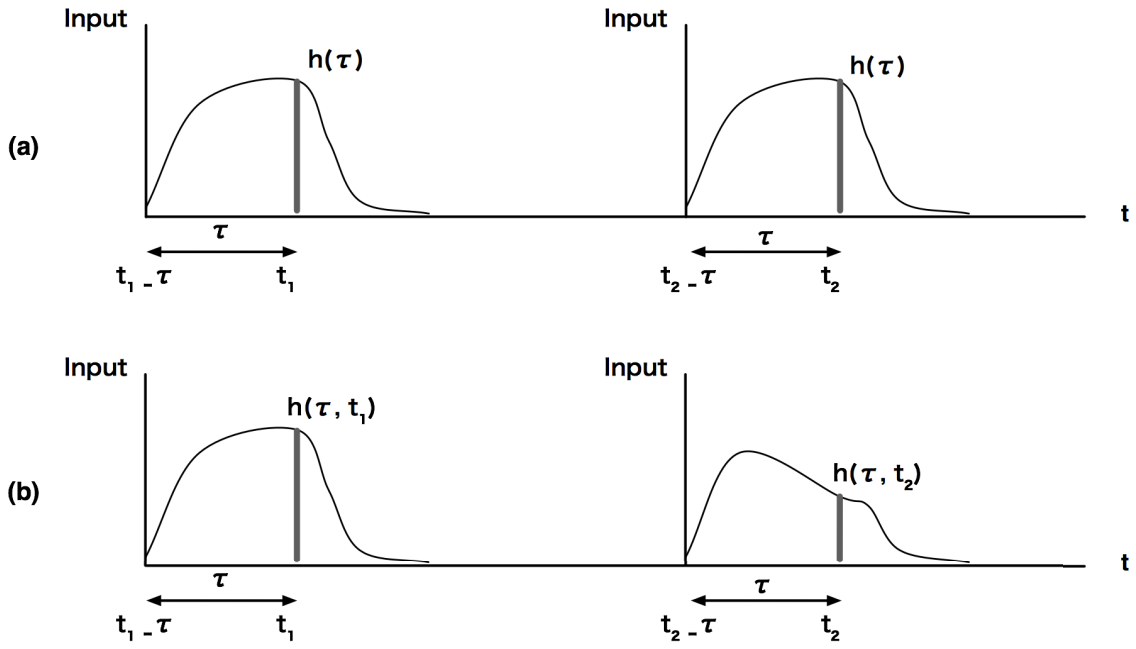

Figure 2.6. Impulse response of (a) time-invariant system and (b) time-varying system

The variable τ in an LTV system has the same features as τ in the impulse response of an LTI system and can be taken to the frequency domain to achieve the transfer function, frequency response and bandwidth. However, since the response

changes in time, a time-varying transfer function can be defined as $H(f,t)$ by taking the Fourier transform of $h(\tau,t)$ with respect to τ [65]:

$$H(f,t) = \int_{-\infty}^{\infty} h(\tau,t)\, e^{-j\omega\tau}\, d\tau \tag{2.7}$$

Here just as it is possible to perform a Fourier transform of a signal which is time dependent, it is also possible to take the Fourier transform of a time-varying impulse response function.

If the system is slowly time-varying then the frequency response concept can be applied to $H(f,t)$ [65]:. While an LTI system has a single impulse response function and a single transfer function, an LTV system could be represented by series of transfer functions and impulse response functions which simplifies the simulation of such system as we will see further in Chapter 4. The input-output relationship of an LTV system can be written based on the definition of impulse response:

$$y(t) = \int_{-\infty}^{\infty} h(\tau,t)x(t-\tau)\, d\tau = \int_{-\infty}^{\infty} h(t-\tau,t)\, x(\tau)\, d\tau \tag{2.8}$$

As is well known, the response of an LTI system, Z_{LTI}, to an exponential input, $e^{j\omega t}$, is:

$$Z_{LTI}\left(e^{j\omega t}\right) = \int_{-\infty}^{t} h(t-\tau)\, e^{j\omega\tau}\, d\tau$$

$$= \int_{-\infty}^{t} h(t-\tau)\, e^{-j\omega(t-\tau)} e^{j\omega t}\, d\tau = e^{j\omega t} Z_{LTI}(j\omega) \tag{2.9}$$

where $Z_{LTI}(j\omega) = \int_{0}^{\infty} h(\xi)\, e^{-j\omega\xi}\, d\xi$ is the frequency response function of the system with $\xi = t - \tau$.

In 1950, Zadeh [60] suggested that the same procedure can be extended to LTV systems:

$$Z_{LTV}\left(e^{j\omega t}\right) = \int_{-\infty}^{t} h(\tau, t)\, e^{j\omega\tau}\, d\tau = e^{j\omega t} \int_{-\infty}^{t} h(\tau, t)\, e^{-j\omega(t-\tau)}\, d\tau = e^{j\omega t} Z_{LTV}(j\omega, t)$$

(2.10)

This equation establishes that the transfer function of an LVT system can be found by using the exponential input, $e^{j\omega t}$, and dividing the response by $e^{j\omega t}$. Unlike the response of an LTI system to a periodic input, the response of an LTV is not necessarily periodic because of the dependence of $Z_{LTV}(f, t)$ on time. However, $Z_{LTV}(f, t)$ is considered a slow and smooth function of t.

Zadeh's method of analysis of time-varying systems inspired researchers in electrical and bioimpedance identification field to apply the method to identification of periodically varying linear systems [61, 66-70]. For example, Sanches et al. successfully estimate the time-varying impedance of a periodically varying bio-impedance within the entire measurement interval [61]. The impedance time-varying transfer function estimation method has been used in many communication and electrical engineering papers [71-73], however, from the bio-impedance transfer function analytical papers, the estimation method has only been used for finding the transfer function of the elastance of left ventricle [74]. In chapter 4 of this thesis we analytically use Zadeh's method for the first time on the respiratory system.

2.5 Piezoelectric Actuators

Piezoelectric actuators have been used for several years in applications such as ultrasonic motors, loudspeakers, dampers, precision position controlling, noise control, relays, acoustics, and pressure sensing [75-78]. Researchers mostly explore the uses of unimorphs, bimorphs, or multilayer morphs in applications as pressure sensors or resonators or in specialized applications [69-72]. The structures of bimorph and unimorph actuators are quite simple. As shown schematically in Figure 2.2, a bimorph actuator consists of two thin ceramic plates bonded together. Two types of connections are often used in bimorph fabrication. One is a series or antiparallel connection, in which two piezoelectric sheets with opposite polarization direction are bonded together by epoxy resin. The electrical voltage is applied across the total thickness and the electrical field

(E) is the voltage divided by actuator total thickness (t). The other is the parallel connection, in which the two piezoelectric layers have the same polarization directions. In this case, the electric voltage is applied between the intermediate electrode and the top and bottom electrodes and E is V divided by the thickness of an individual piezoelectric layer. In both cases, one plate expands while the other contracts and the net result is a bending deflection. In the parallel connection, the driving voltage can be reduced to half the value compared to the series case while keeping the same field strength. Often, a triple-layer structure is used in which a neutral elastic layer is sandwiched between the two piezoelectric layers in a bimorph. In a unimorph actuator, the piezoelectric layer is also bonded to an elastic layer. The elastic layer can provide strength, and also resists the dimension change while the piezoelectric layer is driven to expand or contract leading to bending deformation. Thus the use of an elastic layer can greatly increase the mechanical reliability of the actuator, and alter the mechanical properties of the actuator which are both important features in most applications.

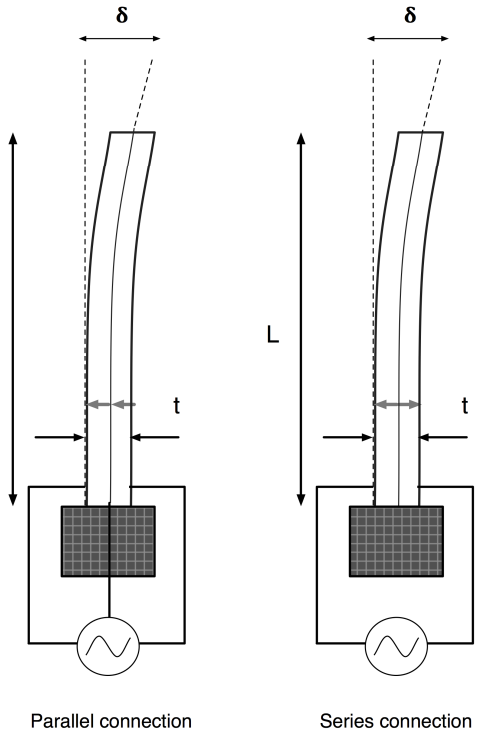

Figure 2.7 Bimorph piezoelectric actuator with length L, and thickness, t, goes under displacement of δ when an AC voltage is applied in parallel and series mode.

In this thesis the review of piezoelectric actuator methodology is limited to the principle of operation and the most common and useful modeling approach appropriate for cantilever operation in an OS device. The thesis is not intended to advance piezo-actuator design or technology, but applies it to a new application of a piezo-driven single frequency OS device.

Modeling Piezoelectric Actuators

Most of the literature has focused on the static behavior of bimorph actuators [83, 84] where the displacement (δ) is composed of a trade off between the input voltage and the force generated by the actuator. This originates the blocking force that it is an assumed external force that can cancel the displacement [83]:

$$\delta = bV + aF \tag{2.11}$$

where a and b are coefficients related to the characteristics of the bimorph: $b = \frac{3d_{31}L^2}{2t^2}$ and $a = \frac{4s_{11}L^3}{Wt^3}$, $s_{11}$is the elastic compliance and d_{31} is the transverse piezoelectric coefficient. Moreover, L, w and t are the length, width, and thickness of bimorph, respectively. The higher the external force, the lower the displacement. Note the external force has a negative sign [84].

There are some common modeling approaches for describing the behavior of piezoelectric actuators [85-90]. Equivalent piezoelectric models can be used for analysis, design and optimization stages of building a device. Model parameters can be obtained using the experimental approach where model parameters are identified based on the transfer function of the system that explains the input-output relationship. Another approach could be using numerical calculations with specific experiments to identify piezoelectric actuator electrical and mechanical properties. Some of these studies have been conducted specifically on piezoelectric bimorphs to address the dynamic aspect of this problem and solved to find the displacement and other intensive quantities of bimorphs. In this category, one of the most important papers in the literature is that

published by Smits et al [85] where by using Euler-Bernoulli beam equations they derive the general form of the dynamic admittance matrix bringing into account the load on the actuator.

In this thesis because we used an off-the-shelf piezoelectric cantilever, we were able to use the experimental approach to fit the results to the chosen model and find model parameters to use in simulations.

Vibrating piezoelectric actuators are often analyzed using electro-mechanical equivalent circuits [86-90]. The model that have been used most commonly by researchers was originally proposed by Cady in 1922 [89] and later expanded by Van Dyke in 1925 [90]. This model that is known as Butterworth Van-Dyke (BVD) brings into account the kinematics of the movements by considering a mass-spring damper system excited by an electric voltage. A disadvantage of the BVD model is that it is valid when the elements being modelled are constant and independent of frequency. However, this is not a problem for an application of an actuator operating on resonance because the system parameters can be assumed constant in the narrow range around the resonance frequency. Considering dielectric losses, structural damping and inertia effects a fixed-free cantilever bimorph actuator's tip deflection (δ) can be predicted by Equation (2.12) [83]:

$$m.\ddot{\delta} + C_d.\dot{\delta} + K.\delta = \alpha_p.V_{in} + F \tag{2.12}$$

where V_{in} is the applied voltage across the thickness of the bimorph, α_p is the electro-mechanical coupling, F is the external load perpendicular to the cantilever's tip, m is the mass, C_d is the damping coefficient, and K is the bimorph stiffness. The BVD model that is shown in Figure 2.8 also consists of a dielectric capacitor, C_p. It is important to mention that the mechanical side of the BVD can also be represented as a circuit consisting of a resistance, an inductor and a capacitor (RLC).

Transforming this equation into the frequency domain using Laplace and assuming that there are no external forces (F=0) yields the input (Voltage) output (displacement) relationship or transfer function of the piezoelectric actuator (TF_{piezo}):

$$TF_{piezo}(s) = \frac{\alpha_p}{m.s^2 + C_d.s + K} \quad (2.13)$$

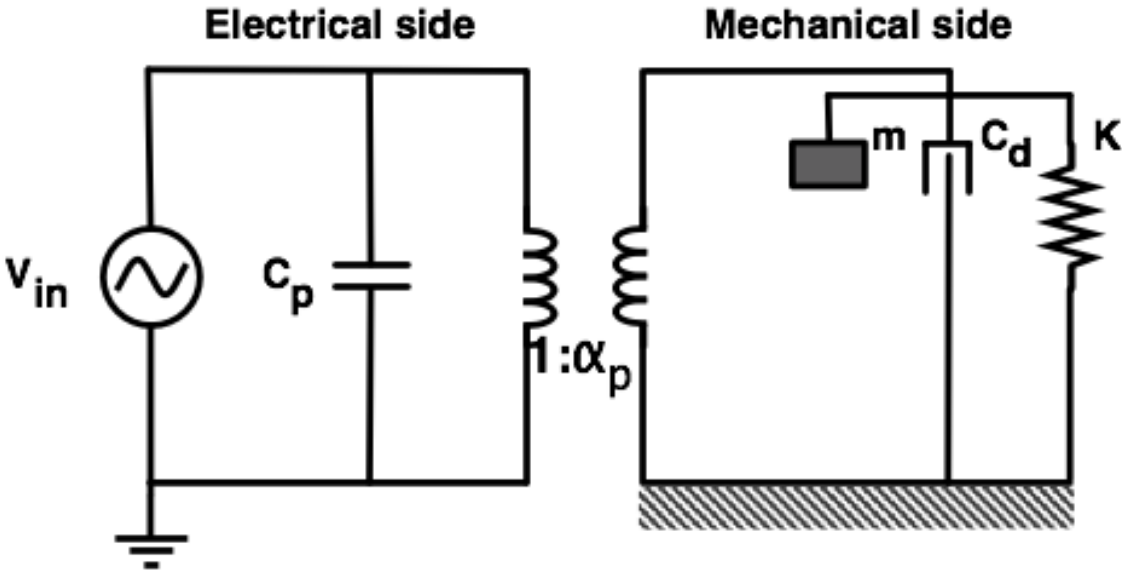

Figure 2.8 Electro-mechanical representation of Butterworth-Van-Dyke (BVD) piezoelectric model.

2.6 Research Hypotheses And Aims

2.6.1 Simulating a Piezoelectric-Based OS Motor

The first objective of this thesis was to simulate a piezoelectric based, small oscillator device to guide the design of an optimal prototype device to measure lung mechanics at a higher frequency not contaminated by breathing.

Brief approach: I implemented a comprehensive model of an OS device using piezo technology in MATLAB/SIMULINK. In the model, I imposed real breathing noise measured from six patients on respiratory system model of different subject populations

including COPD, asthma, children and asthmatic children. This model made possible the evaluation of different potential challenges including: the load of breathing on the actuator, some nonlinearities and airflow leak. The design was used by my co-worker, Lucas Posada, to build a scaled ($3/4^{th}$) prototype device.

2.6.2 Assessing the Accuracy of Tracking Impedance with Time

The second objective of this thesis was to investigate a method to analytically assess the accuracy in temporal tracking of impedance using a time-frequency analysis approach as well as assess the accuracy in a modelling study in tracking a temporally varying respiratory system with current signal processing methods.

Approach: In an analytical study I introduced, for the first time, the time-varying error (TVE) in OS measurements using time-frequency transfer function approach of Zadeh. Also, FFT/DFT were replaced with Goertzel algorithm with the potential benefit of reduced computational cost in practice. To assess the error in tracking time-varying impedance, I used a simulated sinusoidally varying impedance and quantified the estimation error over a range of recorded subject breathing rates.

2.6.3 Influence of Time-Varying Elastance on Frequency Dependence of Resistance

The third objective of this thesis was to develop a method to analyze a time-varying model of the lung that did not assume stationarity and compare this to the more traditional methods of analysis of the respiratory system.

Approach: In an analytical study I first used a time-domain approach to analyze the impedance of a time varying respiratory system. This was achieved by writing the

equation of motion from the single compartment model, but with a time-varying impedance. I used this to specifically examine the influence of time-varying elastance on the frequency dependence of resistance. I also applied the time-frequency analysis approach of Zadeh that I introduced in aim 2, and simulated different impedance conditions using both single and two compartment models to assess the magnitude of this effect relative to the effect of simple heterogeneity.

Chapter 3: A Resonance-Mode Piezoelectric Device For Measurement Of Respiratory Mechanics

Authors

Hamed Hanafi

Lucas Posada

Swati A. Bhatawadekar

Jeremy A. Brown

Geoff N. Maksym

Published, Journal of Biomedical Science and Engineering

2013

This manuscript has been modified from its original format to conform to the structure of this dissertation

3.1 Abstract

This paper presents the design of a novel oscillometry device for the measurement of respiratory mechanics based on piezoelectric bimorph actuator technology. To predict performance for measurement of human respiratory mechanics, a dynamic model was developed based on a bimorph piezoelectric actuator driving a linear resistance mesh screen including subject's respiratory impedance loads, and realistic breathing noise. Model performance was also validated in a prototype device. We found that while breathing noise substantially lowered SNR, the model could produce sufficient pressure and flows for acceptable SNRs exceeding 35 dB, and accuracies exceeding 99%. Satisfactory accuracy could be achieved with load impedance errors less than 3%. Maintaining the air-gap around the oscillating mesh with a resistance against the leak greater than 0.38 $cmH2O/L/s$ maintained good performance, with an acceptable 4 dB decrease to SNR. Moreover, this work provides multiple solutions to host higher amounts of noise and nonlinearities. These results indicate the development of an accurate lightweight portable single frequency FOT device is feasible.

3.2 Introduction

Oscillometry also known as the Forced Oscillation Technique (FOT) superimposes fluctuations in airway pressure on normal breathing to measure the mechanical impedance to airflow of the respiratory system for diagnosing and monitoring lung diseases [91]. Using FOT is possible in very young children to elderly patients as it is easy to perform unlike the current standard approach, which involves a learned maximal forced expiration that is difficult for many patients. Respiratory impedance is a complex quantity with a real part: respiratory resistance (R_{rs}) largely due to airflow resistance and an imaginary part: reactance (X_{rs}) arising from elastic properties of the lung and chest wall and the inertia of the air. The resistance is elevated in diseases such as asthma and COPD associated with airway narrowing and the reactance can also be altered due to loss of airspaces as airways close and limit flow [92].

FOT Devices must reliably produce oscillatory waveforms even when perturbed by breathing, and must accurately measure pressure and flow due to the oscillations, over a wide range of patient respiratory impedances, and compensate for any self-impedance of the device and disposable filter. Current FOT devices use either a loudspeaker or oscillating electromagnetic actuator, which results in a device that is larger or heavier than typical spirometers.

Piezoelectric actuators have been used for several years in applications such as loudspeakers, mechanical dampers, ultrasonic motors, precision position controlling, noise control, relays, phonograph pick-up, acoustics, and pressure sensing [75-77, 93]. We have designed a smaller and less costly FOT device, based on a piezoelectric bimorph actuator using a computer model to help explore the feasibility and design requirements for a suitable device. The design was tested in a prototype device.

3.3 Methods

3.3.1 Simulations

The device is based on a moving mesh in a flow tube and was modeled in MATLAB/SIMULINK as described in following paragraphs. The resonance of the oscillating cantilever was tuned to 6 Hz by varying the mass on the tip [78]. Forced air oscillation at 6 Hz was sent into a respiratory system that modeled different subject populations including healthy, COPD, normal children and asthmatic children with representative impedance values indicated in Table 3.2 [95-100]. We used actual measured breathing waveforms of 6 voluntary subjects (without any apparatus) as realistic noise. Therefore breathing noise was dominant at lowest frequencies, which included a peak at the breathing frequency and a small hump at approximately twice the breathing frequency although it was highly distributed with a long tail that went through the oscillating frequencies. Subjects were recruited as part of a research ethics approved study approved by the Capital District Health Authority (Halifax, NS). The average RMS amplitude of the breathing flow was used as the noise gain of unity. The noise was adjusted in amplitude as a perturbing input to assess the effects of breathing noise on

predicted values as well as on the actuator. The tidal volume (V_T) of the measured volunteer patients was $660 \pm 150\ mL$ ($\pm SD$) while 1/3 of that was used as realistic V_T for the child patient [102]. The predicted actuation characteristics for piezoelectric bimorphs are well known [77] and therefore to achieve sufficient accuracy, signal-to-noise ratio (SNR), low power consumption, and low cost, the model incorporated a novel resonance based piezoelectric actuator design. To model the leak resistance of the moving mesh screen, the mesh resistance comprising the holes on the mesh and the air-gap with the housing was modeled as a resistance in parallel to the respiratory system impedance (This is because the oscillating pressure generates flow that goes both into the respiratory system and also out the back of the device through the mesh. (Figure 3.1)). The device needs to reach high air-gap resistance to conduct the least amount of air loss. From the model we set a design goal for a minimum air-gap threshold resistance to achieve errors less than 10% [2] for different subject loads.

It is important to note that this simulation considered only linear elasticity in the clamp-free cantilever bending model for the piezoelectric actuator. In measurements of the prototype, harmonics were not detectible in monitoring displacement of the actuator during load free oscillation, and added oscillating flows, nonlinear effects appear to be small as no harmonics were detected in flow recordings [9].

3.3.2 Experiments

The simulation was used to verify the design and construction of a prototype device.

Figure 3.1a shows a diagram of the bimorph actuator and Figure 3.1b shows a diagram of the prototype FOT device incorporating the bimorph actuator. An off-the-shelf bimorph actuator (40-2010, American Piezo Ceramics, Mackeyville, PA) with length (L) of 60 mm, width (w) of 20 mm and thickness (h) of 0.7 mm was used. The piezoelectric bimorph was derived by an AC voltage source using a function generator and a pre-amplifier and a mesh screen was attached to actuator's tip in order to generate air oscillation at 6 Hz. The airflow was directed into calibrated reference resistive loads of 5 and 15 $\mathrm{cmH2O/\,L/s}$ (Hans Rudolph Inc, KS, USA). Pressure of airway opening was

measured using a differential pressure transducer (TD-05-AS, SCIREQ Inc., Montreal, Canada) across the mesh screen that was attached to the cantilever and flow was calculated by dividing the pressure across pneumotachograph's mesh by the screen's resistance ($R_p = 0.4\ cmH2O/L/s$). Prior to the tests, transducers were calibrated by applying steps of 0.5 $cmH2O$ using a manometer. Calibration coefficients were calculated based on the results. The breathing noise was generated using a ventilator pump (Bodine Electric Company, Chicago, ILL, USA). The experimental test set up is presented schematically in Figure 3.9b Measurements were repeated for 6 times for each test. Pressure and Flow data were sampled at 1000 Hz and the impedance was computed as previously described [60]. The SNR was determined by Fast-Fourier-Transforming (FFT) the entire duration of data into the frequency domain, and calculating the ratio of the magnitude of the FFT at the frequency of oscillation to the root mean squared average of noise in 1 Hz bandwidth side bands adjacent to the oscillatory frequency.

Section III describes the methods used to model the air oscillometry device shown in Figure 3.1, including the approach used to calculate the oscillation amplitude, and to model the respiratory system and piezoelectric cantilever.

3.3.3 Design and Modeling

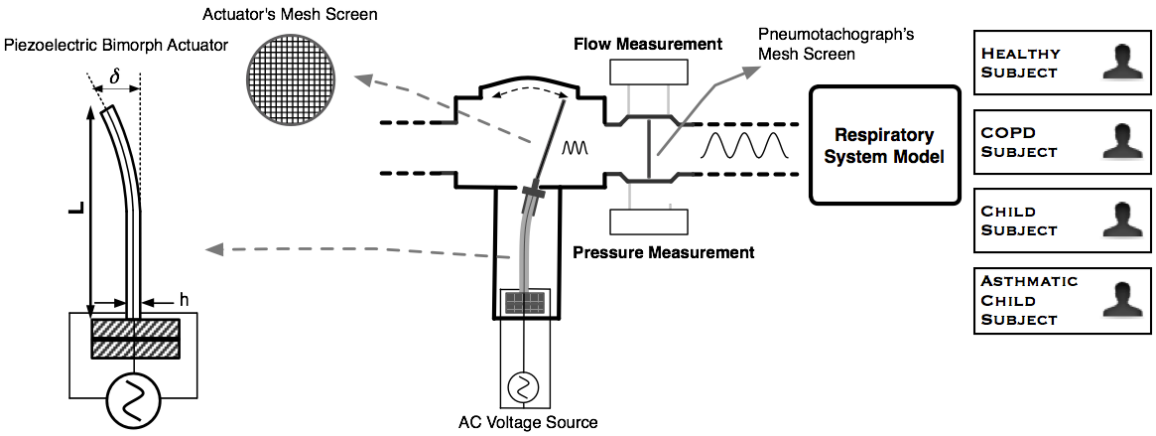

Figure 3.1. (a) Structure of a bimorph actuator with parallel configuration. L, h and δ represent the length, thickness and displacement respectively. (b) Schematic representation of the prototype device attached to the respiratory system model of different subjects for simulations.

Unimorph, bimorph, and multimurph piezoelectric actuators are used in many different applications as a low cost efficient means of converting electrical energy to mechanical energy. Although the total potential energy density remains the same for different multimorph actuators of the same geometry, the more layers incorporated into the multimorph, the lower the amplitude of the required voltage is. Certain bimorph designs however rely on a metallic spacer or vane separating the two relatively thin piezoelectric plates. This type of bimorph actuator reduces the required electric field while maintaining a reasonable displacement and actuator force at a fraction of the cost of multimorph actuators. This is primarily due to the less complicated manufacturing process.

Bimorphs are available in series and parallel configurations. We chose a parallel configuration (Figure 3.1a) since they deflect the same amount as the series for half of the series configuration's applied voltage [76].

3.3.4 Calculations and Piezoelectric Model

Equation (3.1) presents the governing equation for oscillating flow through a mesh screen affixed to the top of the actuator that calculates the oscillation amplitude, δ, at frequency, f:

$$\delta(\omega) = \frac{P}{R_a.\omega.A_r} \tag{3.1}$$

where $\omega = 2\pi f$ is the angular frequency, P is the pressure amplitude expected. $R_a = 0.6\ cmH2O/L/s$ is the resistance of the actuating mesh screen and $A_r = \pi r^2$ is the area of the circular oscillating mesh of radius of $r = 2.45\ cm$.

Taking dielectric losses, structural damping and inertia effects into account, a fixed-free cantilever bimorph actuator's tip deflection (δ), as described in [77], can be predicted by Equation (3.2) as:

$$m.\ddot{\delta} + C_d.\dot{\delta} + K.\delta = \alpha_p.V_{in} - F \tag{3.2}$$

where V_{in} is the applied voltage across the thickness of the bimorph, α_p is the electro-mechanical coupling, F is the external load perpendicular to the cantilever's tip, m is the mass, C_d is the damping coefficient, and K is the stiffness.

Figure 3.2 shows the electro-mechanical representation of the Butterworth-Van-Dyke (BVD) [90] model of the piezoelectric actuator. The parallel capacitor, C_p represents the electrical side of the model. The mechanical side represents a *mass–spring–damper resonant system.*

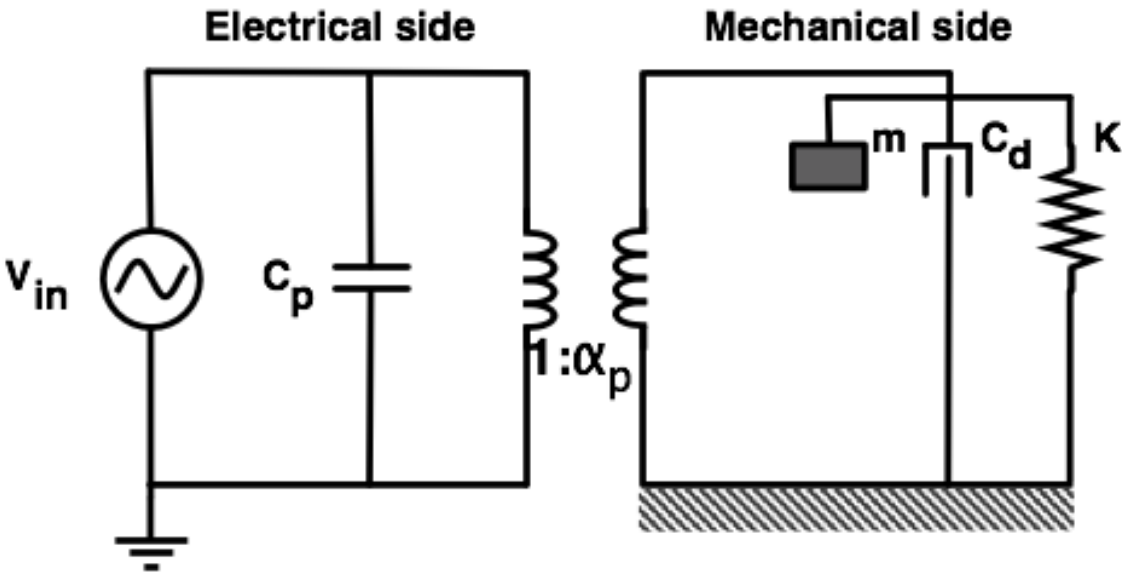

Figure 3.2. Electro-mechanical representation of Butterworth-Van-Dyke (BVD) piezoelectric model.

Transforming Equation (3.2) into the Laplace domain with no load applied for the moment gives the electro-mechanical transfer function (TF_{piezo}) of the piezoelectric actuator:

$$TF_{piezo}(s) = \frac{\alpha_p}{m.s^2+C_d.s+K} \tag{3.3}$$

m, K, C_d, and α where obtained by standard mechanical experiments and using analytical formulas as follows [99]. Briefly: To find m, we calculated and experimentally measured the effective mass of the cantilever and the mass on the tip needed to shift the bimorph resonance down to 6 Hz. At resonance, K was determined from $K = m.\omega_r{}^2$ where ω_r is the resonant angular frequency. The displacement versus frequency data was produced from applying a chirp signal and recording the displacement using a non-contact type laser displacement sensor (AR 200, Acuity, Ortonville, MI). From the curve we obtained the damping ratio $\zeta = \frac{\Delta\omega}{2.\omega_r}$ where $\Delta\omega$ is the angular half-power bandwidth. The damping coefficient was computed as $C_d = 2.\zeta.\sqrt{K.m}$. To find α, this data was least mean squared fit to the transfer function (Equation (3.3)) with $R^2 = 0.97$ (Table

3.1). The movement amplification due to the distance between the tip of the actuator and the center of the mesh screen is added to the model by $\beta = \frac{L+r}{L}$ where $(L + r)$ is the location of the center of mesh (Figure 3.4c).

Table 3.1. Properties of the piezoelectric cantilever

Property	Fitted Value	Approach
α	2.6 N/V	Fitting $R^2 = 0.97$
C_P	190 nF	Manufacturer
m	78 gr	
C_d	0.53 Ns/m	Experiment
K	110.8 N/m	

3.3.5 Respiratory System Model and Impedance

To model the respiratory system impedance, we used the standard single compartment model which is the equation of motion (Equation (3.4)). The resistance (R_{Rs}) was modeled as a single Newtonian resistive tube. The elastance (E_{Rs}) represents the stored elastic energy largely from surface tension, but also from tissue stretching and some gas compression while the inertance (I_{RS}) represents the inertia of the moving gas. (Figure 3.3) [37]

$$P = R_{Rs}.\dot{V} + E_{Rs}.V + I_{RS}.\ddot{V} \tag{3.4}$$

where P is the airway pressure, V is volume, $\dot{V}$ is flow and $\ddot{V}$ is volume acceleration.

The respiratory system impedance, Z_{rs}, is obtained by transforming Equation (3.4) into the frequency-domain:

$$Z_{rs}(j\omega) = R_{Rs} + j(-\frac{E_{Rs}}{\omega} + I_{RS}.\omega) \quad (3.5)$$

This is well established model particularly well suited for the healthy lung, and through altering R_{rs}, E_{rs} and I_{rs}, the model can approximate the major changes in mechanics observed in common lung disease, although a more accurate representation would include some increasing frequency dependence of the parameters, particularly R_{rs} and E_{rs}. For the purposes of design, we have explored a range of mechanical parameters that describe the gross changes commonly encountered using FOT including COPD as well as a child [95-98] (Table 3.2). The changes observed in asthma in an adult would be similar to the increase in R_{rs} and E_{rs} observed in a child.

Table 3.2. Mechanical properties of subject populations

Property	Healthy Male	COPD	Child (8 year old boy)	Asthmatic Child
$R_{rs}\ (cmH2O/\ L/s)$	2.35	10	6.86	9.5
$E_{rs}\ (cmH2O/L)$	33.3	60	82.84	100
$I_{rs}\ (cmH2O/L/s^2)$	0.0146	0.028	0.0092	0.0092

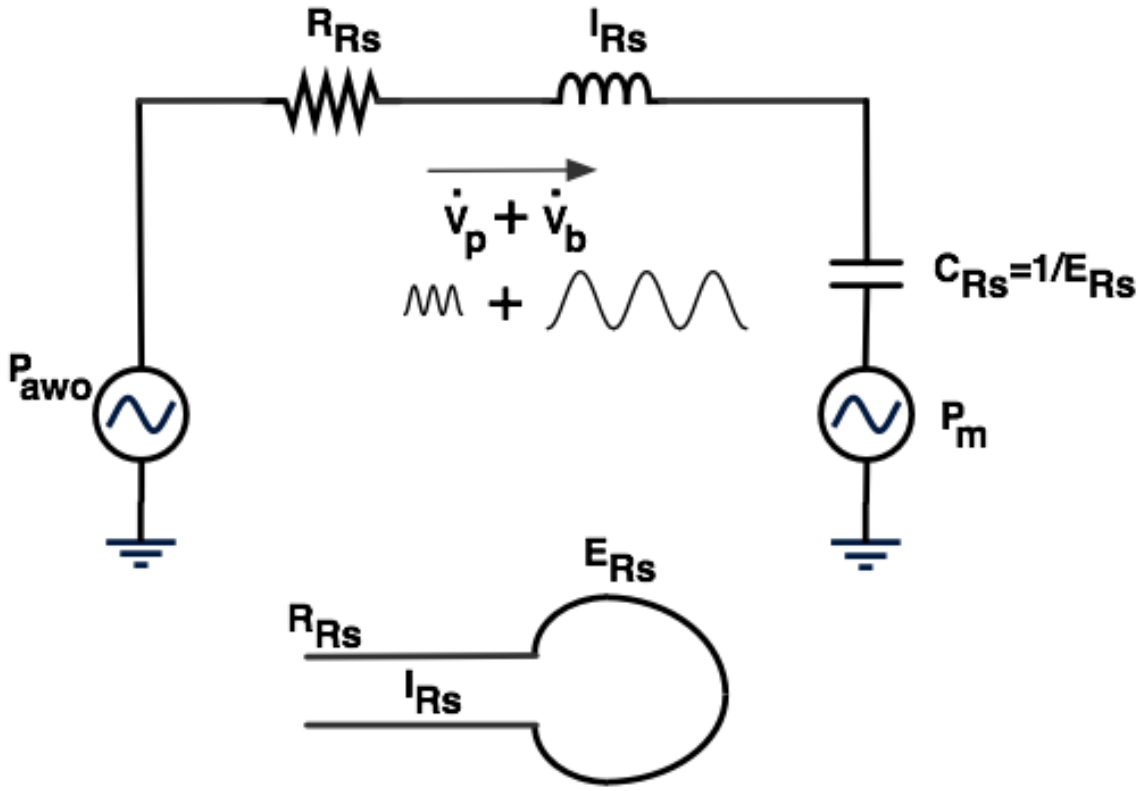

Figure 3.3. Single compartment model of the respiratory system based on linear RLC circuit analogy: R_{Rs} is the resistance of the tubing, E_{Rs} is the elastance of the tissue, and I_{Rs} is the inertance of the flowing gases. P_{awo} is the pressure of airway opening and P_m is the pressure created by muscle effort. $\dot{V}_b$ is the breathing flow/noise and $\dot{V}_p$ is the oscillation flow generated by piezoelectric actuator.

3.4 Results

3.4.1 Simulations

To verify the performance of the single frequency piezoelectric forced oscillation device, simulations of the model presented in section III were performed (Figure 3.4c). The normal breathing of a representative subject with frequency of 0.2 Hz containing the 6 Hz oscillations shown in Figure 3.4b caused fluctuations of approximately 0.2 mm on actuator's tip displacement (Figure 3.4a). This distortion increased with increasing noise

gain. As expected, when the breathing noise amplitude was increased, the flow SNR dropped. The decrease was more severe for the COPD and child simulation with normal tidal volume (V_T) and decreased to 28 dB at the simulated noise gain of 2.5, while the SNR remained higher than 35 dB for noise gains up to 3 for the male subject, the child with realistic V_T and the asthmatic child (Figure 3.5).

The variability in the results is due to the difference in volunteer patients breathing patterns, however, the rank ordering at every breathing noise gain stayed the same amongst subjects.

Increasing the breathing noise up to three times the normal values showed that the error in estimation of impedance of the lung exceeded 10% in the COPD simulation with breathing gain of 2 or more and in the child simulation with adult tidal volume with breathing gain of 3.2 or more, however, the error in the child simulation with realistic tidal volume, the asthmatic child and the healthy male was less than 5% at any breathing noise level (Figure 3.6). For breathing noise gain of unity, the largest absolute error in estimating R_{rs} was 0.175 $\mathrm{cmH2O/\,L/s}$ that represents 1.7% error, which belongs to the COPD subject. The COPD subject also had the largest absolute error in estimating X_{rs} of 0.045 $\mathrm{cmH2O/\,L/s}$. It is not appropriate to use % error representation for X_{rs} because its values are close to zero at respiratory system resonant frequency. Also, Elastance and Inertance cannot be precisely distinguished due to the single frequency measurement described here; therefore, the error in estimation of Reactance is used (Figure 3.6).

Verifying the effect of leak due to air-gap on SNR and the impedance estimation error showed that with total resistance against the leak greater than 0.38 $\mathrm{cmH2O/\,L/s}$ would give SNRs higher than 30 dB and errors lower than 10% for the different simulated respiratory impedances (Figure 3.7).

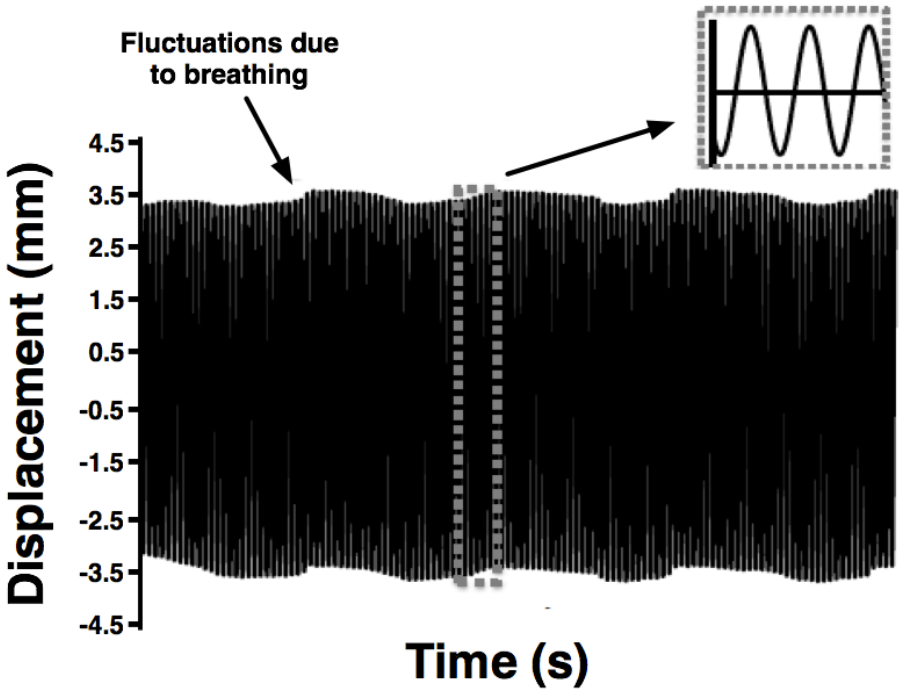
Fluctuations due
to breathing
Displacement (mm)
4.5
3.5
2.5
1.5
0.5
-0.5
-1.5
-2.5
-3.5
-4.5
Time (s)

(a)

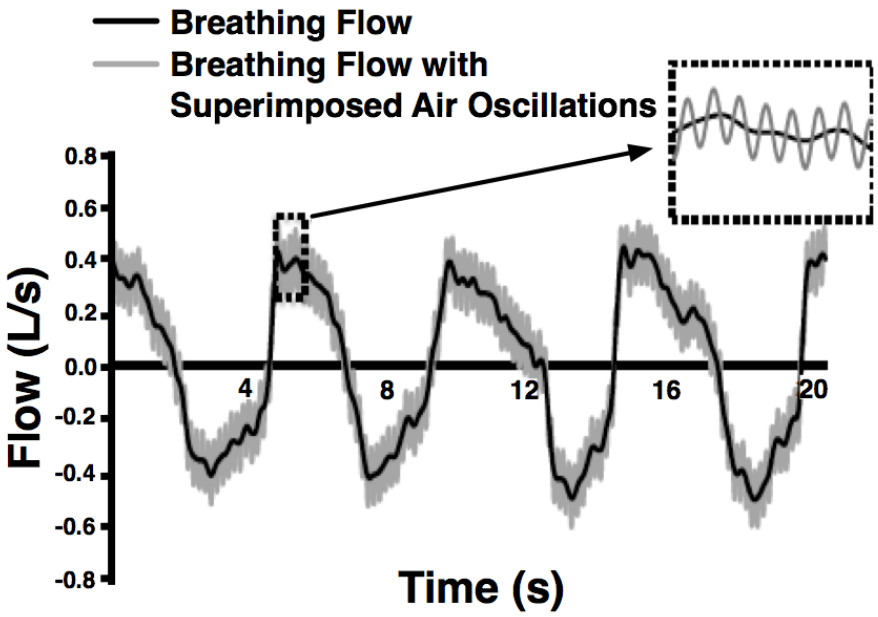
Breathing Flow
Breathing Flow with
Superimposed Air Oscillations
Flow (L/s)
0.8
0.6
0.4
0.2
0.0
-0.2
-0.4
-0.6
-0.8
4
8
12
16
20
Time (s)

(b)

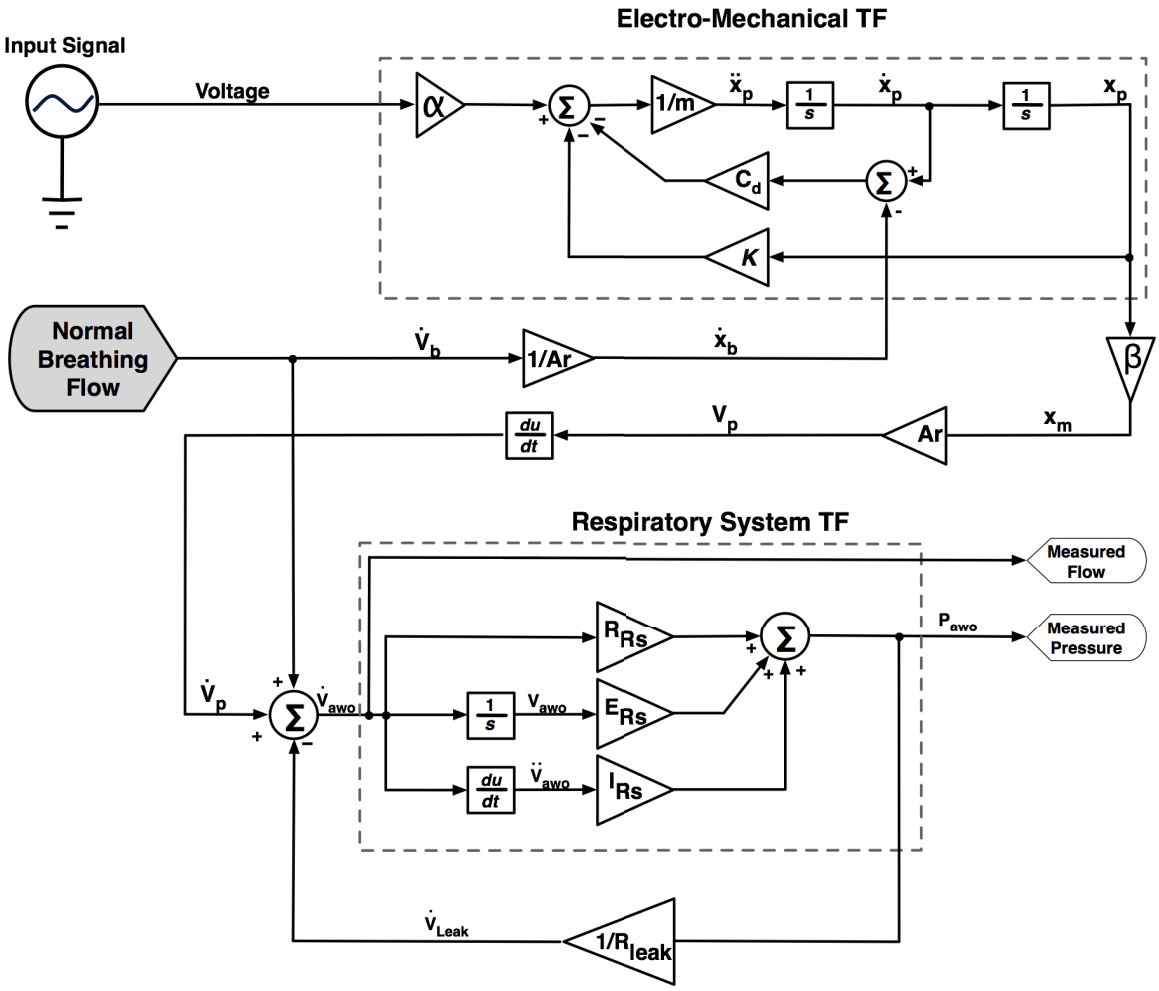

(c)

Figure 3.4. a. Tip displacement affected by breathing noise gain of unity from simulations b. Regenerated measured breathing flow of a volunteer via a pneumotachograph with superimposed oscillations from simulations according to the same time scale as in (a). c. Schematic representation of the modeled system.

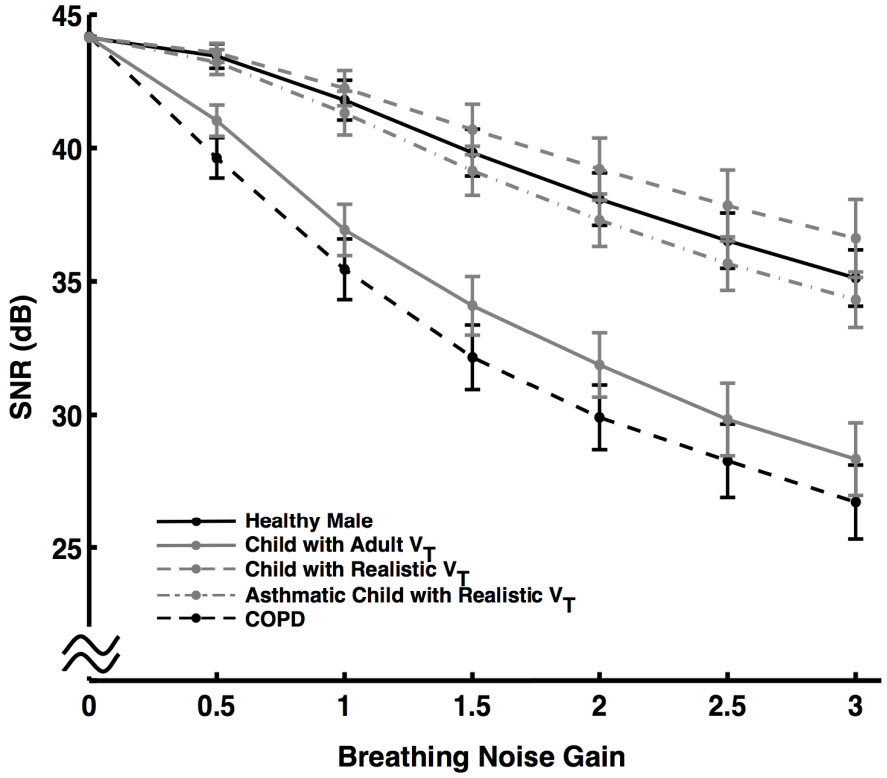

Figure 3.5. The effect of increasing breathing noise on measured flow SNR ratio in different subject populations. Increasing the breathing noise decreased the SNR.

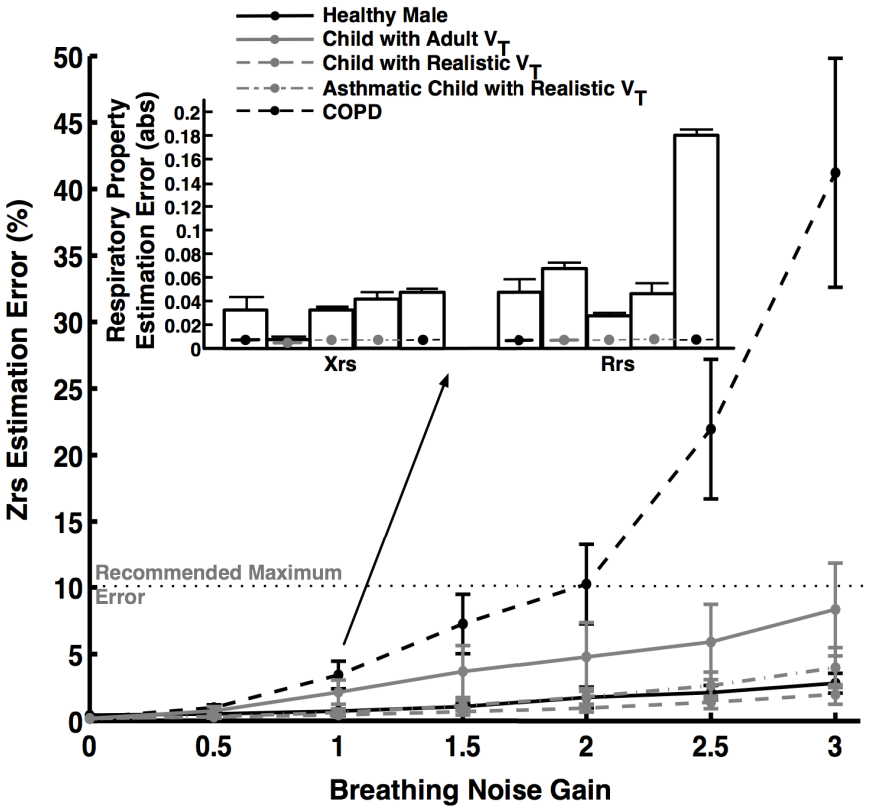

Figure 3.6. Magnitude estimation error of Zrs in percent for different subject populations at different noise levels. The estimation error increased with increasing breathing noise. The insert indicates Rrs and Xrs absolute estimation errors for unit breathing noise gain.

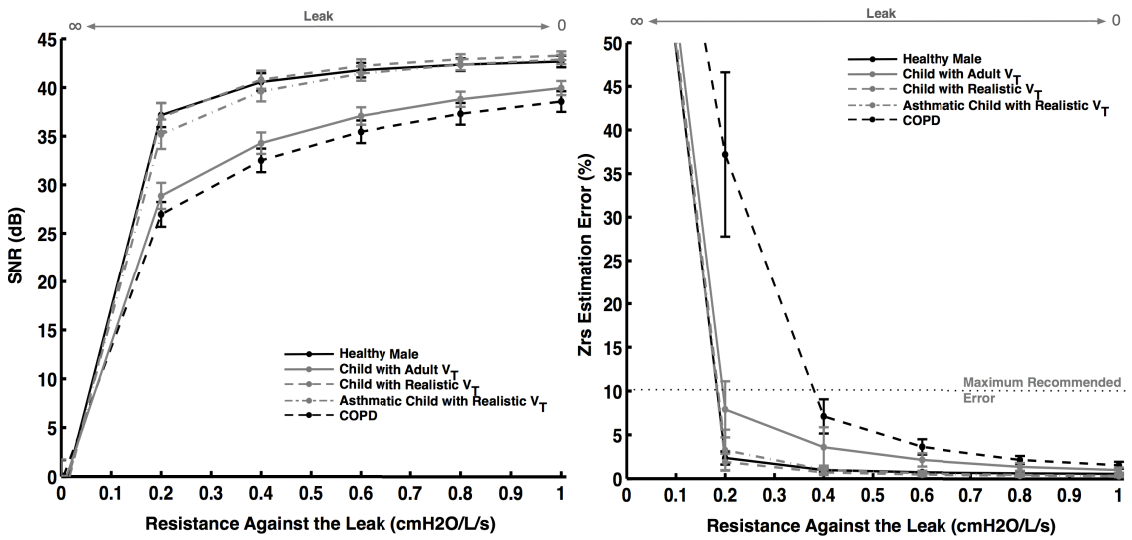

(a) **(b)**

Figure 3.7. SNR (a) and impedance estimation error (b) for different amounts of leak (mesh screen and airgap). As resistance against the leak increases (leak decreases) the SNR increases and the estimation error decreases.

3.4.2 Nonlinearity

The respiratory system model used in this paper was a linear single compartment model. However, there are nonlinearities that can arise such as form the pressure volume curve, and the well-established Rohrer flow nonlinearity. Here we explored the effects of the dependence of the resistance of the airway on flow according to Rohrer equation as follows (Equation (3.6)) that introduces a nonlinearity to the equation of motion (Equation (3.4)):

$$R_u = K_1 + K_2.\left|\dot{V}\right| \tag{3.6}$$

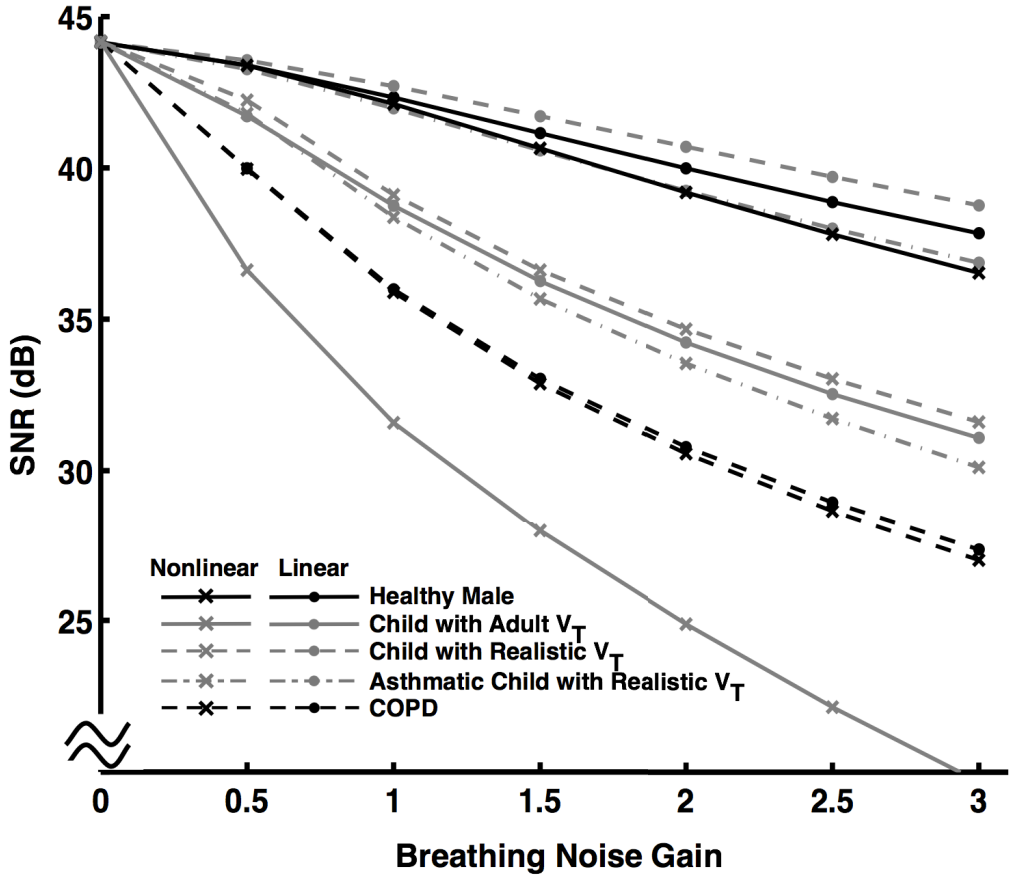
45
40
35
30
25
SNR (dB)
Nonlinear Linear
Healthy Male
Child with Adult V_T
Child with Realistic V_T
Asthmatic Child with Realistic V_T
COPD
0
0.5
1
1.5
2
2.5
3
Breathing Noise Gain

(a)

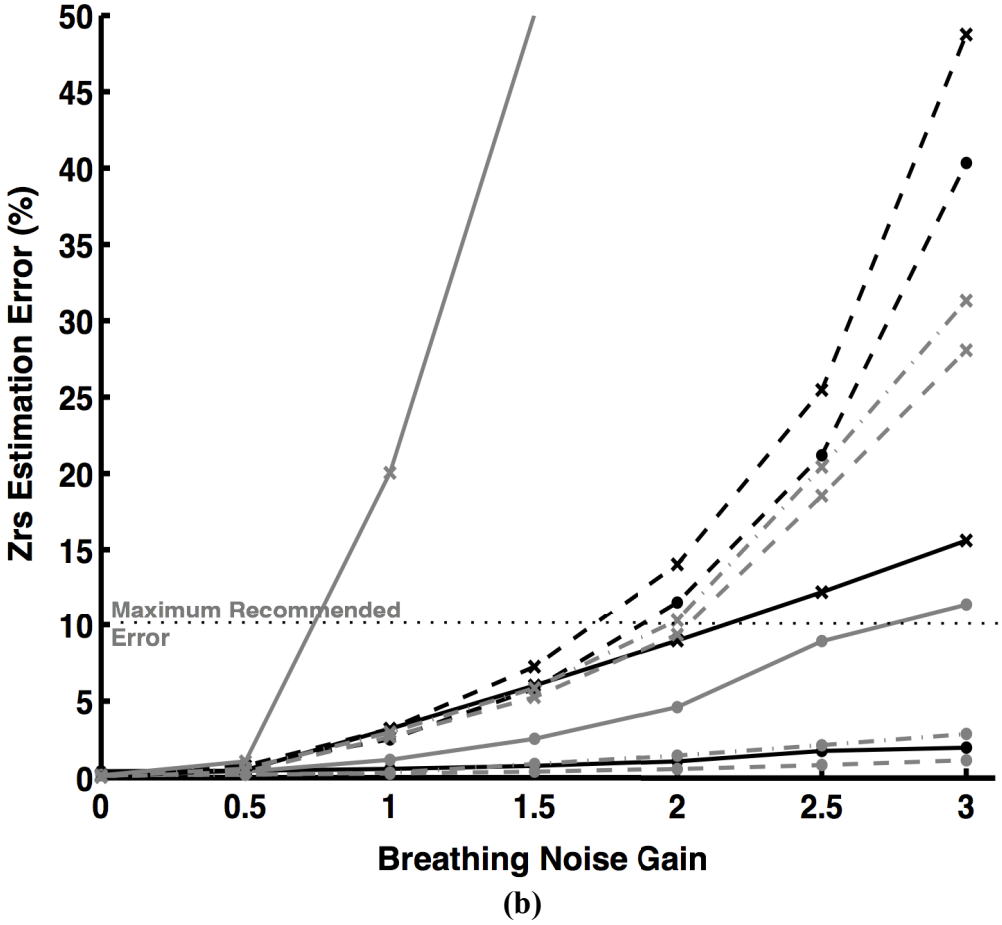

Figure 3.8. The comparison of the nonlinear and linear model in terms of SNR and impedance estimation error for increasing breathing noise in a representative subject. Nonlinearity reduced the SNR and increased the error.

where R_u is the nonlinear flow resistance in the upper airway, K_1 is the linear resistive term and K_2 is the additional resistive term depending on flow. To assess the influence of this nonlinearity on the performance of the device, the linear resistance of the respiratory system was set equal to R_{Rs} so that with zero flow the respiratory resistance would be the same as linear model parameter presented in Table 3.2. The nonlinear coefficient (K_2) was set to 0.2 $\mathrm{cmH2O}/L^2/s^2$ as representative of an adult subject, 7.7 $\mathrm{cmH2O}/L^2/s^2$ as representative of a normal child subject and 11 $\mathrm{cmH2O}/L^2/s^2$ as representative of an asthmatic child subject [101-103].

The effect of introducing this nonlinearity lowered the SNR at all breathing gains with typically less than 3dB difference for all subjects except in the child with adult V_T where the SNR lowered for about 13dB at normal breathing level. The impedance estimation error increased with breathing gain but remained less than 3% at normal breathing amplitudes except for the child with adult V_T. The error in child with adult V_T subject reached 10% at breathing gain of 0.7 while COPD reached the maximum recommended error at breathing gain of 1.7. The asthmatic child, the normal child and the male subject reached the maximum recommended error at breathing noise gain of about 2 (Figure 3.8).

3.4.3 Experiments

To verify the feasibility of the single frequency piezoelectric forced oscillation device in experiments, the prototype device was tested on flow resistive test loads of 5 and 15 $\mathrm{cmH2O/L/s}$ as representatives of a normal and an extremely high respiratory loads with and without generated breathing noise of unit gain using a ventilator pump.

Using the prototype device on test loads with no breathing, the measurement error was less than 1% with SNR of 39.9dB for the 5 $\mathrm{cmH2O/L/s}$ test load and error less than 5% with SNR of 30.1 dB for the 15 $\mathrm{cmH2O/L/s}$ test load (Figure 3.9). Adding the simulated breathing of unit gain through a ventilation pump had an apparent influence on the measurement error where it went up to 5% with deteriorated SNR of 29 dB for the 5 $\mathrm{cmH2O/L/s}$ test load while the measurement error on 15 $\mathrm{cmH2O/L/s}$ test load went up to 10% and its SNR dropped to 19.9 dB (Figure 3.9).

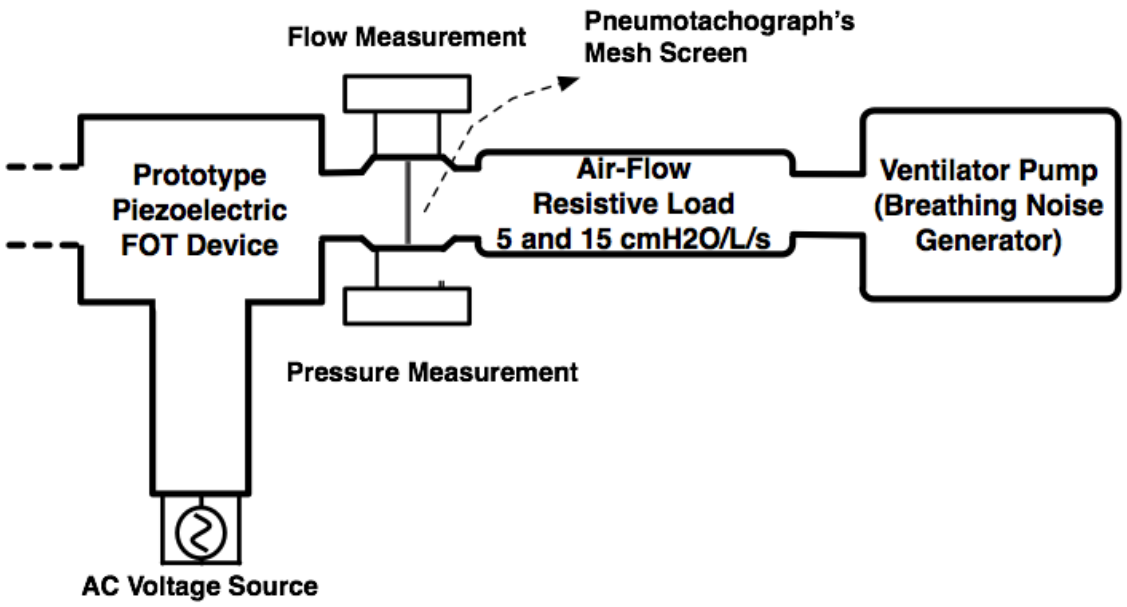
Flow Measurement
Pneumotachograph's
Mesh Screen
Prototype
Piezoelectric
FOT Device
Air-Flow
Resistive Load
5 and 15 cmH2O/L/s
Ventilator Pump
(Breathing Noise
Generator)
Pressure Measurement
AC Voltage Source

(a)

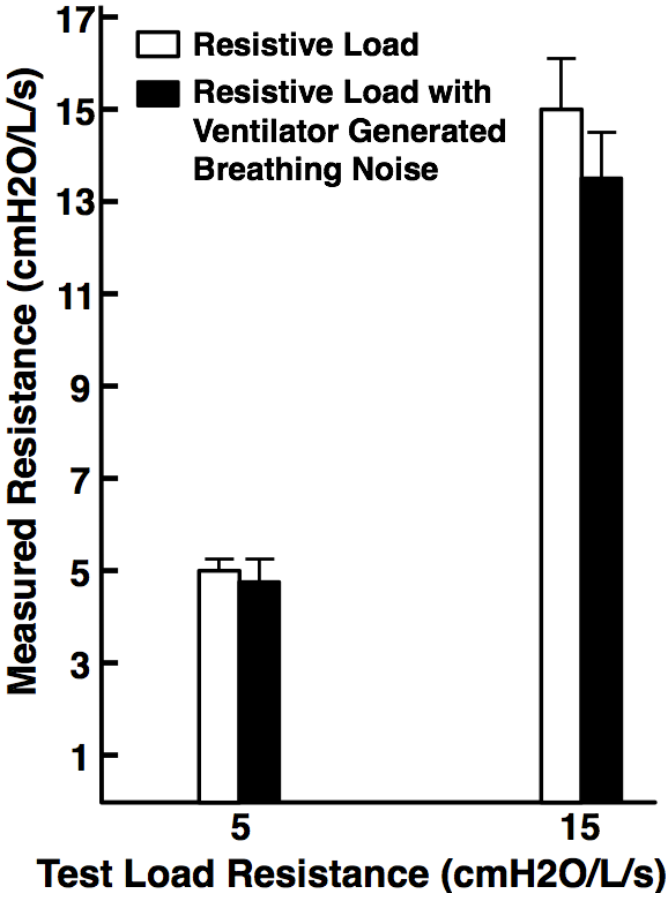
Resistive Load
Resistive Load with
Ventilator Generated
Breathing Noise
Measured Resistance (cmH2O/L/s)
17
15
13
11
9
7
5
3
1
5
15
Test Load Resistance (cmH2O/L/s)

(b)

Figure 3.9 (a) Schematic representation of the experimental test set up on the prototype device. The tests on the air-flow resistive test loads were performed with and without ventilator generated breathing noise of unit gain. (b) Experimentally determined test load measurements. The generated breathing noise increased the estimation error.

3.5 DISCUSSION AND CONCLUSION

3.5.1 Simulations

The aim of this paper was to design an efficient low power forced oscillation device that can meet the standards proposed by Oostveen et al [2] where they recommend a maximum error of 10%. Simulation results presented in the previous section showed that this criterion can be met even with higher noise levels. The healthy male subject and the asthmatic child were influenced similarly by the increasing noise both in SNR drop and the increase in the impedance estimation error. The impedance estimation error in the simulated COPD and child (with high tidal volume) subjects was higher than the healthy male subject (Figure 3.6). The same trend can be seen in Figure 3.5 where the SNR drop in simulated COPD and child impedance was higher than the healthy male subject. To verify the mechanism for this, we calculated the transfer function of the noise on the respiratory system of different subjects (Appendix), taking into account the affect of the breathing noise feedback on the oscillation dynamics of the piezoelectric actuator.

Equation (3.7) presents the total noise transfer function (TF_{NT}):

$$TF_{NT} = \frac{(R_{Rs}+\frac{E_{Rs}}{s}+I_{RS}.s).R_{leak}.(1+\frac{\beta.C_d.s}{m.s^2+C_d.s+K})}{R_{leak}+(R_{Rs}+\frac{E_{Rs}}{s}+I_{Rs}.s)} \quad (3.7)$$

Figure 3.10 shows the magnitude of bode plot of Equation (3.7) around the frequency of oscillation for different subjects. It can be noticed that the noise magnitude in simulated COPD was the highest; the simulated child has a lower peak while the average male impedance has the lowest noise peak at 6 Hz. This is in agreement with the

results in Figure 3.5 and Figure 3.6. It should be noted that the peaks of the bode plot (Figure 3.9b) would shift in magnitude in reality depending on the tidal breathing gain of the specific subject. For example, as shown in Figure 3.5, the simulated child subject with adult tidal breathing exhibits a severe drop in SNR that resembles the COPD simulation. This is because the mechanical impedance of the child and COPD respiratory systems are both high in value (Table 3.2). However when the realistic amounts of tidal volume is applied to the child's respiratory system, the noise decreases, and the SNR is maintained even higher than that of the healthy male simulation.

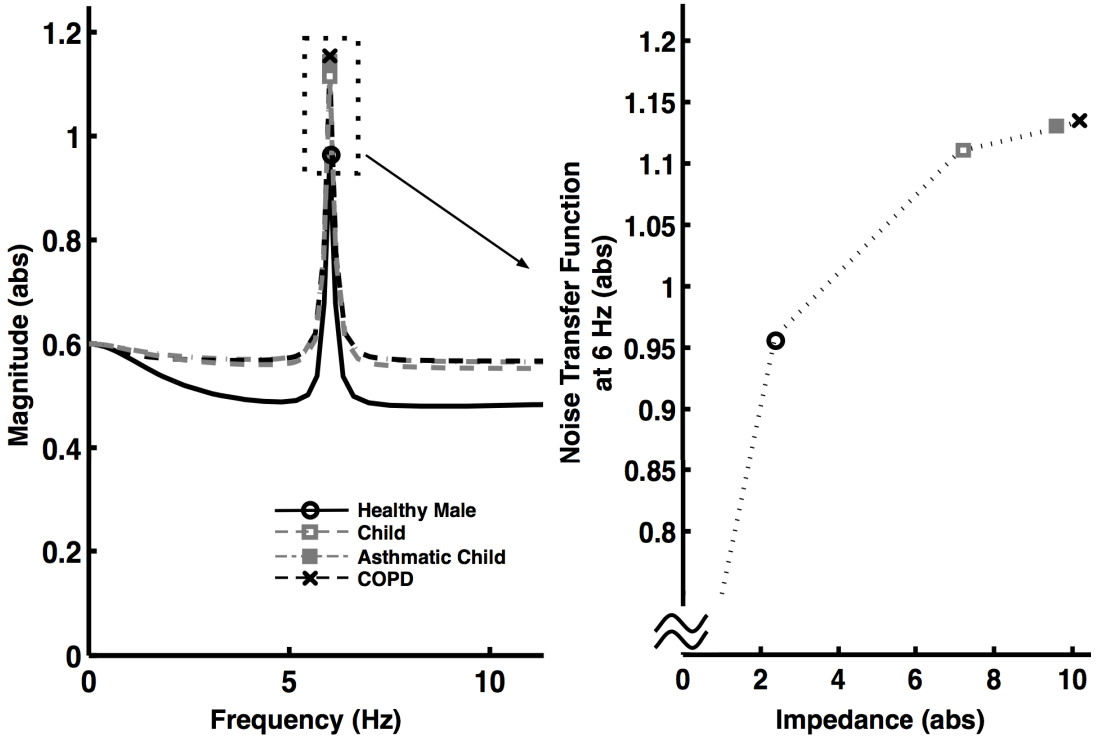

Figure 3.10. Magnitude of the bode diagram of noise transfer function and the noise magnitude vs impedance at 6 Hz. Increasing the impedance increased the noise.

Producing oscillations of air through a moving mesh screen includes the intrinsic problem of some of the resistance originating from the mesh screen with the remainder arising from the gap between the mesh and the housing tube. Considering the impedance using an electrical analog model, the resistance of air-gap is in parallel with mesh resistance and thus the total equivalent resistance is smaller than the mesh resistance. In

this work the equivalent resistance of the mesh screen and air-gap was defined to be $0.6\ cmH2O/L/s$ (Figure 3.7). An interesting conclusion from Figure 3.7 is that if the resistance against the leak due to air-gaps in the device is maximum (open circuit), the mesh screen can be replaced with one with resistance as low as $0.38\ cmH2O/L/s$ while maintaining the impedance estimation error less than 10% and the SNR higher than 30 dB. It should be noted that guidelines recommend the total resistance that subjects breath through including an anti-viral/antibacterial filter in series with the mesh resistance should be smaller than $1\ cmH2O/L/s$. This is small such that subjects can easily breath on devices that meet this criterion.

Simulating the effects of nonlinearity on different simulated subjects had the most substantial effect on the impedance estimation error of the child with adult V_T. The effects on the male, the child with realistic V_T and the asthmatic child subject were also substantial while the effect on the COPD was the smallest (Figure 3.8). The small effects of the nonlinearity in the COPD subject were because the nonlinear term was small relative to the linear resistance, while in the healthy male the linear resistance is small relative to the nonlinear term. However, while nonlinearity led to increases in errors, the errors were only unacceptable for the healthy male, the realistic child and the asthmatic child subjects at larger flows than normal. At normal flow levels and at the normal tidal volume for the child subject, the error was acceptable in all subjects.

3.5.2 Experiments

The tests on the prototype device without breathing noise resulted in very low errors and high SNRs. As expected, after adding the breathing noise the SNR dropped and errors increased. However in the case of the 15 $\mathrm{cmH2O/L/s}$ test load which is higher than would be anticipated for adult subjects, but possible for children with airway obstruction [12] the error reached the maximum recommended value (Figure 3.9b). Children fortunately have lower breathing noise, and thus this design is likely suitable for a large range of subjects. These are for normal or nearly normal tidal volumes. However if measurements are to be made under larger ventilation conditions such as with exercise, the reduction in SNR would begin to cause larger errors in estimating impedance. If this

is unacceptable then larger oscillatory flows would be recommended using one or a combination of following techniques:

- Movement amplification techniques including mechanical lever and/or using longer customized piezoelectric multimorphs and/or using multiple actuators at the same time for increasing the applicable force.
- Using an actuator with higher surface area to generate higher pressure oscillations.
- Reducing the amount of leak due to air-gaps.

3.5.3 Conclusions

In this paper, for the first time, an oscillometry device was designed based on optimization in a simulation that included the device characteristics together with changes in subject impedance and including perturbations from breathing. Although breathing noise reduced the SNR, the performance remained acceptable and demonstrates a useful design approach that led to the development of a feasible accurate lightweight portable single frequency FOT device. Reducing the leak and improving the measurement accuracy of the transducers as well as modifications in the oscillating mesh and the actuator can improve the results from the prototype device.

3.6 APPENDIX

The aim of this appendix is to calculate the total noise transfer function that appears in output pressure including the effect of breathing noise on the screen mesh.

From Figure 3.4c we can write:

$$[V_{in}.\alpha - (K.x_P + (\dot{x}_P - \dot{x}_b).C_d)].\frac{1}{m.s^2} = x_P \qquad \text{(A 3.1)}$$

If we assume $V_{in} = 0$ and knowing that $\dot{x}_b = \frac{\dot{V}_b}{Ar}$ and $V_P = \beta.x_P.Ar$, with rearrangement we have:

$$TF_{NO} = \frac{\dot{V}_P}{\dot{V}_b} = \frac{\beta.C_d.s}{m.s^2+C_d.s+K} \quad \text{(A 3.2)}$$

Where TF_{NO} is the transfer function of feedback noise influence on oscillations of piezo actuator. Transforming Equation (3.4) into s-domain we have the transfer function of the respiratory system as below:

$$TF_{Rs} = R_{Rs} + \frac{E_{Rs}}{s} + I_{RS}.s \quad \text{(A 3.3)}$$

Therefore we can write (Figure 3.3c):

$$(\dot{V}_b + \dot{V}_b.TF_{NO} - \frac{P_{awo}}{R_a}).TF_{Rs} = P_{awo} \quad \text{(A 3.4)}$$

Rearranging and using Equations (A 3.2) and (A 3.3), gives the total noise transfer function (TF_{NT}) of:

$$TF_{NT} = \frac{P_{awo}}{\dot{V}_b} = \frac{TF_{Rs}.R_{leak}.(1+TF_{NO})}{R_{leak}+TF_{Rs}} \quad \text{(A 3.5)}$$

3.7 ACKNOWLEDGEMENTS

Hamed Hanafi and Lucas Posada were supported by the NSERC CREATE program at Dalhousie University, S.A.Bhatawadekar was supported by the NSERC.

The authors thank Guy Drapeau at Thorasys Medical Systems for his great feedback especially for experiments. They also thank Andre Bezanson for his help with piezoelectric actuators.

Chapter 4: Analysis Of The Error In Tracking Linear Time-Varying Respiratory Mechanics

Authors

Hamed Hanafi

Kamal El-Sankary

Ubong Peters

Marwa Al Amer

Andrew Milne

Dietrich Henzler

Geoffrey N. Maksym

To be submitted to IEEE transactions on biomedical engineering

4.1 Abstract

Within-breath analysis of respiratory mechanics is recently being developed to provide new insights on the health of the respiratory system. Estimating of time-varying mechanics of the respiratory system can be done either by time-domain approaches or by methods based on the short time Fourier transform (STFT), but little work has been done estimating their accuracy. In this study we analytically and computationally assess the accuracy of the time-frequency transfer function to evaluate the accuracy in determining the time-varying parameters of respiratory impedance. To reduce the computational cost of FFT/DFT, the Goertzel algorithm was used to perform STFT. We introduce and evaluate the ability of an analytical method to estimate the error arising from time variation, termed the time varying error (TVE). This could reasonably estimate error without noise in the model, and demonstrated how TVE increased with increasing breathing rate independent of breathing noise amplitude. The TVE did not account for additional error caused by the addition of real recorded breathing noise from seven children with asthma, but we also computed the true error, which similarly increased with breathing rate, to as much as 25% for shorter window sizes (0.2s and 0.4s) at breathing rates of 0.4 Hz. For breathing rates less than 0.4 Hz, we found that current common analysis methods could be moderately accurate with less than 5% error, and recommend that subjects with higher breathing rates should be trained to breathe with lower rates.

4.2 INTRODUCTION

Oscillometry, also known as the forced oscillation technique, superimposes fluctuations of airway pressure on normal breathing while measuring pressure and flow to determine the mechanical properties of the respiratory system. The mechanical impedance is the ratio of the oscillatory pressure to the flow in the frequency domain, which is expressed as a complex quantity versus frequency, real part being the respiratory system resistance and the imaginary part being the respiratory system reactance. The fundamental assumption behind nearly all current computational methods implemented to evaluate the impedance is that the underlying impedance is a linear time invariant system,

at least for short durations. That is for short periods, the respiratory system behaves as a linear time invariant system (LTI), and the varying mechanics are tracked as successive piecewise solutions of a time-varying (TV) system.

Linear time invariant (LTI) systems are widespread for modeling many physiological and nonphysiological systems and their analysis has been generalized in the literature [106]. The respiratory system is inherently time-varying as dilation with inspiration and renarrowing with exhalation impose temporal physical variations in the diameters of the airways and stretch of the tissues, and hence lead to temporal changes in the respiratory parameters that can be altered in disease [54, 58, 109]. To track temporal changes in respiratory impedance a common approach has been to use windowing in time or frequency domain techniques and to assume stationarity within the boundaries of the window, assuming errors due to underlying time variation within the window are small. For example, the time-domain recursive least-square (RLS) method tracks the impedance over time and is explained in detail in [37, 58-60, 108, 110]. The parameters are identified including matrix inversion fitting a linear input-output model, and each inversion uses a block of time that assumes the system is stationary, and this window is shifted in time to allow estimates of the parameters identifying the parameters of the model in a piecewise temporally varying manner. Included in the fit, is a single time constant filtering function, also known as the forgetting factor, which smooths the parameter variation, and dictates how the temporal responsiveness of the estimator changes in the underlying system [37]. However, given the time-varying aspect of respiratory mechanics, we felt it may be useful to explore utilizing time-frequency methods that take into account the underlying time varying behavior of the respiratory system, and to evaluate the error incurred by assuming piecewise time invariance.

Perhaps more common is to employ Fourier transform methods computing the respiratory impedance, also within short duration windows, within which the system parameters are assumed to be stationary as noted above. This essentially uses the time-frequency analysis method of the short-time Fourier transform (STFT) to compute impedance over short windows and thus tracks Zrs over time [61-64]. Like RLS, this method also uses windows in the time-domain with the assumption of stationarity within the boundaries of window, then transforms pressure and flow to the frequency domain

and calculates the impedance for that specific block. Making the window shorter improves the ability to track temporal changes, but makes the estimates more susceptible to noise. To our knowledge no detailed analysis of the effects of this approach on time variation of respiratory parameters has been carried out.

Another approach would be to generalize the analysis of LTV systems to account for non-stationarity of the underlying system parameters. Indeed, Zadeh developed a novel method for analysis of LTV systems [60], and introduced the first generalized frequency analysis method of variable systems.

In this work, we use Zadeh's technique to find the time-varying transfer function of a single compartment lung model. We also analyze the accuracy of the current commonly used STFT method [111, 112]. Since oscillometry is usually applied only at a few frequencies (typically 3 to 20 frequencies, and sometimes only 1 frequency), we also apply the Goertzel algorithm that reduces the computation of the frequency components to only the desired frequencies separately [107, 110].

The paper is organized as follows. Materials and methods used in simulations, measurements of subjects and data analysis are explained in section II. The TV transfer function of the single-compartment lung model is calculated, TV error (TVE) is introduced and a TVE prediction method is proposed in section 4.3. Section 4.4 explores the STFT using the Goertzel algorithm. Section 4.5 presents the results from simulations without noise and verifies the results by adding measured noise from children. Results are discussed in section 4.6 and conclusions are provided in section 4.7.

4.3 Materials and Methods

Oscillometry is performed by measuring pressure and flow during normal tidal breathing with superimposed small oscillations of airflow. Pressure and flow signals of subjects are often filtered to remove the predominantly low frequency breathing noise, then, the data is divided into blocks of equal length and windowed. The window function is normally chosen to be a duration that is an integer number of oscillatory cycles. Additionally errors caused by lack of periodicity (also known as errors due to edge

artifacts) can be reduced by using windowing functions such as Hanning or Hamming that progresses smoothly from zero on the edge to unity at its center and back to zero on the other edge. These windows will reduce errors even if the data is not periodic within the window. Respiratory parameters are then calculated by calculating the complex impedance and separating the real part which is the resistance from the imaginary part which is the reactance.

Where the average impedance is being calculated, in addition to or instead of temporally varying impedance, various studies have shown improvement in data analysis and mean impedance estimation using variety of filters such as high-pass, band-pass and resonance-filters [65, 66, 93], however, narrow-band filters that result in higher SNRs and better coherence need long acquisition times and as well as having the potential of removing some of the important modulated information around the oscillation frequency where the temporal variation in impedance is located [113].

The objective of our study was to assess the accuracy of computation of time-varying Z_{rs} using STFT, and to computationally investigate Z_{rs} analysis using Zadeh's approach, to develop an estimator of the error incurred when tracking temporally varying impedance.

4.3.1 Simulations

The respiratory system was modeled as a single-compartment lung model (Figure 4.1) in MATLAB/SIMULINK. The model consists of a resistance (R_{rs}) and an elastance (E_{rs}). R_{rs} represents a single Newtonian resistive tube while E_{Rs} represents the stored elastic energy largely from surface tension, but also from tissue stretching and some gas compression. Since single sinusoids of low frequency are most common for tracking respiratory impedance the oscillometry was assumed to be an ideal sinusoidal signal at 5 Hz. Later, measured breathing noise was added to flow signal to achieve pseudo-realistic conditions.

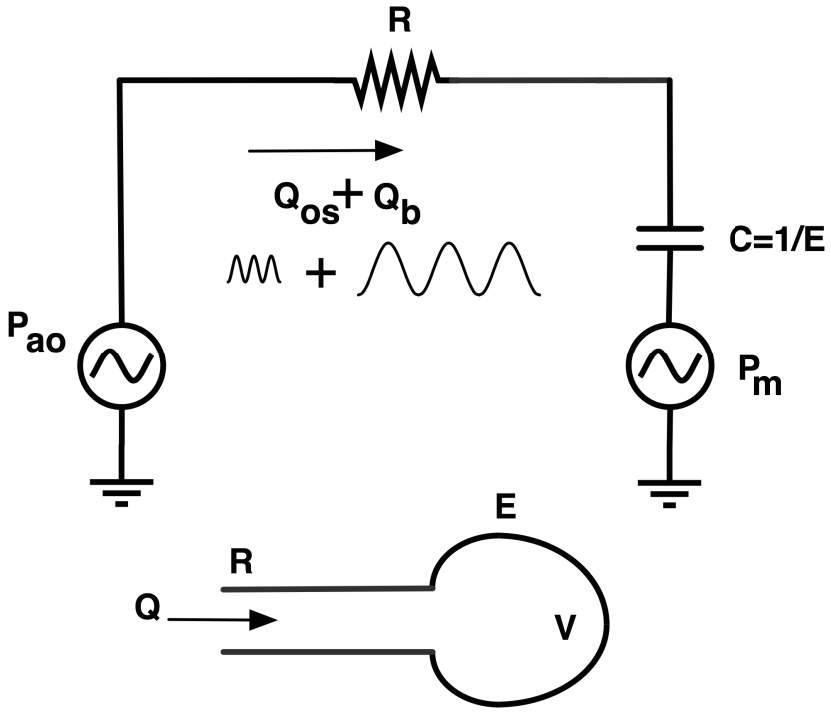

Figure 4.1. Single compartment model of the respiratory system based on linear RC circuit analogy: R is the resistance of the tubing and E is the elastance of the tissue. P_{ao} is the pressure of airway opening and P_m is the pressure created by muscle effort. Q_b is the breathing flow/noise and Q_{os} is the oscillation flow generated by the airwave oscillometry device.

4.3.2 Subjects

To obtain measurements of breathing noise seven children with asthma (4 males and 3 females) were enrolled following obtaining informed consent. The study was approved by the Capital Health Research Ethics Board (REB) (Table 4.1).

Table 4.1: Subject characteristics

Male/Female	4/3
Age (years)	9.9 (2.8)
Height (cm)	137.4 (16.2)
Weight (kg)	36.6 (13)
FEV1 (%)	96.3 (12.8)
FVC (%)	111.3 (11.9)

Table 4.2: Fundamental breathing noise Frequency of subjects

BrN #	Frequency (Hz)
1	0.25
2	0.31
3	0.31
4	0.37
5	0.37
6	0.43
7	0.50

4.3.3 Measurements

To obtain realistic samples of breathing noise for use in the simulations, pressure and flow data were measured with sampling rate of 256 Hz using an airwave oscillometry device (tremoFlo™ Airwave Oscillometry System, THORASYS Thoracic Medical Systems Inc., Montreal, Canada) (Figure 3.2). The duration of measurements were 16 seconds, and measurements were repeated 3 times for each subject based on recommendations and common practice [114].

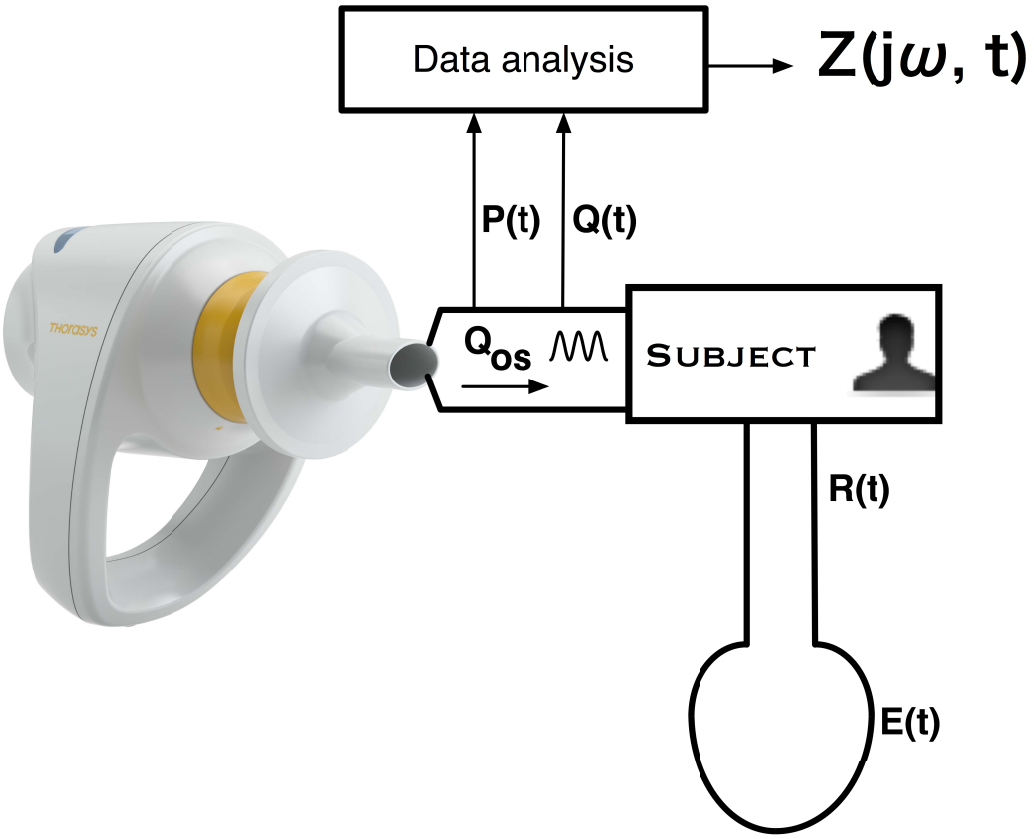

Figure 4.2. Schematic representation of the test set up using tremoFlo™ Airwave Oscillometry System, THORASYS Thoracic Medical Systems Inc., Montreal, Canada.

4.3.4 Data Analysis

Breathing noise data was analyzed using MATLAB. We Fourier transformed the pressure and flow data to the frequency domain and removed the input signal at the 5 Hz oscillation frequency and then applied the inverse Fourier transform and removed the imaginary component to produce the three breathing noise signals from each subject. We then computationally produced a pure sinusoidal oscillatory probe signal of 0.2 L/s peak-to-peak at 5 Hz. We then added the breathing noise to the flow signals to use the subject data as realistic noise, and to be able to arbitrarily vary the signal to noise ratio. We added noise of different amplitudes ranging from 0.45 to 0.75 L/s at the main breathing frequency thus achieving SNRs between 30-40 dB at the oscillation frequency.

For noise-free simulations, we modeled the impedance for two different cases as follows. For both cases, we assumed as is commonly done, the respiratory system to be a Single-Input Single-Output (SISO) linear system, but with periodically varying respiratory impedance at the breathing frequency. The first case represented a child subject with typical mean resistance of $R_{m_{Ch}} = 7\ cmH2O/\ L/s$ and mean elastance of $E_{m_{Ch}} = 80\ cmH2O/L$ with respective sinusoidal variations of $R_{v_{Ch}} = 2\ cmH2O/\ L/s$ and $E_{v_{Ch}} = 10\ cmH2O/L$ [116]. For the second case, we simulated a typical COPD adult subject with mean resistance of $R_{m_{COPD}} = 7\ cmH2O/\ L/s$ and mean elastance of 100 $E_{m_{COPD}} = 100\ cmH2O/L$ with respective sinusoidal variations of $R_{v_{Ch}} = 3\ cmH2O/\ L/s$ and $E_{v_{COPD}} = 50\ cmH2O/L$ [112]. The variations were set to be at the fundamental breathing frequency of the subject for simplicity [65]. Also, resistance and reactance were both varied in phase with flow (peak Rrs and Xrs occurred with peak expiratory flow) to mimic the observation from the few studies that show the time-course of both parameters versus time in a specific oscillation frequency in COPD [111] and even healthy subjects [109].

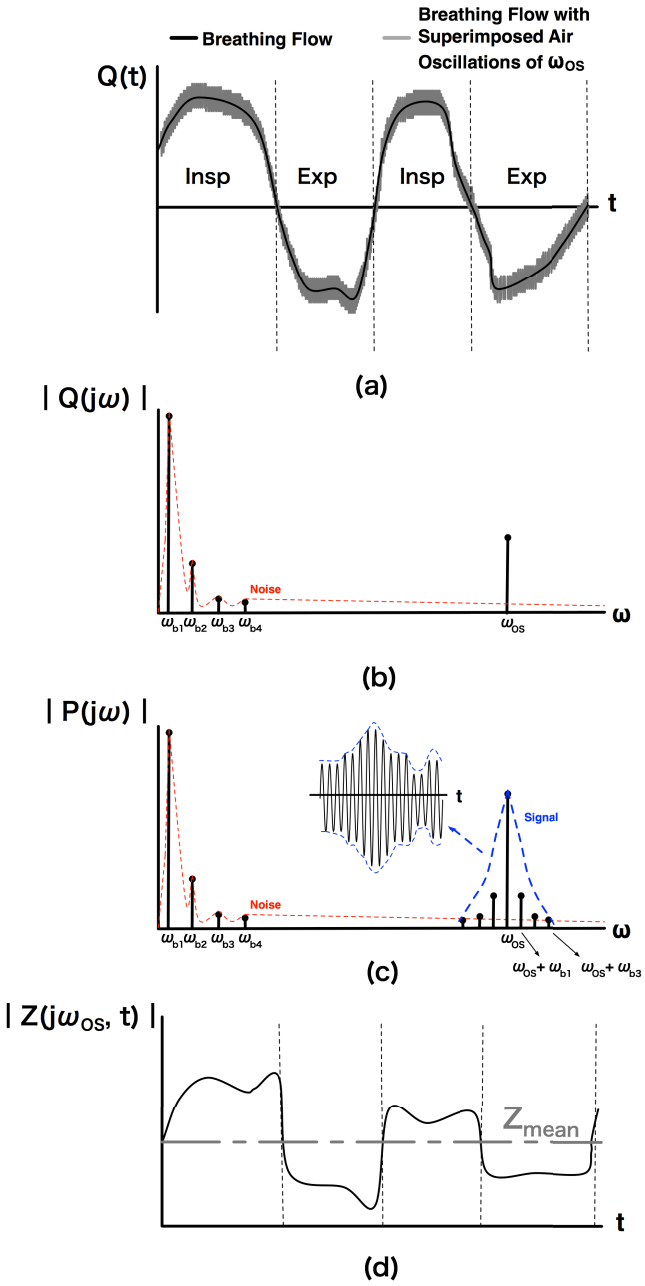

Figure 4.3. Schematic illustration of (a) Breathing flow with superimposed oscillations (b) Breathing flow in frequency-domain (c) pressure in frequency-domain (d) Time-frequency impedance at oscillation frequency and mean impedance. Q and P represent flow and pressure signals while ω, ω_{OS} and ω_b represent the angular frequency, angular frequency of oscillation and angular frequency of breathing respectively. Breathing noise is simplified to the main breathing frequency and its harmonics.

4.3.5 Time-Frequency Analysis Of Pressure And Flow

The time–frequency content of the FOT signals were analyzed using STFT, which is the repeated application of the Fourier transform in sequential time windows, which were 50% overlapping. We used the Goertzel DFT to reduce the computational cost of the algorithm (described further in section 4.3).

The time-frequency resolution of the STFT is limited by the uncertainty principle, and there is a trade-off between high frequency resolution obtained with long windows, and time resolution obtained with short windows.

We used windows of .2s, .4s, .8s and 1s with 50% overlap and each segment was multiplied by a Hanning window function as is commonly employed [92].

We performed the tests with a high-pass filter (3rd order Butterworth) at 1 Hz on pressure and flow signals to remove much of the breathing noise. Moreover, because high frequency variations in the estimate influenced accuracy when short window sizes were used, we tested the performance of adding a low-pass filter (LP) with cut-off frequency of 10 Hz to the estimated impedance.

4.4 Time-Varying Error (TVE)

In this section we first illustrate the effect of time-varying parameters on FOT, then after developing the method proposed by Zadeh applied to the respiratory system, we analytically derive the time-frequency transfer function of the respiratory system.

The simulated flow signal, $Q(t)$, composed of breathing noise (ω_{b1} as the fundamental breathing frequency and ω_{b2-bn} as its harmonics) with superimposed oscillations at ω_{OS} is shown in Figure 3.3a. Fourier trasformation of $Q(t)$ to the frequency-domain $Q(j\omega)$ (Figure 4.3b) shows schematically the influence of breathing noise on the signal which reduces the signal-to-noise ratio (SNR) and eventually the accuracy of the measurements especially in lower oscillation frequencies (e.g. 5 Hz). The output is the pressure signal showing the oscillatory signal at the oscillation frequency as well as side lobes which are the result of the amplitude-modulation (AM) of the input

signal arising from the sinusoidal variation in impedance at the breathing signal frequency [64] (Figure 4.3c). Given that ω_{b1} is the fundamental breathing frequency with the largest amplitude, the largest side lobe amplitude is located at $(\omega_{OS} \pm \omega_{b1})$. It should be mentioned that in communication systems ω_{bn} is known as the spectral shift and $2\ \omega_{bn}$ is the spectral spread [118].

The side lobe carries the time dependent variation of the impedance of the respiratory system and therefore needs to be recovered for temporal tracking of the respiratory system, and estimation of $Z(j\omega_{OS}, t)$ as depicted in Figure 4.3d. One method to do this analytically is to define a time-frequency transfer function for impedance, which we develop below using Zadeh's approach.

4.4.1 Zadeh's Time-Frequency Transfer Function Estimation

Here we first elaborate Zadeh's transform [2] and then use the method to obtain the time-frequency transfer function of the single-compartment lung model (Figure 4.1).

First we illustrate his practical definition for the transfer function of a LTV system. The nonstationary process of H_{TV} is defined in (4.1) by taking the convolution of the impulse response of an LTV system, $h(t, \xi)$, to input $x(t)$:

$$H_{TV}\{x(t)\} = \int_{-\infty}^{\infty} h(t, \xi)\, x(\,\xi)\, d\xi \tag{4.1}$$

where $t = \xi$ is the time when the unit impulse occurs.

Applying an oscillatory signal as an input $x(t) = e^{j\omega t}$ to equation (4.1) repeatedly over a range of frequencies can be used to provide a transfer function of the LTV system:

$$H_{TV}\left\{e^{j\omega t}\right\} = \int_{-\infty}^{t} h(t, \xi)\, e^{j\omega \xi}\, d\xi \tag{4.2}$$

$$H_{TV}\left\{e^{j\omega t}\right\} = e^{j\omega t} \int_{-\infty}^{t} h(t, \xi)\, e^{-j\omega (t-\xi)}\, d\xi = e^{j\omega t} H_{TV}(t, j\omega) \tag{4.3}$$

Therefore if input oscillatory signals are applied individually, the time varying transfer function can be defined as,

$H_{TV}(t, j\omega) = {response\ of\ the\ LTV\ system\ to\ e^{j\omega t}}\Big/_{e^{j\omega t}}$ which is the same as the input-output relationship of a stationary system.

On the other hand, in the time-domain, assuming that signal-to-noise ratio of the system is high enough to be able to ignore the influence of noise on the transfer function, modeling the system without noise and using ordinary differential equation (ODE) and assuming a_n and b_n as continuous functions of time we have:

$$a_n(t)\frac{d^n y(t)}{dt^n} + \cdots + a_1(t)\frac{dy(t)}{dt} + a_0(t)y(t) = b_m(t)\frac{d^m x(t)}{dt^m} + \cdots + b_1(t)\frac{dx(t)}{dt} + b_0(t)x(t) \tag{4.4}$$

If equation (4.4) is presented instead in its compact form, $D\left(\frac{d}{dt}, t\right)y(t) = N\left(\frac{d}{dt}, t\right)x(t)$, the time-varying impulse response using equation (4.3) with $x(t)$ replaced with an impulse at time $t = \xi$ can be presented and calculated as:

$$D\left(\frac{d}{dt}, t\right)h(t, \xi) = N\left(\frac{d}{dt}, t\right)\delta(t - \xi) \tag{4.5}$$

where D and N are polynomial operators.

Transforming equation (4.5) with respect to ξ using (3) yields Zadeh's transform [17] of $H(j\omega, t)$:

$$D\left(\frac{d}{dt}, t\right)H(j\omega, t)e^{j\omega t} = N\left(\frac{d}{dt}, t\right)e^{j\omega t} \tag{4.6}$$

that is the response of $H(j\omega, t)e^{j\omega t}$ to $e^{j\omega t}$. Expanding the left hand side of equation (4.6) yields:

$$D\left(\frac{d}{dt},t\right)H(j\omega,t)e^{j\omega t} = H(j\omega,t)D\left(\frac{d}{dt},t\right)e^{j\omega t} + \frac{dH(j\omega,t)}{dt}\frac{\partial D\left(\frac{d}{dt},t\right)}{\partial\frac{d}{dt}}e^{j\omega t} + \cdots +$$

$$\frac{1}{n!}\frac{d^nH(j\omega,t)}{dt^n}\frac{\partial^nD\left(\frac{d}{dt},t\right)}{\partial(\frac{d}{dt})^n}e^{j\omega t} \quad (4.7)$$

Knowing that the operator $\frac{d}{dt}$ is equivalent to multiplication by $j\omega$ in frequency-domain gives:

$$\left[\frac{1}{n!D(j\omega,t)}\frac{\partial^nD(j\omega,t)}{\partial(j\omega)^n}\right]\frac{d^nH(j\omega,t)}{dt^n} + \cdots + \left[\frac{1}{D(j\omega,t)}\frac{\partial D(j\omega,t)}{\partial(j\omega)}\right]\frac{dH(j\omega,t)}{dt} + H(j\omega,t) = \frac{N(j\omega,t)}{D(j\omega,t)} \quad (4.8)$$

To solve equation (4.8) a differential equation approximation solution is used that starts by splitting the transfer function into series of blocks:

$$H(j\omega,t) = H_1(j\omega,t) + H_2(j\omega,t) + \cdots \quad (4.9)$$

$H_1, H_2, \ldots$ expand H as a parallel-series group of stationary systems with varying gains. It can be seen from equation (4.8) that if coefficients vary close to their mean, less contribution of derivative terms would be involved and equation (4.9) would be rapidly convergent.

4.4.2 Respiratory System Model And Impedance

In this section, we introduce the equation of motion as the dominant equation explaining the mechanics of the respiratory system, then we modify the common stationary equation to a time-varying version and apply Zadeh's method to achieve the new time-varying transfer function

The equation of motion for the LTI model of the respiratory system [37] is presented as

$$P(t) = R_{rs}.Q(t) + E_{rs}.V(t) \tag{4.10}$$

where $P(t)$ is the airway pressure, $Q(t)$ is flow and $V = \int_{-\infty}^{\infty} Q(t)\,dt$ is volume.

Here R_{rs} and E_{rs} are static and thus the system is stationary. Transforming equation (4.10) into the frequency domain and dividing both sides by $Q(t)$ yields the LTI respiratory system impedance, $Z_{rs}(j\omega)$:

$$Z_{rs}(j\omega) = R_{rs} + \frac{E_{rs}}{j\omega} \tag{4.11}$$

This is a well-established model that is particularly well suited for the healthy lung. However, since the resistance and elastance of lung are not constants and vary with breathing, for within-breath analysis, a time-varying single compartment model could be better suited. Hence, rewriting the equation of motion in frequency-domain with TV resistance and elastance gives:

$$j\omega.P(j\omega) = [R(t).j\omega + E(t)]\,.Q(j\omega) \tag{4.12}$$

To calculate the time-varying Zadeh's transfer function of the respiratory system we write equation (4.12) in the same format as equation (4.8) knowing that $\frac{\partial D(j\omega,t)}{\partial(j\omega)} = \frac{\partial(j\omega)}{\partial(j\omega)} = 1$:

$$\frac{dZ}{dt} + (j\omega).Z = R(t).j\omega + E(t) \tag{4.13}$$

4.4.3 Applying Zadeh's Time-Frequency Transform To Respiratory Impedance

To solve the differential equation (4.13) we use an approximation technique shown in [60] under conditions when the rate of change in time-varying parameters are

lower than frequency of oscillation (slowly time-varying systems). Rearrangement of equation (4.13) in the format of equation (4.9) yields:

$$Z = \frac{R(t).j\omega + E(t)}{j\omega} - \frac{1}{j\omega}\frac{dZ}{dt} \tag{4.14}$$

Therefore defining the 1st and 2nd terms as Z_1 and Z_2 we have,

$$Z_1 = \frac{R(t).j\omega + E(t)}{j\omega}$$

$$Z_2 = -\frac{1}{j\omega}\frac{dZ_1}{dt} \tag{4.15}$$

Substituting Z_1 in Z_2 gives:

$$Z_2 = -\frac{(j\omega).\frac{d(R(t))}{dt} + \frac{d(E(t))}{dt}}{(j\omega)^2} \tag{4.16}$$

Adding Z_1 and Z_2 provides the second order approximation to Z:

$$Z(j\omega, t) = R(t) + R_{tv}(t) + \frac{E(t) - E_{tv}(t)}{j\omega} \tag{4.17}$$

where $R_{tv}(t) = \frac{\frac{d(E(t))}{dt}}{(\omega)^2}$ and $E_{tv}(t) = \frac{d(R(t))}{dt}$.

Equation (4.17) reveals added terms $R_{tv}(t)$ and $E_{tv}(t)$ that depend on the rate of change of R and E. We refer to these as bias error terms since they indicate a frequency dependent bias error from the mean values of R(t) and E(t), since they appear in the transfer function and represent deviations in the estimated impedance form the transfer function from R(t) and E(t). Thus $R_{tv}(t)$ is the bias error for resistance and $E_{tv}(t)$ is the bias error for elastance and together these two terms indicate a bias error

that will be observed from estimates of the impedance we term the time-varying error (TVE). Here we are limiting the scope of our analysis to examining if these predicted error terms are useful in predicting the magnitude of any error that occurs during standard FOT from time variation from simulated subjects with different breathing rates assuming simple time variation in R(t) and E(t) that may occur with breathing. We choose children as these subjects breathe more rapidly than adults to explore this effect.

The TVE can be computed analytically from computational modelling when R(t) and E(t) are known such as in simulation from Equation (4.17). But the TVE cannot be directly computed during measurement in practice, as it requires that R(t) and E(t) are known. Therefore, we propose a practical TVE prediction method based on calculating the rate of change from the estimated time-varying resistance and elastance ($\widehat{TVE}$). Here we use simulations to compare the actual TVE and estimated TVE with and without noise in section 4.5.

4.4.4 Time-Varying Resistance And Elastance

Time varying respiratory system parameters are shown to be correlated to the variation in lung volume and thus vary at the breathing frequency [65] of the specific subject. This variation is quasi-sinusoidal containing harmonics, but for simplicity, in this paper we restrict the variation in resistance and elastance to the fundamental and assume sinusoidally varying resistance and elastance as equation (4.18) and equation (4.19).

$$R(t) = [R_m + R_v.\cos(\omega_{b1}t)] \tag{4.18}$$

$$E(t) = [E_m + E_v.\cos(\omega_{b1}t)] \tag{4.19}$$

where $b1$ is the dominant or fundamental component in the breathing flow signal (Figure 4.3).

Using equation (4.17) and considering $\frac{d(R(t))}{dt} = -\omega_{bn}.R_v.\sin(\omega_{bn}t)$ and $\frac{d(E(t))}{dt} = -\omega_{b1}.E_v.\sin(\omega_{b1}t)$, the time-varying impedance function becomes:

$$Z(j\omega,t) = R_m + R_v.\cos(\omega_{b1}t) + \frac{E_m+(\sum_{n=1}^{nb} E_v.\cos(\omega_{b1}t))-(\sum_{n=1}^{nb} \omega_{b1}.R_v.\sin(\omega_{b1}t))}{j\omega} + \frac{-\sum_{n=1}^{nb} \omega_{b1}.E_v.\sin(\omega_{b1}t)}{(j\omega)^2} \quad (4.20)$$

A multifrequency sinusoidal FOT oscillation signal can be written as:

$$x(t) = \sum_{k=1}^{p} a_k.\cos(\omega_k t + \phi_k) \quad (4.21)$$

where a_k and ϕ_k are the magnitudes and phase angles of the components at frequencies ω_k $(k = 1 \dots p)$.

We continue the analysis here using a single frequency oscillation for simplicity, thus taking equation (4.21) into frequency-domain and with $k = 1$ gives:

$$X(j\omega) = A_1\{\delta(\omega - \omega_1) + \delta(\omega + \omega_1)\} \quad (4.22)$$

where, δ, is the Dirac Delta function.

Applying equation (4.22) in equation (4.20) as input yields:

$$Z(j\omega,t) = \left[R_m + R_v.\cos((\omega_1 - \omega_{b1})t) + \frac{E_m+E_v.\cos((\omega_1-\omega_{b1})t)-\omega_{bn}.R_v.\sin((\omega_1-\omega_{b1})t)}{j\omega} + \frac{-\omega_{b1}.E_v.\sin((\omega_1-\omega_{b1})t)}{(j\omega)^2}\right] \quad (4.23)$$

Equation (4.23) illustrates the terms in impedance due to breathing variations that cause amplitude modulation of flow which appears as side-lobes around the oscillation frequency on pressure signal.

4.5 STFT Using Goertzel Algorithm

4.5.1 Demodulation with short-time-Fourier transform (STFT)

In this section we explain how STFT is used to track time-varying signals versus time.

STFT is one of the simplest approaches for analysis of time-varying systems that are based on time localization of frequency components of the signal. This is done by windowing the measured signal into smaller segments and transforming each segment into frequency-domain. Using STFT, $Z(j\omega, t)$ can be considered as an LTI system during the period of the window.

The STFT of a signal, $x(t)$, is defined as equation (4.24) in continuous time [4]:

$$X_{STFT}(\omega, t) = \int_{-\infty}^{\infty} x(\tau) w(t-\tau) e^{-j\omega\tau}\, d\tau \tag{4.24}$$

where $w(t)$ is the window function which can be simplified to $FFT\{w_m[x(t)]\}$ and m represents the window index.

STFT can also be interpreted as series of modulations of the signal that are low-pass filtered by the window. This modulation brings the frequency components near ω_{OS} down to DC. Low-pass filtering act of the window maintains these frequency components in the output, and rejects the remaining components. The bandwidth of X_{STFT} is equal to the bandwidth of the window. Moreover, X_{STFT} contains the frequency components of the signal that are within $\pm nW$ of ω_{OS} where nW is the bandwidth of the window. Therefore, the impedance calculated using STFT can be shown as equation (4.25):

$$Z_{rs_{STFT}}(\omega_{OS}, t) = \frac{FFT\{w_m[P(t)]\}}{FFT\{w_m[Q(t)]\}} \tag{4.25}$$

4.5.2 Goertzel Algorithm

An N-point DFT can be used to obtain information from the frequency of interest, but calculates the results at frequencies that are not of interest, and thus wastes computational effort. However, as illustrated in Figure 4.4, the Goertzel algorithm directly computes a single DFT output, the amplitude and phase at the oscillation frequency with reduced calculations.

In this paper, the sampled pressure and flow signals were first Hanning windowed into smaller segments with 50% overlap, and the Goertzel filter was applied at the frequency of interest, ω_{OS}, to attain the pressure and flow signals of that frequency at each moment in time (depending on the window size). Then the pressure and flow were divided at the oscillation frequency to calculate impedance.

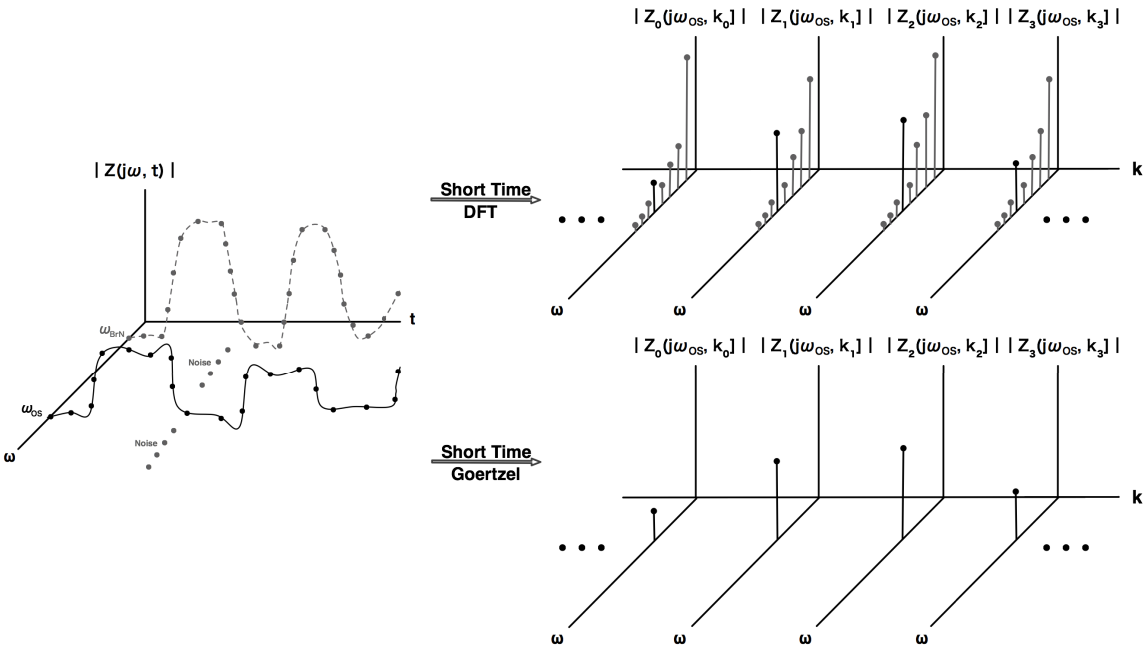

Figure 4.4. Comparison of Goertzel algorithm with DFT on a signal that varies in time and frequency. While DFT calculates the amplitude and phase of signal components at every frequency, the Goertzel approach only performs the DFT calculation at a specific frequency or at a few specific frequencies.

4.6 Results

4.6.1 Noise-Free Verification Of TV Error And Prediction Methods

To assess the analytically found time-varying error in (17), simulations were performed in MATLAB/SIMULINK followed by time-frequency analysis described in Methods. The percent normalized-sum-squared error ($pNSSE$) was calculated equation (4.26) to quantify the error.

$$pNSSE\% = 100\times\frac{\sum\left(\hat{Z}_{rS}(t)-Z_{rs}^{i}(t)\right)^{2}}{\sum\left(Z_{rs}^{i}(t)\right)^{2}} \tag{4.26}$$

where $\hat{Z}_{RS}(t)$ was the calculated impedance from equation (4.25) and $Z_{Rs}^{i}(t)$ is the ideal target impedance from the set model parameters. From equation (4.26) it can be seen that when the average squared error is equivalent to the variance of the measured data, the $pNSSE$ is 100% of the variance of the data.

Simulations were repeated with different window sizes, from 0.2 to 1 second, initially in the absence of noise. In the child example, errors increased with increasing breathing rate. Using the shortest window (0.2 s), errors remained lower than 1% even at 0.8 Hz breathing rate (Figure 4.5a). As the window length increased to 0.4s, the increase in TVE increased to about 4% at 0.8 Hz breathing rate and errors increased further with 0.8s and 1s window length up to 10% at 0.5 Hz breathing rate. In the COPD example, there was little difference in TVE for 0.2 and 0.4 sec windows ranging from 0.1% at breathing frequency of 0.1 Hz to about 5 % at 0.8 Hz (Figure 4.5b). However, when we used longer window sizes (0.8 s and 1 s), the error increased ranging from 0.05% at 0.1 Hz to about 10% at 0.5 Hz. To provide an example of the error relative to $pNSSE$, representative target and estimated impedances with 4% and 9% errors are illustrated in Figure 4.5c.

In both examples the TVE increased with increasing breathing frequency of the modeled subject. This was expected as the dependence on the rate of change of impedance was described by equation (4.17).

Moreover, we tested both proposed TVE predictors. It can be seen in Figure 4.5a that the practical prediction method was only able to predict the increase in error for window sizes of 0.2 s and 0.4 s with good precision for the COPD (bigger) load but not for the child. However, the predictions were not acceptable for long window sizes.

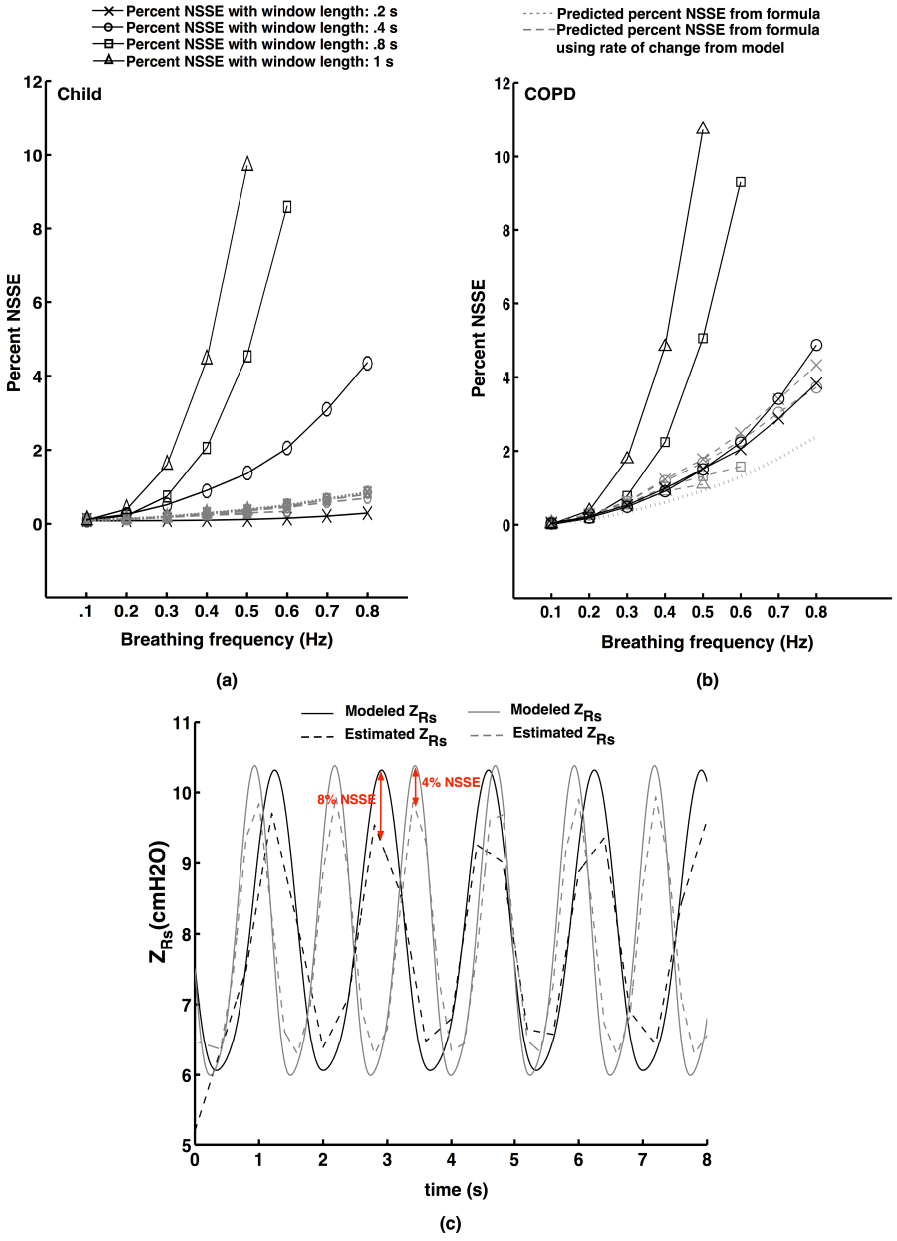

Figure 4.5. Percent normalized sum-squared error ($pNSSE$) without noise for (a) Child load where TVE increased with increasing breathing frequencies but predictions didn't precisely follow simulation results and (b) COPD load where TVE increased with increasing breathing frequency and predictions could follow simulation results using short window lengths (0.2 s and 0.4 s). This error is only plotted before reaching the Nyquist frequency of the window. (c) The estimated and target impedance versus time for a 4% and a 8% representative $pNSSE$ errors.

4.6.2 Adding Subject Noise To Simulations

To test the analytical model of TVE in the presence of realistic noise, the noise obtained from each of the 7 children was added back to the simulated flow signals again with impedance varying in time as in the noise free simulations (Table 4.2). A high-pass filter was applied to the pressure and flow data (1 Hz cut-off) as well as a low-pass filter (10 Hz cut-off) to the estimated impedance (Figure 4.6). Given that the prediction methods did not account for the STFT and that the results from noise-free simulations showed that the prediction methods were not able to precisely follow simulation results from all subjects, they were not applied to noisy simulations.

First, to compare the results with common practice, a time-invariant estimation was applied by calculating the mean of estimated impedance from all windows. Percent error from all window sizes remained lower than 2% and coherence remained higher than 0.9 (Figure 4.7).

Second, TVE was computed by plotting $pNSSE$ for each subject. For all window sizes, TVE similarly increased with increasing breathing rate. Compared to the short window sizes (0.2 s and 0.4 s), other window sizes had lower overall errors ranging from about 7% in the subject with the lowest breathing frequency (BrN#1) to about 20% in BrN#6 (Figure 4.8a). However, in the subject with the highest breathing frequency BrN#7, the window size of .8s had the lowest amount of error (7%).

Finally, we plotted $pNSSE$ for each subject with all window sizes which illustrated a decreasing trend in error to window sizes of 0.8 s, followed by an increase for windows of 1 second (Figure 4.8b).

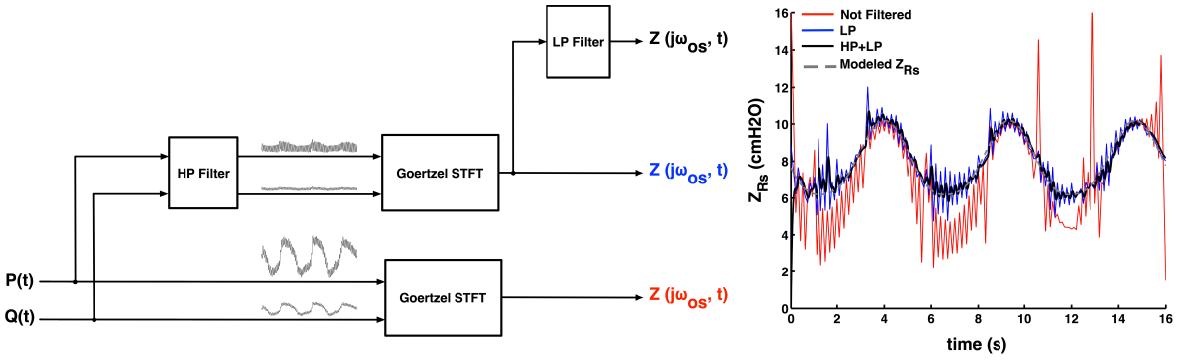

Figure 4.6. Influence of using a high-pass filter on pressure and flow and a low-pass filter on the estimated impedance

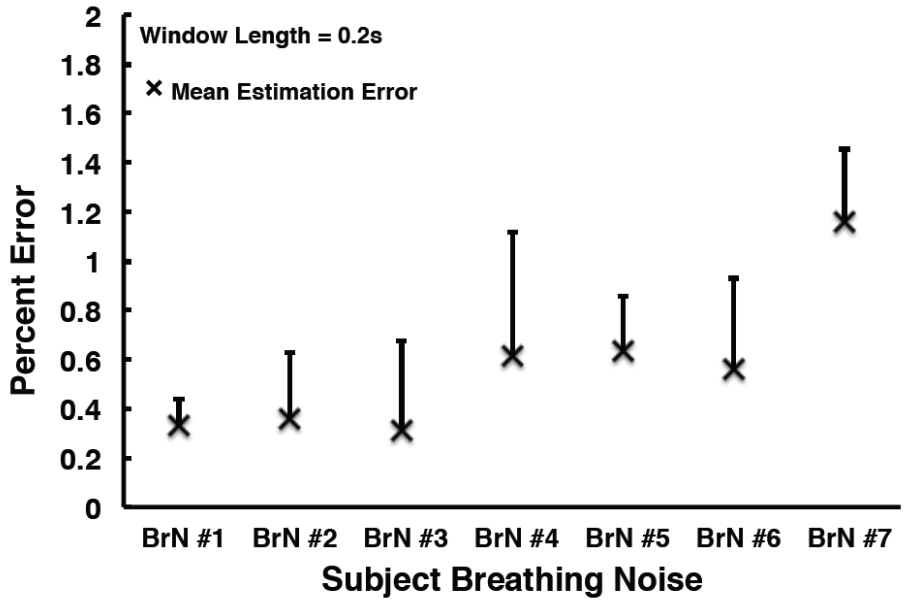

(a)

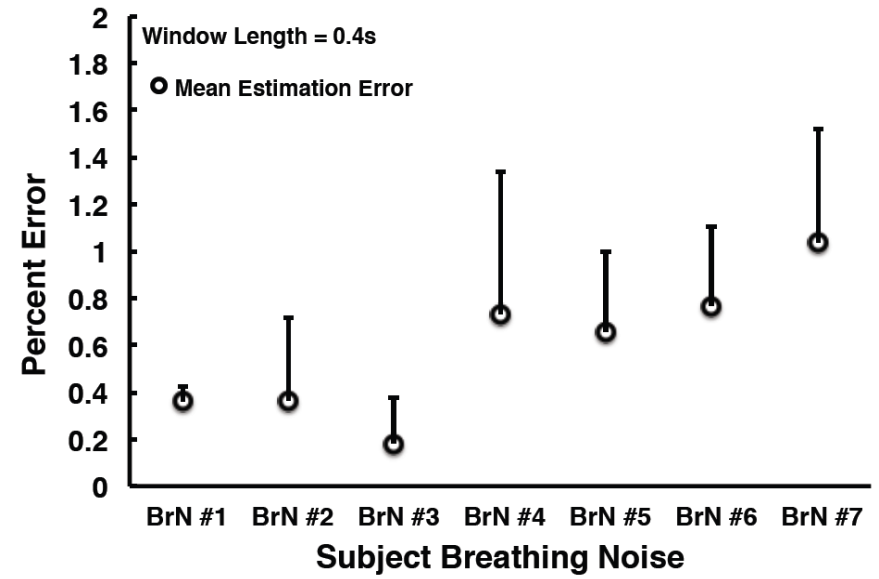
Window Length = 0.4s
Mean Estimation Error
Percent Error
2
1.8
1.6
1.4
1.2
1
0.8
0.6
0.4
0.2
0
BrN #1
BrN #2
BrN #3
BrN #4
BrN #5
BrN #6
BrN #7
Subject Breathing Noise

(b)

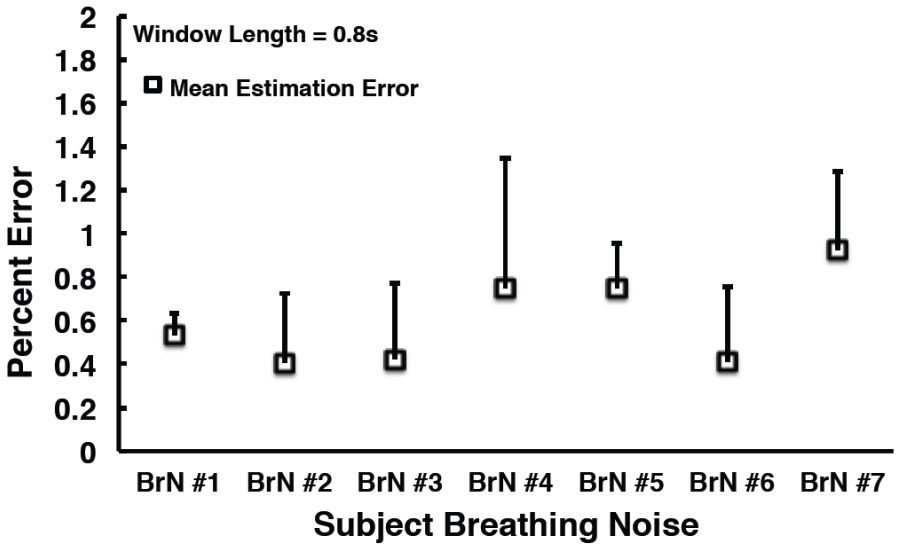
Window Length = 0.8s
Mean Estimation Error
Percent Error
2
1.8
1.6
1.4
1.2
1
0.8
0.6
0.4
0.2
0
BrN #1
BrN #2
BrN #3
BrN #4
BrN #5
BrN #6
BrN #7
Subject Breathing Noise

(c)

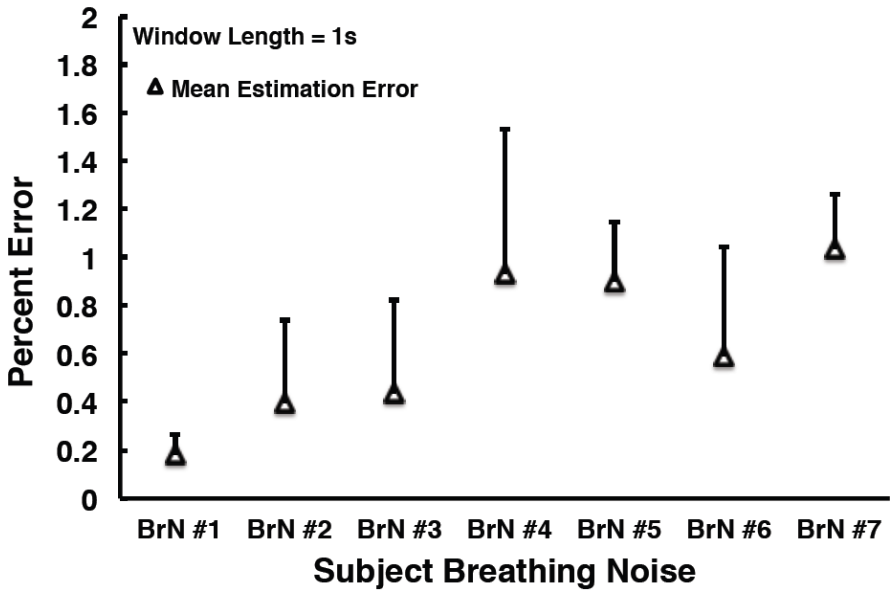

(d)

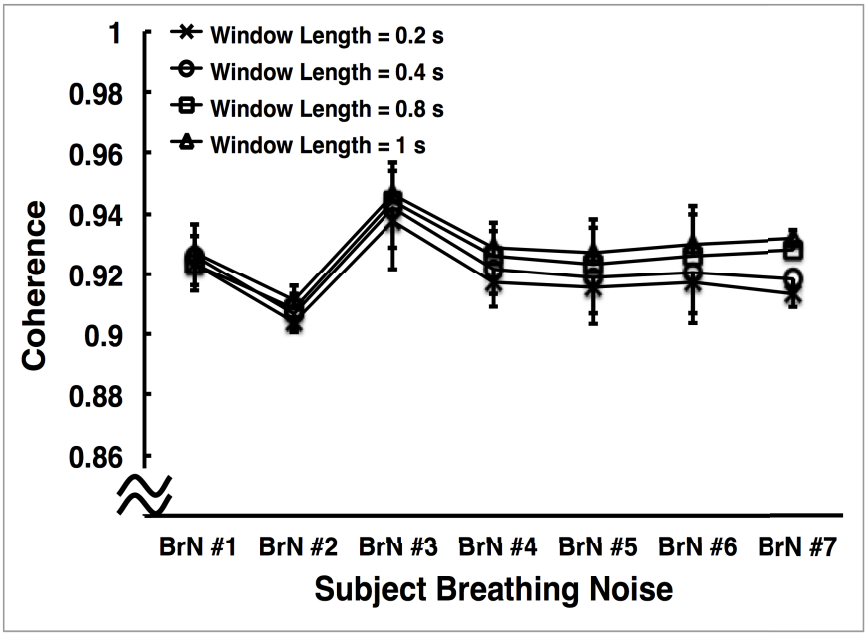

(e)

Figure 4. 7. Mean percent error using for different window sizes using subject noise with increasing breathing frequency and coherence (e) for different window sizes. Coherence improved with increasing window size.

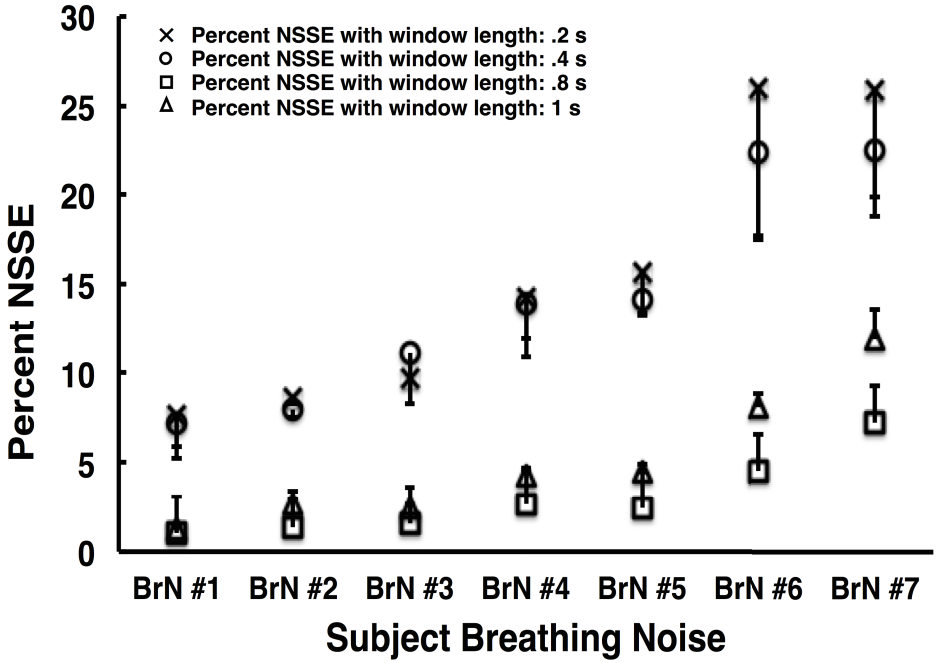

(a)

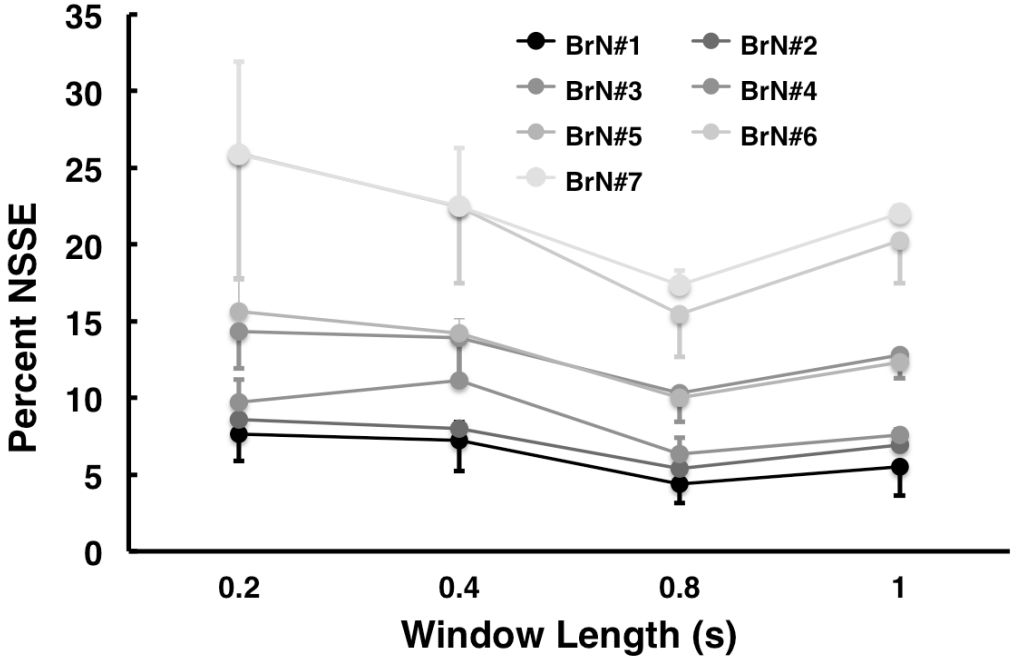

(b)

Figure 4.8. (a) Percent normalized sum-squared error for different window sizes using subject noise with increasing breathing frequency. (b) $pNSSE$ for different subject noises using different window sizes. 0.8s window had the lowest error for all subject noises.

4.7 Discussion

Oscillometry is a well-accepted method to measure average respiratory impedance over a range of frequencies, and is a highly accurate at reproducing known test loads of known fixed impedance [2]. All analysis methods for oscillometry assume that the system behaves linearly and is stationary, at least over short durations. Using small amplitude oscillations and avoiding high flow rates helps to reduce the effects of nonlinearities, but may not help reduce any errors associated with non-stationarity. Methods designed to track time variation in impedance recognize the limitations in using time invariant analysis methods, and utilize short windows over which they assess respiratory impedance, albeit at the expense of decreased signal to noise [110-114]. While it is assumed that the impedance estimates are reasonably accurate for physiological interpretation, the accuracy of the estimates of time-varying impedance has not been quantitatively assessed in detail to our knowledge.

Some researchers have successfully employed time-domain approaches to track the impedance [37, 54, 58, 104, 115, 116]. For example, Lauzon *et al* [58] developed an RLS algorithm and optimized the forgetting factor to track slowly changing single-compartment model impedance. They successfully tracked modeled varying impedance with a five fold change in resistance and two fold change in elastance that occurred over 10 seconds. However, these changes occurred slower than they would occur within a breath and are in excess of changes that occur with breathing. Kaczka *et al* [104] performed a study on both single-compartment and two-compartment models and found that the error for single-compartment tests were identical between the FFT approach and continuous-time time-domain approach with the least amount of error (<5%). Although their resistance and elastance were not time-varying in simulation studies (LTI system) they investigated the effect of noise by adding zero-mean, white Gaussian noise with different standard deviations of the peak-to-peak amplitude. Indeed, adding white noise is an effective method, but it does not quite represent the real breathing noise, which includes high amounts of noise in lower frequencies and reduces as the frequency increases (Figure 4.3).

We similarly used a single-compartment lung model and added noise to verify its effect on accuracy. However, we included time-varying impedance, which modeled the resistance and elastance varying with the breathing frequency of the subject. Moreover, we used actual recorded noise from subjects. This is important especially because real breathing noise does not over emphasize noise at higher frequencies.

Using multiple windows sliding in time as employed in the STFT but with overlapping windows, is the common method to estimate impedance as it is robust against noise and windows with artifacts such as coughs can be eliminated [59, 62, 108-110, 188]. To perform STFT, most researchers use FFT/DFT on windowed data. Studies that only report mean impedance use longer window sizes, for example, Farré *et al* [109] and Lorino *et al* [63] use a 4 s window. However, studies that report time-varying impedance use shorter window sizes, for instance, Nirav [118] and Lall et al [98] and Bhatawadekar *et al* [59] use a 1 s window size, Dellaca *et al* [92] used a 0.2 s window size and Que et al [126] used 1/6 sec windows.

Short window sizes help tracking rapid changes in system parameters, but have the disadvantage of increased sensitivity to noise and spectral leakage [37], therefore, we used a range of window sizes with realistic noise and subjects with realistic impedance to assess the tradeoff between temporal tracking and sensitivity to noise. Because this is a simulation study we know exactly the accuracy of the estimated impedance. In addition, because in oscillometry, only the data at oscillation frequency is of importance (Figure 4.4), we used Goertzel algorithm instead of the commonly used FFT/DFT to reduce the computational complexity of STFT [107, 120].

In this paper, we assessed the accuracy of tracking the time-varying impedance and showed with and without noise this error increases with increasing breathing rate. We also showed that using STFT is fairly accurate if used in lower breathing rates and with the right window size.

A limitation of this study was that we only investigated sinusoidally varying resistance and elastance. Variations can happen more rapidly than the breathing frequency, for example with the onset of flow limitation and its reversal, which can occur in COPD [92]. Also we only investigated children with asthma that although have high impedance, their breathing amplitude is small, and thus the noise may be larger in COPD.

Choosing to record real breathing noise from children was important because children generally breathe faster. However, higher rates of breathing would be encountered with exercise and with larger noise, but oscillometry is generally restricted to normal breathing. It is also possible that in a different population such as COPD, the noise would have a slightly different frequency distribution but we speculate that our findings would likely be similar and translatable to COPD.

Another limitation of this study was the assumption of resistance and elastance varying in phase with flow. Although this assumption is supported with evidence from some of the research on COPD [111], asthma and even healthy subjects [109], one could also explore the amount of TVE with assumption of resistance and elastance varying in phase with volume, which we explore further in Chapter 5. Here, analytically for estimating TVE, this would not make a difference as the error arises solely from the magnitude of the rate of change of impedance. This is the derivative of the magnitude, which is not different between sine or cosine and is independent of the phase.

Our model was also limited because it assumed that the impedance varied only with the fundamental breathing frequency. Also, we simplified our simulations to only 5 Hz oscillations. The TVE if measured at another frequency could have a different magnitude, however, since the breathing noise is less at higher frequencies, our results should be characteristic of the worst case.

Moreover, we found that the TVE matched the actual error for only for the noise-free COPD load when using short windows but not for added noise. We believe this is because the TVE assumes continuously varying parameters which does not include errors incurred by the edge artifacts induced by choice of windowing. Thus the TVE is not an estimate of the actual errors incurred in the current analysis of time varying respiratory parameters, but is an underestimate of the error in that case. Therefore it is more reasonable to state that the TVE likely provides a value of the minimum bias or error that occurs in estimating the parameters of an ‘average’ time invariant frequency domain transfer function from a time-varying system.

It is also important to note that here we applied Zadeh’s transform to illustrate that the estimates of impedance deviated from the actual impedance parameters, using a single compartment model. The same would be true if we used multi- compartment

models, where a TVE based deviation in Zrs would similarly result from the time-derivative of the underlying impedance parameters as indicated by application of equation (4.17). However, we do not know how aspects such as model heterogeneity might influence the magnitude of this error.

We also analytically derived the time-frequency transfer function of a time-varying single-compartment model. This revealed an inherent analytical error we term TVE, that arises from using a time-invariant methodology to analyze a time-varying respiratory system equation (4.17).A phenomenon that can be readily seen in equation (4.17) is that faster variations in impedance would result in higher TVE. This agrees with the dependence in actual error we observed with higher breathing rates. However, this increase was more dramatic for longer window sizes in noise-free simulations which can be partly because the Nyquist frequency of a longer window is closer to the breathing frequency of the modeled subject. These results are important because they show that TVE, independent of the breathing noise, can be as high as 5% using short windows and 10% using long windows depending on subject's fundamental breathing frequency. Another interesting observation from equation (4.17) is that the variations in resistance influence the elastance estimates and the variations in elastance influence the resistance estimates. Here we found that with short windows less than 0.4 s and without added noise the TVE or $\widehat{TVE}$ accurately predicted the deviation observed in the estimated impedance in COPD example, and fairly accurately predicted the deviation in the child example. This is important since for greater loads, the variation in impedance is harder to track accurately. In all cases TVE increased with increasing breathing rate, which means that the rate of subject's breathing during OS will affect the precision of measurement.

To verify the phenomenon of increasing TVE with increasing breathing frequency in the presence of noise, breathing signals of a relatively high-noised population (children) were measured and added to the simulations. While an impedance estimation error of 10% for mean impedance is the maximum recommended error in the literature [2], our plots showed very small errors of 1.5% are achievable for every window size (Figure 4.7). This implies that high accuracy is achievable with standard analysis methods in estimating mean impedance values.

On the other hand, the error in tracking time variation of impedance is much higher and depends on both window size and breathing rate. The dependence on breathing rate was consistent with every window size (Figure 4.8a). Notably as well, the error was largest with the shortest window as expected. However, window size of 0.8 s had the lowest error in every subject's breathing rate (Figure 4.8b). This implies that there is an optimum window size to be found that balances the tradeoff between the influence of noise and precise tracking of varying impedance.

Small amounts of error observed in low breathing frequencies indicate that the current airwave oscillometry devices and post data processing are relatively suitable for within-breath estimation of impedance. However, errors were larger than 10% for subjects with higher breathing rate and in particular with short windows. Technologically, accuracy can be improved with larger signals to improve signal to noise, as long as peak pressures are within acceptable maximums (5 cmH20/l/s) and accepted by the patient. However from a clinical point of view, as the subject's breathing rate increases and breathing noise is added (as in children, COPD, or a normal subject during exercise), it is harder to have a precise estimation of variations in impedance. This could be partly resolved by asking the subjects to breathe at a lower rate. A similar procedure was employed Nirav [118] where they asked and trained every subject to breathe at 0.2 Hz.

4.8 Conclusion

This paper, for the first time, introduced a time-varying error calculation procedure for linear time-varying respiratory system models based on Zadeh's transform also using Goertzel algorithm to reduce computational cost in practice. Using STFT with multiple windows is a very accurate method for estimating average impedance despite time-variation of underlying impedance, however, it is not as accurate for tracking the variations of impedance.

Chapter 5: Frequency Dependence Of Impedance Due To Time-Varying Respiratory Mechanics

Authors

Hamed Hanafi
Kamal El-Sankary
Jason H.T. Bates
Geoffrey N. Maksym

This article is to be submitted to the Annals of Biomedical Engineering. The content of this chapter was conceived and developed by Hamed Hanafi with supervision from Dr. Maksym. Dr. El-Sankary provided assistance applying the approach of Zadeh to the respiratory system. Dr. Bates was very helpful in providing feedback and critique on the development and novel predictions of the time-domain varying single compartment respiratory mechanics model.

5.1 Abstract

Frequency dependence of respiratory mechanics is a well-established behavior of the respiratory system, attributed to both tissue viscoelasticity and heterogeneity of airflow in the lung. It is important as it is beginning to be used clinically as an indicator for obstructive disease. Additionally, despite the fact that respiratory mechanical parameters are known to vary in time, all analysis methods assume quasi-stationarity in the parameters used to describe the respiratory system, and the effects of this assumption have not yet been examined in any detail. Here we first analyzed a simplified respiratory system model with time-varying parameters in the time-domain, then we developed a theory for time-varying respiratory mechanics according to Zadeh's method for analysis of linear time-varying systems. In this report, we find that a number of characteristic features arise analytically. These include: we find that accounting for the time-varying behavior of the respiratory system predicts an inverse frequency dependence for the resistance; This is dependent on the amplitude of the time variation of the elastance; and finally we predict that hysteresivity, η, increases with the amplitude of the time variation of the respiratory system in the frequency spectrum. These findings are important because this is a novel mechanism for a well observed behavior of resistance, and we have theoretically demonstrated how increases in time variation in elastance are linked to increases in frequency dependence of Rrs, both of which are known to increase in obstructive disease.

5.2 INTRODUCTION

The respiratory system resistance follows a nearly inverse power-law frequency dependence. This frequency dependence has been established to originate from both tissue viscoelasticity [32, 33, 46, 121] as well as from airflow heterogeneity [26, 31]. *Hantos et al* [36, 39] in an inverse modeling approach developed the constant-phase (CP) model to account for the frequency dependent impedance data. This model has since become well established over the past two decades being able to well describe impedance data from all species measured with few free parameters [13, 23, 31, 37-41, 37, 122]. Equation (5.1) presents the constant phase tissue impedance transfer function including a Newtonian airway resistance (R_L) as:

$$Z_{\mathrm{CP}} = R_L + \frac{\mathrm{G} - i*\mathrm{H}}{\omega^{\alpha}} \tag{5.1}$$

where G reflects the viscous energy dissipation and H describes lung stiffness respectively. The exponent α is not an independent parameter, and is defined from G and H as:

$$\alpha = \frac{2}{\pi}\tan^{-1}\frac{\mathrm{H}}{\mathrm{G}} \tag{5.2}$$

In the healthy lung, since ventilation is thought to be largely homogenous all frequency dependence is commonly thought to arise from the respiratory system tissue mechanics. But with the development of non-uniform obstruction of the lung, this leads to heterogeneity in impedances down multiple pathways, which requires description via a distributed model with multiple effective time constants, with the time constant arising from the product of a resistance and compliance for each path [123]. Otis *et al* [26] showed in a parallel two compartment model that the presence of unequal time constants leads to frequency dependence of the impedance. Indeed, complex multiple branch airway tree models that utilize standard linear resistance elements for airways and compliances for terminal tissue elastance elements can account for the inverse frequency

dependence without employing constant phase tissue mechanics. Additionally, although the constant phase model is homogeneous, it has been shown that it is possible to describe the onset of ventilation heterogeneity by allowing the ratio of G/H, known as the hysteresivity (η), to vary. Indeed it has been shown in experimental studies that η, increases with nonuniform ventilation [31, 125], and the rise in η has been interpreted as an increase in heterogeneity [28, 124], however, the reason for this has not been completely found analytically, and indeed in models with extreme heterogeneity, η contradictorily decreases [25, 125].

On the other hand, it is well established that temporal variations in Rrs and even in Xrs occur during respiration and these can increase in disease. Variations in Rrs have been used as a severity index in asthma where resistance increases with severity of obstruction [98, 126, 127, 128]. In other studies, variations in Xrs, specifically the differences between expiratory and inspiratory Xrs at 5 Hz, which is largely associated with elastance, has been used as an index of airflow limitation in COPD [92, 110, 127, 128] (Figure 5.1). However, when the complex impedance of the respiratory system is described, it is common to present only the average Rrs and Xrs behavior over the measured frequency range. This is normally computed from averaging impedance estimated from Fourier methods from multiple finite overlapping windows, or from averaging over the time course computed from recursive time domain methods that also effectively examine short duration overlapping periods. Each of these techniques assume that within a short window, the mechanics of the respiratory system are time-invariant, and the pressure and flow data are assumed to have the property of stationarity, that is non-time dependent statistical properties. In this paper we examine the validity of this assumption, and the impact of the violation of this assumption may have on the estimates of impedance in the frequency domain.

To explore the calculation of impedance without violating non-stationarity, we first analyze the model using a time-domain analytical approach to provide the pressure-flow relationship across frequency, producing the frequency response of the system, and we also employed a method developed for calculation of the frequency domain transfer function of linear time-varying (LTV) systems developed by Zadeh. [60]. This method

and similar approaches have not been previously applied to the respiratory system, despite the time-varying nature inherent in the respiratory system, but have been applied to a variety of systems including some other physiological systems such as solving for the pressure-flow frequency response accounting for time-varying elastance of the left ventricle's elastance [74] and also to predict voltage-current frequency response of bioimpedance using a dummy time-varying electrical circuit [67]. Here we principally were able to show using the two approaches applied to the single compartment model of the respiratory system that the frequency dependence of Rrs can arise from time-varying mechanics and we further demonstrate that when there is temporal variation in respiratory mechanics, η can reflect in part this variation.

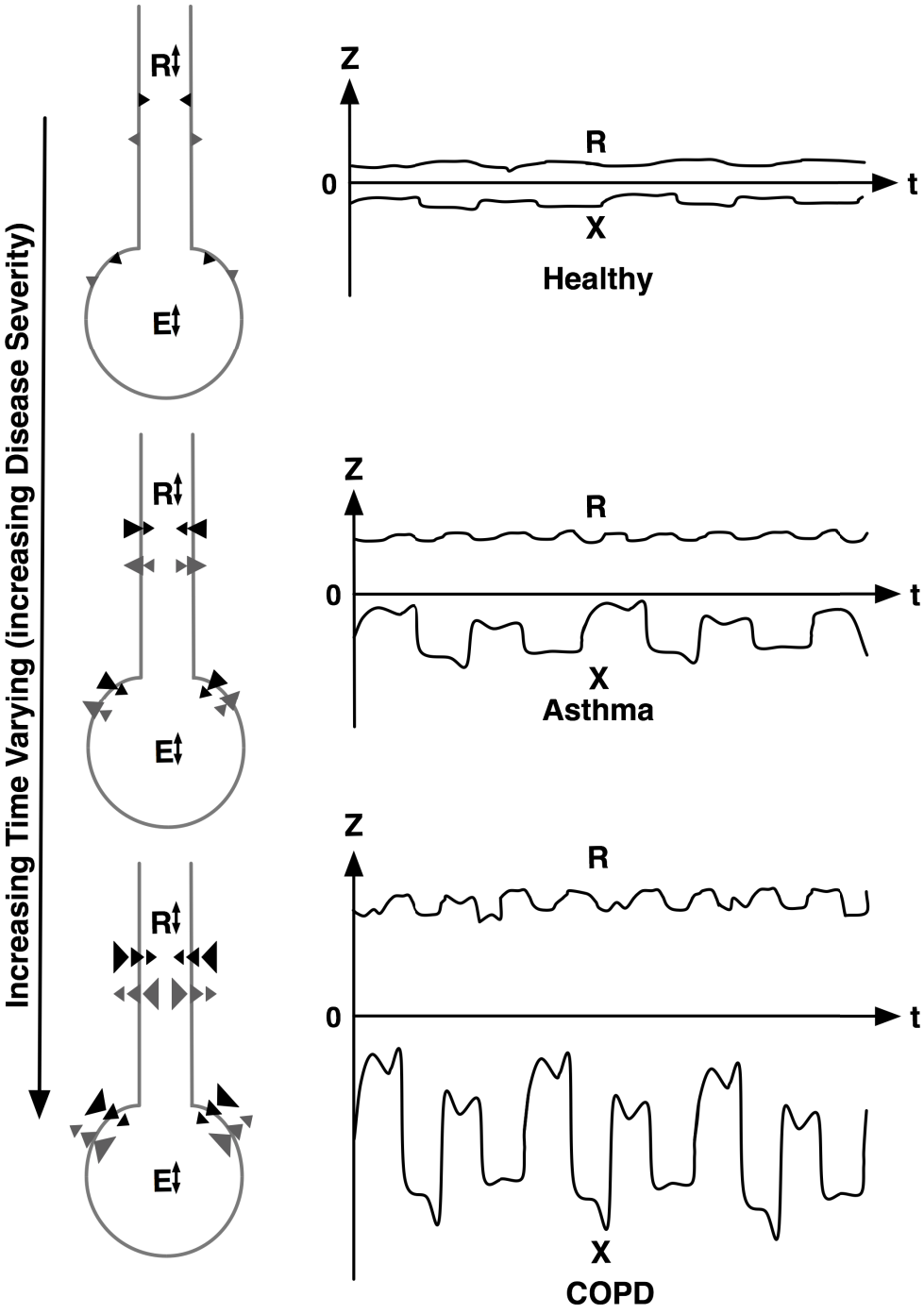

Figure 5.1: Symbolic demonstration with time-varying resistance and elastance in a single compartment lung model that could occur in different obstructive disease. Triangles represent the rate of time-varying alterations in airway diameter and elasticity of tissue.

5.3 ANALYTICAL METHODS AND RESULTS

5.3.1 Single-Compartment Time-Varying Transfer Function in Time-Domain:

The single compartment model is the simplest and perhaps the most commonly used model representation of the lung [37]. This model represents the pressure-flow relationship of the conductive airways as a tube with constant Newtonian resistance (R_L) and the pressure-volume behavior of the elastic tissues as a balloon with constant elastance (E_L). The resulting relationship between pressure and flow forms the so-called single compartment equation of motion for across the lung during normal respiration:

$$P(t) = P_{pl} - P_{ao} = R_L.Q + E_L.V \tag{5.3}$$

where $P(t)$ is the pressure difference across the lung, P_{pl} is the pleural pressure and P_{ao} is the pressure of airway opening, Q is flow and V is volume.

If we consider applying an oscillation of air of the model at frequency, f_{os}, we can consider that the dimensions of the lung, and thus the model may also vary at f_{os}. Thus the airway diameter increases with inflation and decreases with deflation, and it is also expected that the elastance can vary also at this frequency, whether due to the nonlinear nature of the PV curve for the lung, or arising from the onset of flow limitation which increases elastance on exhalation relative to inhalation. Thus we can conceive of both variations in resistance and elastance that may occur at the same frequency of oscillation. Indeed this is what happens during spontaneous ventilation or mechanical ventilation by a ventilator. In general for what we will derive below, we could consider variations of R and E of different phases relative to the flow or volume. However, we can initially simply consider a common occurrence observed in obstructive disease, based on published data (Figure 5. 2) [92, 110] and even in healthy subjects [118] where variations in resistance

appear to be actually more commonly in phase with flow and elastance inversely proportional with flow.

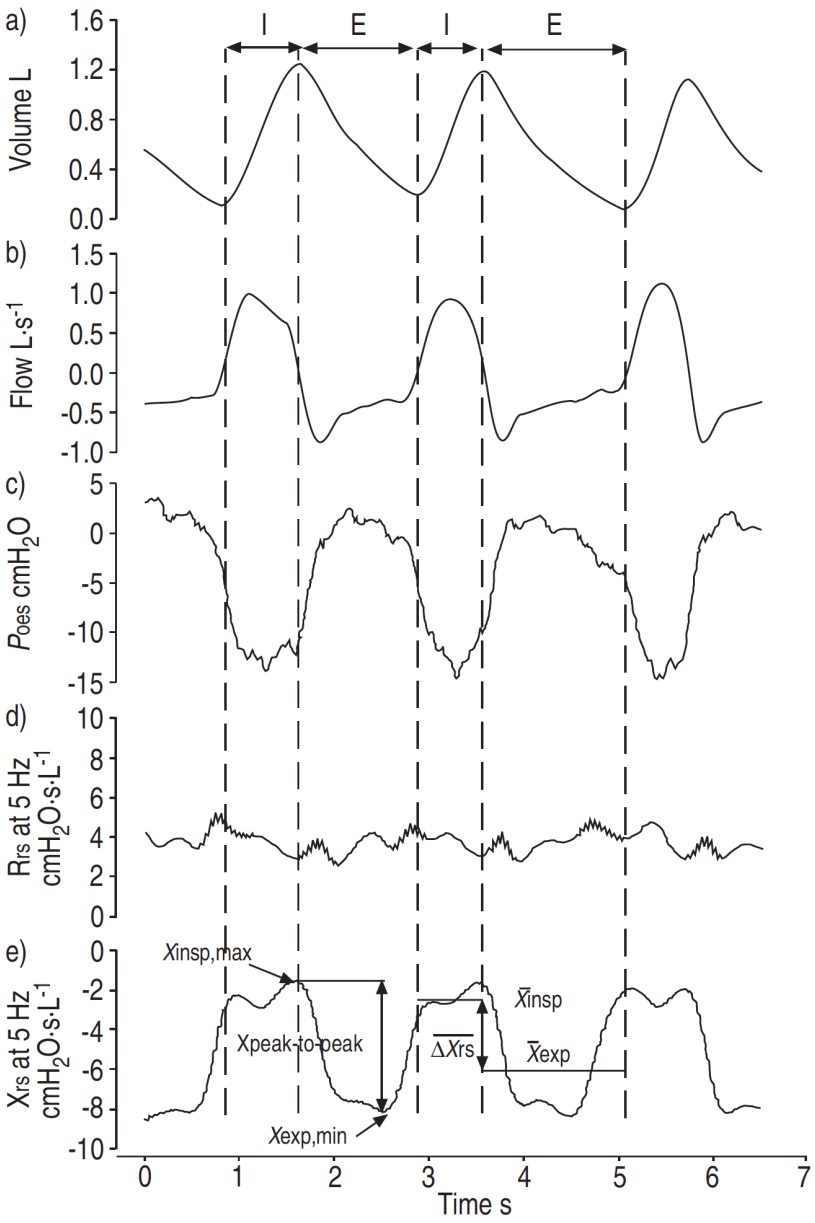

Figure 5. 2: Experimental tracing from a representative flow-limited patient and definition of the indices used to characterize the respiratory system reactance (X_{rs}) time course during a single breath. a) Respiratory volume, b) flow at the airway opening, c) oesophageal pressure, d) total respiratory input resistance (R_{rs}) and d) X_{rs} at 5 Hz. X_{insp}: mean value of X_{rs} during inspiration; X_{exp}: mean value of Xrs during expiration; $X_{exp,min}$: minimum value of X_{rs} during expiration; $X_{insp,max}$: maximum value of X_{rs} during inspiration. Since reactance was expected to decrease during expiratory flow limitation, the difference between X_{insp} and X_{exp} (ΔX_{rs}) and the difference between $X_{insp,max}$ and $X_{exp,min}$ (Xpeak-to-peak) was considered. Indices were defined in two different breaths for clarity. I: inspiration; E: expiration; P_{oes}: oesophageal pressure. Reproduced with permission from [110]

If we assume a sinusoidal volume oscillation at frequency f_{os} with amplitude A, $V(t) = -A\cos(2\pi f_{os}t) + V_{mean}$, and hence the flow, $Q(t) = A(2\pi f_{os})\sin(2\pi f_{os}t)$, where we arbitrarily choose a negative cosine in volume such that flow is of positive sign for convenience. Then resistance and elastance can be simplified to equation (5.4) and equation (5.5) respectively:

$$R_L(t) = R_{mean} + R_{var}\sin(2\pi f_{os}t) \tag{5.4}$$

$$E_L(t) = E_{mean} + E_{var}\sin(2\pi f_{os}t) \tag{5.5}$$

with R_{mean} and E_{mean} as the constant part of time-varying resistance and elastance and R_{var} and E_{var} the amplitude of the variable part. Here we have assumed that R_L and E_L vary sinusoidally, whereas for simplicity neglecting possible effects of nonlinearities which would induce smaller contributions at harmonics of f_{os}.

If we write the time-varying form of equation (5.3) using equation (5.4) and equation (5.5), $P(t) = R_L(t).Q(t) + E_L(t).V(t)$, with rearrangements we have:

$$P(t) = R_{mean}A2\pi f_{os}\sin(2\pi f_{os}t) + R_{var}A2\pi f_{os}\sin^2(2\pi f_{os}t) - E_{mean}A\cos(2\pi f_{os}t) - E_{var}A\sin(2\pi f_{os}t)\cos(2\pi f_{os}t) + V_{mean}E_{mean} + V_{mean}E_{var}\sin(2\pi f_{os}t) \tag{5.6}$$

Eliminating all the terms that don't belong to the frequency of oscillation we thus only have the following:

$$P(t)|_{f=f_{os}} = R_{mean} A 2\pi f_{os} \sin(2\pi f_{os} t) - E_{mean} A \cos(2\pi f_{os} t) + V_{mean}\, E_{var} \sin(2\pi f_{os} t) \quad (5.7)$$

The first term is in phase with flow, and governed by R_{mean} and the magnitude of the flow ($A2\pi f_{os}$), the second term is in phase with volume and governed by the magnitude of the volume and E_{mean}, and most importantly, there is a third term which is also in phase with flow governed by V_{mean} and E_{var}. The first two terms depend on the magnitude of the average resistance, and average elastance, and the magnitude of the flow. However the third term, $V_{mean}\, E_{var} \sin(2\pi f_{os} t)$, is in phase with the real part of impedance, and is also right at the frequency of oscillation but it's origin is from variations in elastance and any mean volume present in the system.. If there is no variation, $E_{var} = 0$, this term disappears, and indeed the pressure-flow relationship reduces only to being dependent on R_{mean}, E_{mean} and the frequency of oscillation. However, with variations in elastance at the frequency of oscillation, there are two contributions to the pressure time-course that are both in phase with flow.

Although from separate sources since they occur at the same frequency they cannot be separated from the recorded pressure signal, and thus the pressure signal amplitude is increased over and above the normal component due to the resistive load R_{mean}, by an amount proportional to the variation in elastance, and together these sources contribute to the pressure a total magnitude of ($R_{mean} A 2\pi f_{os} + V_{mean}\, E_{var}$). In using this data to compute the resistive component of the impedance, which can be done by dividing the measured pressure signal that is in phase with flow by the flow signal, or equivalently taking the real part of the ratio of the Fourier transform of pressure to the Fourier transform of flow, even if we first remove the means of both pressure and flow signals, nothing can be done that removes the biasing effect of the $V_{mean}\, E_{var}$ on the calculated resistance as:

$$R(t)|_{f=f_{os}} = \frac{P(t)}{Q(t)|_{f=f_{os}\ \&\ in\ phase\ with\ flow}} = R_{mean} + \frac{V_{mean}\, E_{var}}{A2\pi f_{os}} \quad (5.8)$$

Equation (5.8) reveals a source of frequency dependence of resistance dependent on the magnitude of the variation in elastance, and the mean volume in the system. As stated above, without variation, this dependence on the mean disappears, but in a time-varying system, because $E_{var}\sin(2\pi f_{os}t)$ occurs at the frequency of oscillation, $V_{mean}\ E_{var}\sin(2\pi f_{os}t)$ must be added to the oscillatory pressure. Moreover, from mechanical system point of view, V_{mean} is an intrinsic property of the single compartment model, and also for the lung. In a system with a chamber with a volume, if one makes the volume zero, there is no gas in the system, and so nothing to generate pressure. In the single compartment model with no flow, P = EV, which states for any increase in volume, pressure will be generated. It also states that any constant volume, if E is increased, pressure will be increased. Although we may arbitrarily subtract the mean volume and pressure, this relationship requires an increase in pressure for any real system with an actual non-zero volume if either E or V are increased. To demonstrate this effect, a simple simulation with $E_{mean} = 40\ cmH2O/L$, $E_{var} = 0,\ 12.5\%, 25\%, 37.5\%\ and\ 50\%\ of\ E_{mean}$, $R_{mean} = 2\ cmH2O/L/s$, and $R_{var} = E_{var} = 0,\ 12.5\%, 25\%, 37.5\%\ and\ 50\%\ of\ R_{mean}$ was performed in MATLAB. A typical inertance of 0.028 ($cmH2O/L/s^2$) was added for reactance to cross zero and increase with higher frequency. V_{mean} was set to 2 L and the amplitude of airflow was set to $A = 2\ L/s$ to have an equal ratio of $\frac{V_{mean}}{A}$, however in practice, this ratio changes depending on the specific subject's physiology and mechanics. For analysis, the means of pressure and flow signals were first removed, and the data was Hanning windowed with window length of two oscillation cycles with 50% overlap, FFT of pressure was divided by FFT of flow to calculate impedance in each window, real and imaginary parts were separated as resistance and reactance respectively, then mean resistance, R, and reactance, X, were calculated. Later, elastance was calculated from $E = -2\pi f_{os}X$. To produce the frequency domain behavior for R and E, this was repeated at oscillation frequencies of 0.2, 0.3, 0.4, 1, 2, 4 and 5 Hz. To check the influence of Hanning windowing, the same simulations were repeated without applying windowing.

The resistances calculated by equation (5.8) predicted exactly the same frequency dependence produced by simulations without windowing, however, applying Hanning window reduced the frequency dependence by about 50% at all frequencies (Figure 5.3).

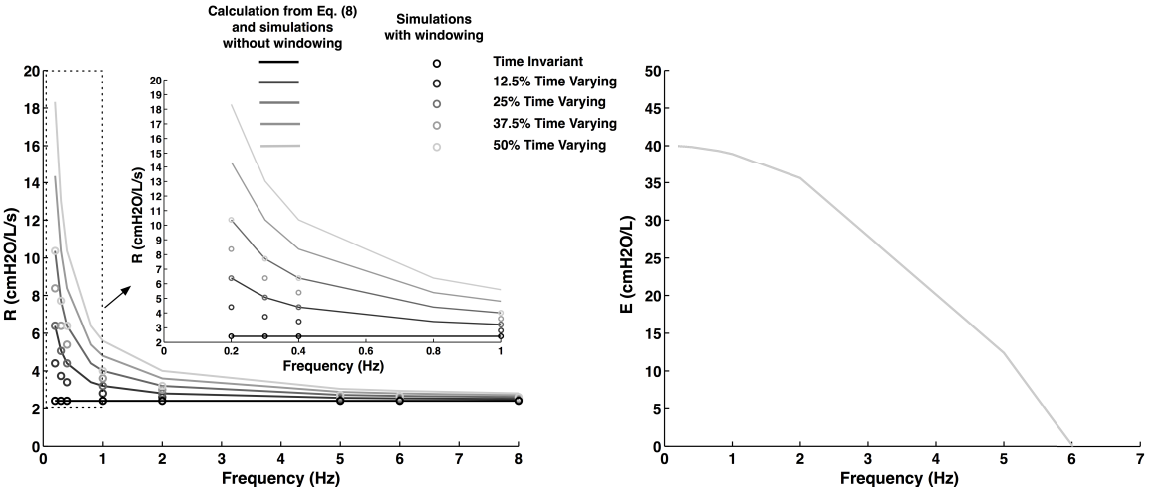

Figure 5. 3: Resistance, R and elastance, E versus frequency using FFT with time-varying elastance and resistance in phase with flow. Calculated resistance from equation (5.8) and impedance estimated from simulations without windowing showed the same frequency dependence of resistance (solid lines), however simulations with Hanning windowing reduced the frequency dependence but did not remove the effect.

Equation (5.8) also reveals that the frequency dependence is existent at all phases of any variation in elastance

$$E_L(t) = E_{mean} + E_{var}\sin(2\pi f_{os}t + \varphi) \tag{5.9}$$

except when the varying part of elastance varies completely in phase with volume ($\varphi = 90$).

This is explored by increasing the phase difference (φ) from 15-90 degrees on the same healthy single-compartment model with 50% time-varying magnitude. Frequency dependence of resistance decreased with increasing phase (Figure 5.4).

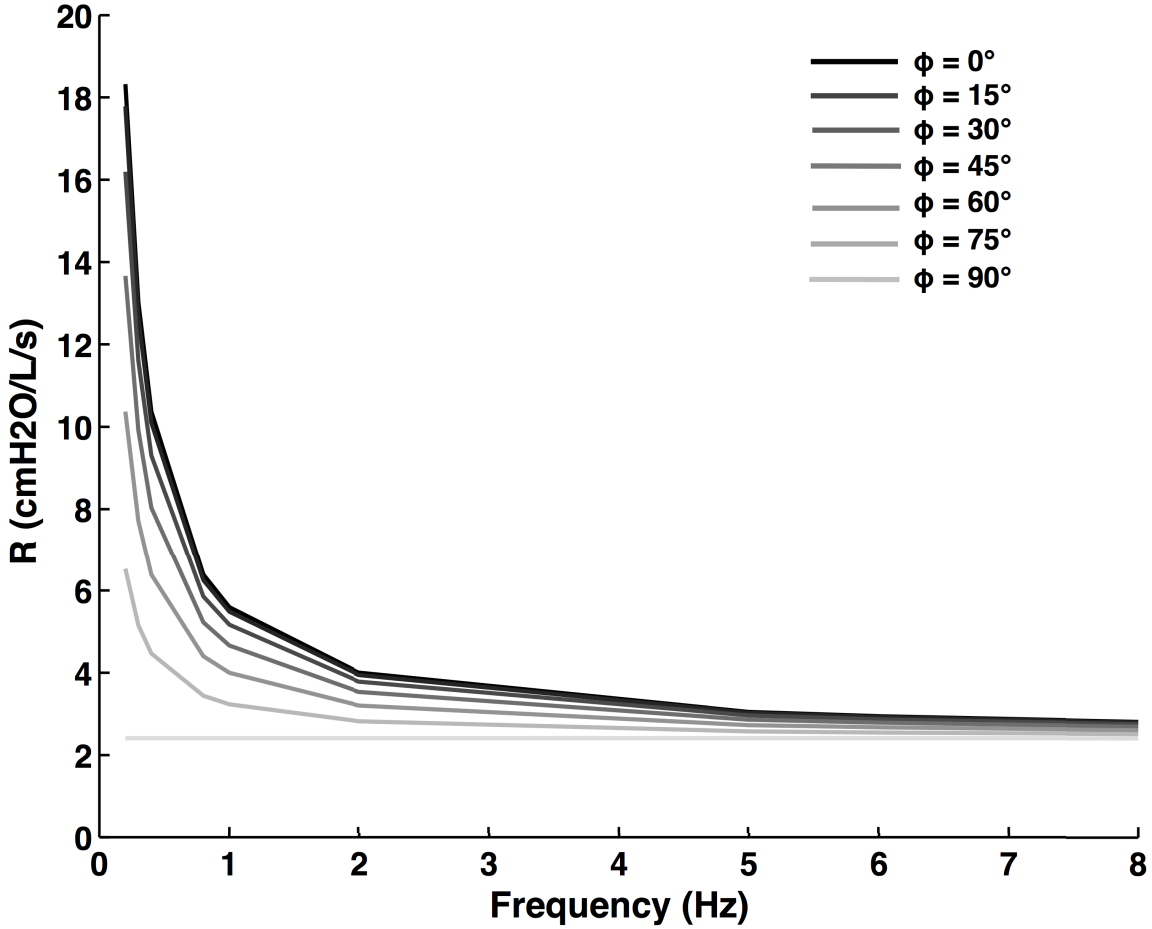

Figure 5. 4: The influence of phase difference between variations of elastance and oscillatory flow signal on frequency dependence of resistance. The frequency dependence decreased as phase increased and dissapeared at $\varphi = 90$.

5.3.2 Single-Compartment Time-Varying Transfer Function Using Zadeh:

We also approached the same problem via an alternate method and developed a time-frequency domain transfer function for the time varying single compartment model of the respiratory system using an approach for LTV systems developed by Zadeh [60]. First we demonstrate this on the time invariant system as follows. We first transform equation (5.3) to frequency domain, which forms the linear time-invariant (LTI) single-compartment impedance transfer function:

$$Z(j\omega) = R_L + jX_L \tag{5.10}$$

where, $X_L = -\frac{E_L}{\omega}$ is the reactance of the lung.

For time variant, we re-write equation (5.1) with time-varying resistance ($R(t)$) and elastance ($E_L(t)$) and using Zadeh's transformation (See Appendix) which yields the time-frequency transfer function of single-compartment impedance:

$$Z(j\omega, t) = R_L(t) + \frac{\dot{E_L}(t)}{\omega^2} + \frac{E_L(t) - \dot{R_L}(t)}{j\omega} \tag{5.11}$$

where $\dot{R}_L(t)$ and $\dot{E}_L(t)$ are the derivatives of $R_L(t)$ and $E_L(t)$ with respect to time.

Note equation (5.11) describes a temporally changing impedance, which is unfamiliar but is a necessary consequence if the parameters of the linear system are varying. equation (5.11) shows that the impedance has a real component arising from the expected temporal variation in resistance $R_L(t)$, but also another term as part of the real part of impedance that is dependent on the rate of temporal variations in elastance ($\frac{\dot{E_L}(t)}{(\omega)^2}$). The reactance, which is the imaginary part, has the expected dependence on the variation in elastance $E_L(t)$, but also a dependence on the rate of temporal variations in resistance ($\dot{R}_L(t)$).

This surprising result, as we derived similarly for equation (5.8), shows that frequency dependence of reistance could arise from the temporal variations in elastance (Figure 5.1) and similarly a component of the reactance can arise from any variations present in the resistance.

The real part of impedance from equation (5.11), $\frac{\dot{E_L}(t)}{\omega^2}$ could give rise to the same effect seen in equation (5.8) from $\frac{V_{mean}\, E_{var}}{A\omega}$. Considering a sinusoidally varying elastance (equation (5.5)), $\dot{E}_L(t) = \omega . E_{var} \cos(\omega t)$ and therefore $\frac{\dot{E_L}(t)}{\omega^2} = \frac{E_{var}}{\omega} \cos(\omega t)$ which has the same amplitude as $\frac{V_{mean}\, E_{var}}{A\omega}$ if $\frac{V_{mean}}{A} = 1$. This could be possible if for example the functional residual capacity (FRC) in the lung would be $V_{mean} = 2\ L$ and the amplitude

of airflow generated by oscillometry/OVW would be $A = 2\ L/s$. We plotted the amplitude of these variations versus frequency to explore these results together with those of the time-domain simulations.

To explore this phenomenon over a range of temporal variation in R and E, we simulated a single compartment model with resistance and elastance values typical for a healthy subject [17] and with different amplitudes of variations in resistance and elastance (R_{var} and E_{var}) as previously applied to time-domain simulations of the single compartment model. Again, inertance was added representing the inertial properties of the lung (Table. 5.1). For simplicity, the variations of resistance and elastance were assumed to be sinusoidal and we explored the frequency range commonly used for the optimal ventilator waveform from 0.2 Hz to 8 Hz.

At zero amplitude for R_{var} and E_{var}, there was no frequency dependence for Rrs, but this increased with increase in magnitude of variation (Figure 5.5). While the effect on resistance was easily observed, there was little effect on elastance since $\dot{R_L}(t)$ is so small relative to $E(t)$. Also, comparing the resistance versus frequency from Figure 5.5 and Figure 5.3 confirms that under the current assumptions, the amplitude of resistance in equation (5.11) yielded the same frequency dependence observed from time-domain simulations and predicted by equation (5.8).

Table 5.1: Mechanical properties of a healthy subject in a single compartment model

Property	
$R_L\ (cmH2O/\ L/s)$	2.41
$R_v\ (cmH2O/\ L/s)$	$(R_L/2)\times(0, 12.5, 25, 37.5 \text{ and } 50)$ %
$E_L\ (cmH2O/L)$	40
$E_v\ (cmH2O/L)$	$(E_L/2)\times(0, 12.5, 25, 37.5 \text{ and } 50)$ %
$I_L\ (cmH2O/\ L/s^2)$	0.028

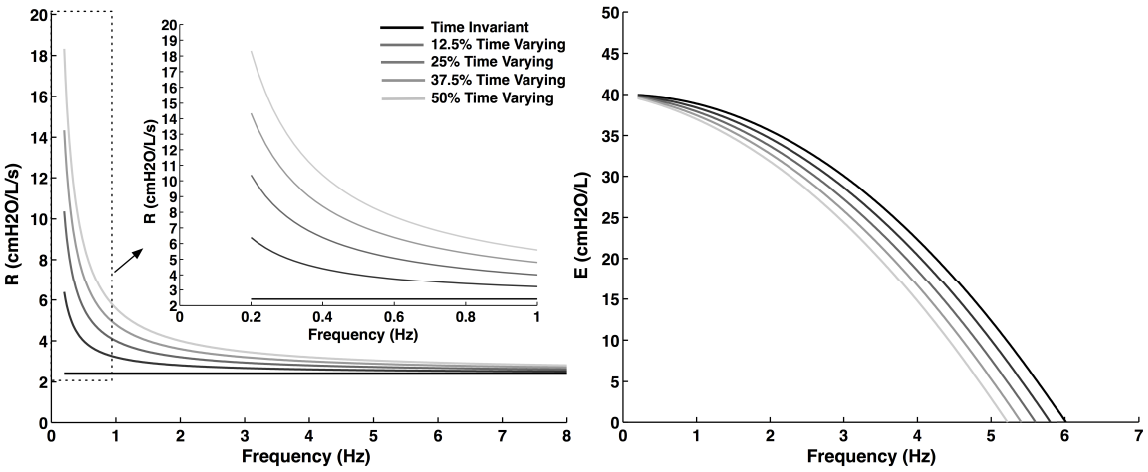

Figure 5. 5: Single compartment model with different time-varying percentages. Frequency dependence increases with increasing time-varying

5.3.3 Two Compartment Model

We wanted to compare the magnitude of the frequency dependence predicted from time variation of impedance to the effect of heterogeneity which can also produce frequency dependence of impedance. The single compartment model has no heterogeneity; therefore, to compare the time-varying nature to what might occur with heterogeneity, we implemented a two compartment (TC) time-varying system (Figure 5.6). In this case, we simulated the model representative of reported data from different disease conditions including healthy, mild asthma, severe asthma [17] and COPD [92, 110] (Table 5.2). The healthy subject was modeled homogeneously ($R_2 = R_1 \; and \; E_2 = E_1$) and the subject with mild asthma was modeled with heterogeneous airway diameters but identical terminal elastances ($R_2 = 5R_1 \; and \; E_2 = E_1$). The elastance for the mild asthma model was larger than that in health as is commonly reported [17]. A greater degree of heterogeneity was chosen to model severe asthma and COPD. In these simulations heterogeneity was limited to only the difference in airway diameter effecting resistances. This is because we wanted to compare the effect of percent variations of elastance on frequency dependence of resistance and also having heterogeneous elastance would make it harder to separate contributions to frequency dependence of resistance,

although this would be interesting to examine (Table 5.2). The common airway resistance (R_c) was set to 1 $cmH2O/L/s$.

$$Z_{\mathrm{TC}} = R_C + \frac{\mathrm{Z}_1\,\mathrm{Z}_2}{\mathrm{Z}_1+\mathrm{Z}_2} \tag{5.12}$$

where Z_1 and Z_2 are the impedances of first and second lobes respectively. Calculating R_{TC}, the real part of Z_{TC} yields:

$$R_{\mathrm{TC}} = R_C + \frac{\omega^2 R_1 R_2 (R_1+R_2)+(\mathrm{El}_2^2 R_1+\mathrm{El}_1^2 R_2)}{\left(\dot{R}_1+\dot{R}_2-\mathrm{El}_1-\mathrm{El}_2\right)^2+\left(\frac{\dot{\mathrm{El}}_1}{\omega}+\frac{\dot{\mathrm{El}}_2}{\omega}+\omega(R_1+R_2)\right)^2} + R_{TV} \tag{5.13}$$

And calculating E_{TC} from the imaginary part of Z_{TC} yields:

$$E_{\mathrm{TC}} = \frac{El_1 El_2 (El_1+El_2)+\omega^2 (El_2 \mathrm{R}_1^2+El_1 \mathrm{R}_2^2)}{\left(\dot{R}_1+\dot{R}_2-\mathrm{El}_1-\mathrm{El}_2\right)^2+\left(\frac{\dot{\mathrm{El}}_1}{\omega}+\frac{\dot{\mathrm{El}}_2}{\omega}+\omega(R_1+R_2)\right)^2} + E_{TV} \tag{5.14}$$

where R_{TV} and E_{TV} are the portion of two compartment resistance and elastance that would be zero with no time-varying (see Appendix. B). Note that in the absence of time-varying, equation (5.13) and equation (5.14) reduce to the familiar equation presented by Bates *et al* [125] ($R_{\mathrm{TC}} = R_C + \frac{\omega^2 R_1 R_2 (R_1+R_2)+\mathrm{El}_2^2 R_1+\mathrm{El}_1^2 R_2}{(\mathrm{El}_1+\mathrm{El}_2)^2+\omega^2 (R_1+R_2)^2}$ and $E_{\mathrm{TC}} = \frac{El_1 El_2 (El_1+El_2)+\omega^2 (El_2 \mathrm{R}_1^2+El_1 \mathrm{R}_2^2)}{(\mathrm{El}_1+\mathrm{El}_2)^2+\omega^2 (R_1+R_2)^2}$).

When we altered the parameters to simulate the different diseases in he double compartment model, we found that the COPD and the severe asthma cases had the highest frequency dependence while the healthy subject had the lowest (Figure 5.7 a, b, c). For the healthy case in panel (a) the results were very similar to the single compartment time variant model (Figure 5.5). For the asthma cases in panel (b), the solid black lines represent resistance from time invariant parameters where the heterogeneous asthma exhibit some frequency dependence previously describe for two compartment models as seen in Bates *et al* [125]. In all cases adding time variation 25% and 50%

increased the frequency dependence of the resistance (Figure 5.7 a, b, c). Comparing the 25% time varying models in panel a (homogeneous) to the 25% time varying models in panel b (heterogeneous asthma) shows that adding heterogeneity in the presence of time variation increased the frequency dependence slightly. However at 50% time variation, heterogeneity has a stronger effect, and the frequency dependence was doubled. In the heterogeneous severe asthma case with 25% time-varying, the frequency dependence was even above 50% heterogeneous mild asthma and was increased further with 50% time-varying.

It is important to note that time variation representative of what is observed in asthma or COPD can produce frequency dependence comparable to what may be representative of heterogeneity in these diseases, albeit simplified to a two compartment model.

Panel (d) shows the reactance for all of the cases. Reactance was lower (more negative) with increasing disease severity as expected due to the increases elastance values for each model, however, within each group, time-variation only slightly increased each subject's reactance at all frequencies. Examining reactance further, we can estimate an elastance from $\hat{E} = -\omega X$ [28]. This is only valid at low frequencies, as it neglects any inertive component, which becomes important at higher frequencies. We can see in panel e, that for the time invariant and homogenous model the estimate of elastance is constant at low frequencies, but then begins to descend as inertance begins to draw this downward. Moreover, the strong upward frequency dependence of elastance at low frequencies with heterogeneity is remarkably similar to the data presented by Lutchen *et al* [28].

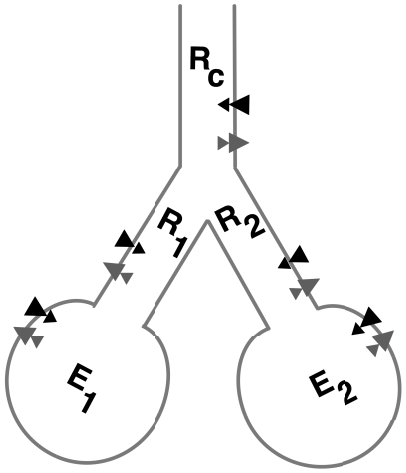

Figure 5. 6: Two compartment time varying model.

Table 5. 2: Mechanical properties of subject populations in a two compartment model

Property	Healthy	Homogeneous Asthma	Heterogeneous Mild Asthma	Heterogeneous Severe Asthma	COPD
$R_1\ (cmH2O/L/s)$	2	6	3.6	6.66	7.46
$R_{1v}\ (cmH2O/L/s)$	0	3	1.8	3.33	3.73
$R_2\ (cmH2O/L/s)$	2	6	18	60	111.9
$R_{2v}\ (cmH2O/L/s)$	0	3	9	30	55.95
$E_{1,2}\ (cmH2O/L)$	8	147.6	147.6	200	300
$E_{v1,2}\ (cmH2O/L)$	1	73.8	73.8	100	150
$R_c\ (cmH2O/L/s)$	1	1	1	1	1
$I_c\ (cmH2O/L/s^2)$	0.028	0.028	0.028	0.028	0.028

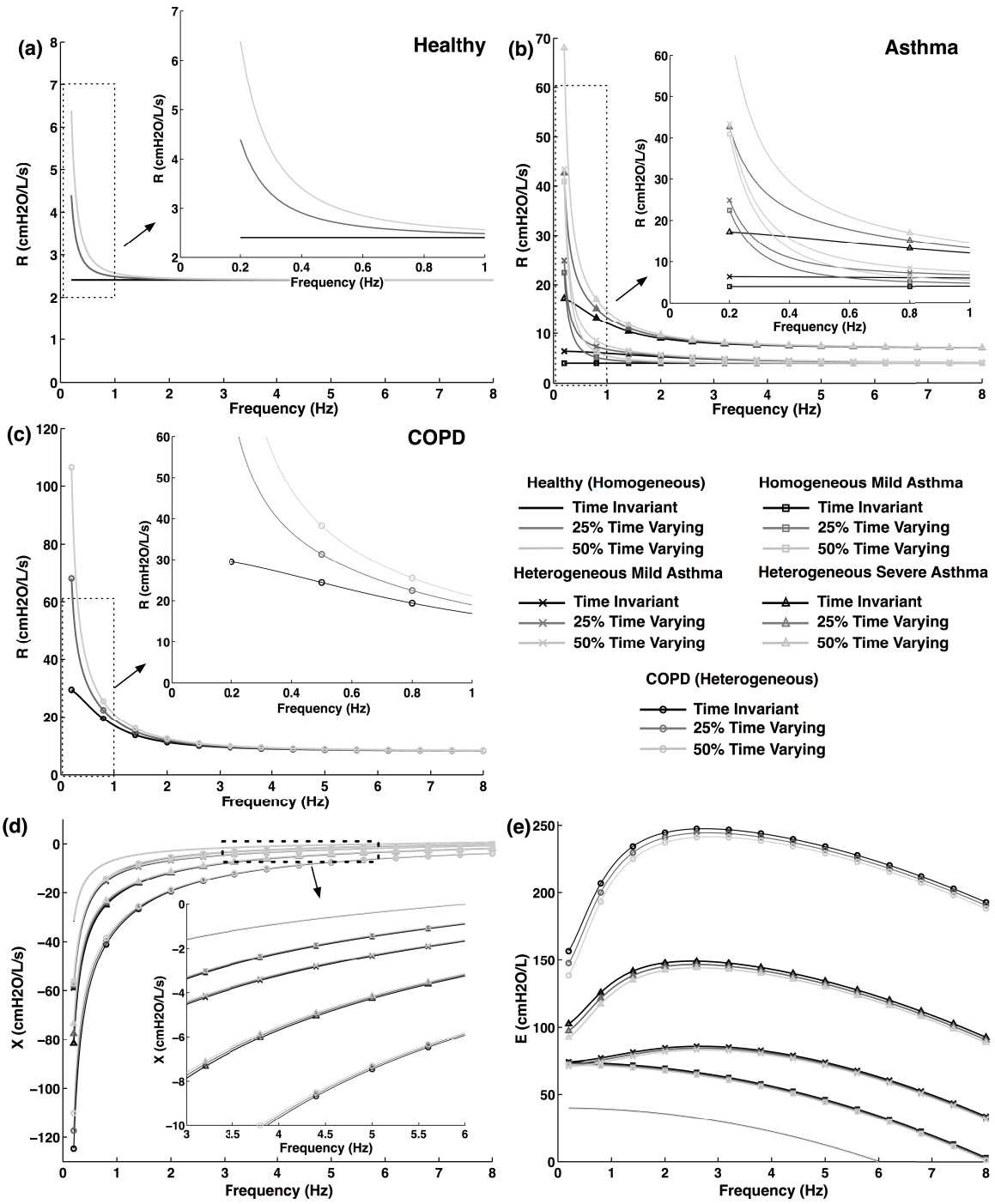

Figure. 5. 7: Two compartment model for different subject cases. Resistances are presented in panels a, b and c for healthy, asthma and COPD cases. Reactances are presented in panel d elastances in panel e.

5.3.4 Hysteresivity

A quantity sometimes employed in the interpretation of respiratory mechanics, applied to lung tissue, is the hysteresivity, η. It is defined as the ratio of real part to imaginary part of the impedance, and is a very fundamental quantity defining the ratio of energy lost to frictional processes such as viscous dissipation, to the energy stored elastically. In lung tissue, η is generally largely constant over a wide range of frequencies, and despite large differences in mechanical properties across species, the value of η is very consistent at about 0.1 to 0.3 [37]. η in the constant phase model it is $\frac{G}{H}$, but in the single compartment model it is:

$$\eta = \frac{\omega R}{E} \tag{5.15}$$

However when obtained from the respiratory impedance, using the constant phase model with Newtonian resistance accounting for airway resistance, η is established to increase with increasing heterogeneity. Thus is has been proposed as an indicator for the development of heterogeneity in ventilated animals [28, 124]. Therefore when we calculate η as in Bates *et al* [125] removing the airway resistance of $\frac{R_1 R_2}{R_1+R_2}$ from the two compartment parallel resistance, we can compare η in models with different degrees of heterogeneity.

To explore the effect of time-varying mechanics on hysteresivity in the presence of heterogeneity, we simulated a homogeneous ($R_1 = R_2$) and three heterogeneous models ($R_1 = 5R_2, R_1 = 10R_2 \; and \; R_1 = 15R_2$) with and without 25% time-varying (Table 5.3). Elastance was kept the same for all models. Figure 5.8 plots η versus frequency for the simulated scenarios. The solid black lines represent models with heterogeneity and grey lines represent η with 25% time-varying for each case. We found that in the homogeneous case, increasing time-varying increases η. At presence of heterogeneity with no time-varying (i.e. $R_2 = 5R_1$ time invariant), η increased in lower frequencies but decreased it in higher frequencies. Having both heterogeneity and time-varying also showed that an increase in heterogeneity does not guarantee an increase in η

at all frequencies. For example, when $f < 1.5$ Hz, $\eta_{R_2=10R_1} > \eta_{R_2=5R_1}$ but when $f > 1.5$ Hz, $\eta_{R_2=10R_1} < \eta_{R_2=5R_1}$. It is important to note that in these simulations η can be zero because a model with no time varying and no constant phase component doesn't have any tissue viscoelasticity.

Table 5. 3: Mechanical properties of two compartment model with increasing heterogeneity used to calculate hysteresivity

Property	$R_1 = R_2$	$R_1 = 5R_2$	$R_1 = 10R_2$	$R_1 = 15R_2$
$R_1\ (cmH2O/\ L/s)$	1	6	5.5	5.33
50% $R_{v1}(cmH2O/\ L/s)$	2.	1.5	1.37	1.33
$R_1\ (cmH2O/\ L/s)$	1	30	55	80
50% $R_{v2}(cmH2O/\ L/s)$	2.	7.5	13.7	20
$E_{1,2}\ (cmH2O/L)$	1	147.	147.	147.6
50% $E_{v1,2}\ (cmH2O/L)$	3	36.9	36.9	36.9

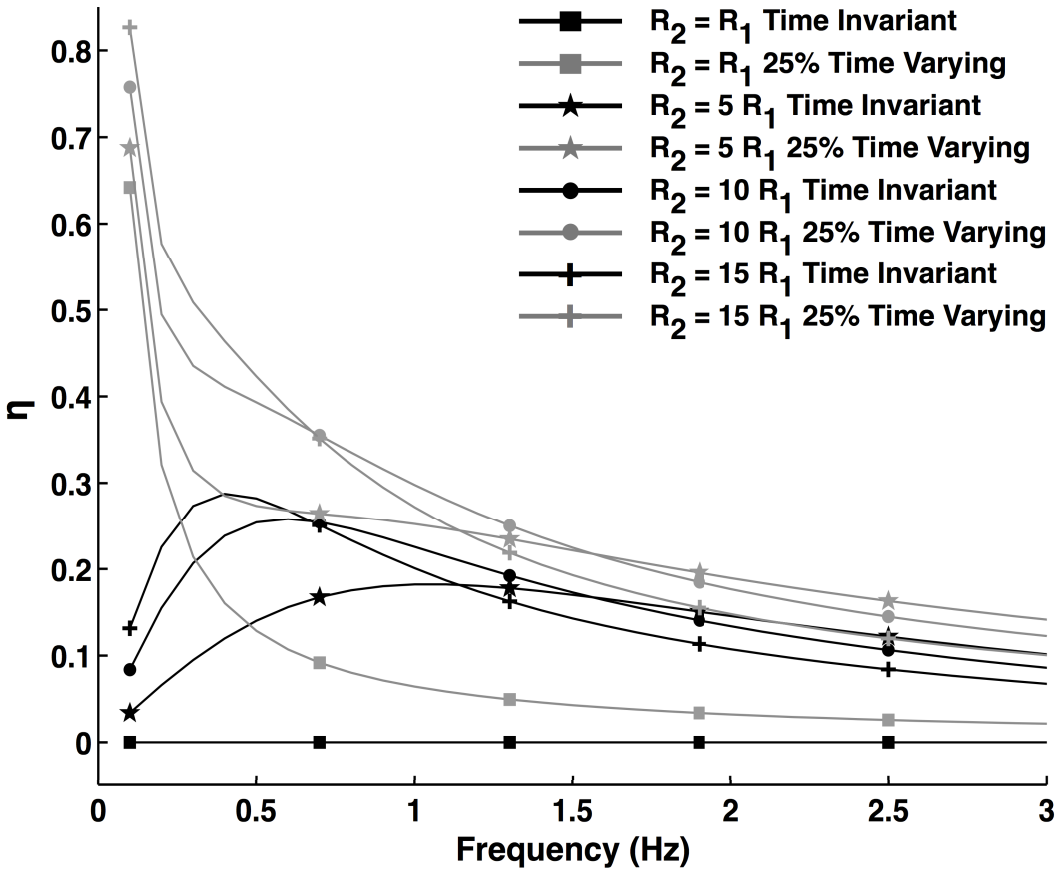

Figure. 5. 8: η in double compartment models for increasing heterogeneity. The parallel equivalent of all R_1s and R_2s are 5 cmH2O/L/s. The same elastance has been used for comparison based on increasing heterogeneity.

5.4 DISCUSSION

Our principal finding is that frequency dependence of resistance can arise wholly or in part from temporal changes in elastic mechanics of the respiratory system. This is an analytical result that necessarily originates from solving for the transfer function of linear time-varying systems which we have demonstrated using a time-domain analysis, and using a second approach developed for linear time varying systems which is a predominantly frequency domain approach. Using these approaches that make no

assumptions of time invariance is important, as it has not been done before. Indeed, all analysis and interpretation of respiratory mechanics previously assumes linear time invariance, approximating the mechanical behavior from the time-varying respiratory system generally assuming the underlying mechanical parameters vary slowly enough that the approximation to time-invariance is valid. Here we show that if this limitation is removed, that time-varying elastance can contribute to the well-recognized frequency dependence of resistance, which has become an indicator of lung disease. We further show that although Hanning windowing can reduce from the frequency dependence of resistance originated from time-varying elastance, it does not remove it.

Frequency dependence of resistance is nearly a universal finding in respiratory mechanics. In healthy human it is present at very low frequencies [11, 28]. In small animals [39, 23, 38, 41] or with obstructive disease in humans [74] the frequency dependence shifts to higher frequencies, and has been recently used as index of dysfunction. Frequency dependence of resistance has been ascribed to originate in from the fundamental viscoelastic mechanics of the lung tissue, but can also arise from the development of heterogeneity amongst airway diameters in both animals and humans. It is understood from respiratory impedance measurement alone that it is not possible to distinguish whether the frequency dependence of resistance is due to tissue viscoelasticity or heterogeneity, or a combination and other measurements are required. For example in asthma, where an increase in frequency dependence is commonly observed that increases with severity [17], either this can be attributed to a change in the viscoelastic properties of the tissue itself (parenchyma) and/or the shift in frequency dependence to higher frequencies is due to heterogeneity, or possibly both contribute in lung dysfunction. In asthma, the airways are altered, with remodelling, and mucous plugging, which may alter parenchymal viscoelasticity, or through increased airway narrowing, the added tension on the parenchyma through airway tissue parenchymal interdependence may alter the tissue viscoelasticity. Whether these effects are sufficient to alter lung mechanics, which is dominated by central airway resistance, and peripheral tissue elasticity of the parenchyma is unclear. However it is well established that heterogeneity of ventilation is substantial in asthma, inferred from forced oscillation measurements, measured from nitrogen breath washout or observed directly form hyperpolarized inhaled gas imaging.

Here we saw that heterogeneity was able to produce frequency dependence (Figure 5.7) although perhaps to a lesser degree than observed in severe asthma. The frequency dependence was at a lower frequency that can be observed in severe asthma (Cavalcanti et al [17]). This model only had two compartments, and multiple compartment models are able to produce heterogeneity and frequency dependence observed in asthma (Lutchen et al [133]). Although the frequency dependence in our two compartment model was modest with time invariant parameters, in a model with typical time variation of elastic parameters was included, we found clearly that this alone can cause frequency dependence, again albeit less than typical for asthma. However, when combined with a small amount of heterogeneity, these two effects combined can give rise to typical levels of frequency dependence observed in modeling or experimental studies [11, 17, 28].

As imaging studies have shown the presence of heterogeneity [133-135], computational studies have modeled the human airway tree to simulate ventilation heterogeneity based on well described experimental data [24, 123, 133-136, 138, 139]. For example, Tgavalekos et al [139] narrowed peripheral airways to account for the alterations in lung elastance which are located spatially according to regions of poor ventilation acquired by imaging gas-flows. To account for the resistance and its frequency dependence, they had to invoke substantial heterogeneity in the airway diameters of the non-defective regions of the lung. However, since temporal variations in elastance is evident in asthma [127, 128] and perhaps even more so in COPD [110], according to our findings it is possible that the exhibited frequency dependence in resistance of subjects may also have been due in part to the temporal variations in elastance. Thus while it is clear that heterogeneity is present and contributes to the frequency dependence of resistance, this may mean that the heterogeneity they needed to account for the data was overestimated.

The frequency dependence of resistance that is described to account for tissue viscoelasticity is most frequently modeled using the constant phase model. We can compare our result to the constant phase formula, by rearranging equation (5.11) as:

$$Z(j\omega,t) = R_L(t) + \frac{\frac{\dot{E_L}(t)}{\omega} - j\left(E_L(t) - \dot{R_L}(t)\right)}{\omega} \tag{5.16}$$

The similarity to the constant phase model equation (5.12) is readily apparent, with G $= \frac{\dot{E_L}(t)}{\omega}$, $H = E_L(t) - \dot{R_L}(t)$ and $\alpha = 1$. Here G depends on the derivative of E_L and is frequency dependent. However as G is estimated from oscillatory perturbations [52], the derivative of any oscillatory component in $E_L(t)$ will bring out an ω in $\dot{E_L}(t)$, canceling ω in $\frac{\dot{E_L}(t)}{\omega}$, predicting a constant G. This is true in the case of either linear or nonlinear pressure-volume relationships. For example, see appendix C where we have derived $\dot{E_L}(t)$ utilizing the Salazar and Knowles pressure-volume equation [132]. Turning our attention to H, the tissue elastance, our results indeed include $E_L(t)$ but also the term time derivative of $R_L(t)$. It is important to note that the variations in resistance are smaller than elastance. In our case, for example in health, R_L is 8 times smaller than E_L and almost negligible although we included it in our simulations. Lastly, the constant phase model has an exponent, α, that is due to the fact that $\frac{1}{\omega}$ dependence in resistance is not perfectly hyperbolic, with α typically just slightly smaller than unity [37]. In fact, when fitting the constant phase model, it is usual to start by fitting G and H with the data and tuning α for an more optimal fit. Here we can show that time-varying can account for the bulk of constant phase behaviour but only for $\alpha = 1$. Any remaining deviation from hyperbolic form could arise from tissue viscoelasticity.

It is very important to note that even a very small time-varying behavior in elastance will increase the resistance at low frequencies due to the amplification factor of $\frac{1}{\omega}$ in the real part of equation (5.11). This finding is important because it is established that the variability of both resistance and reactance increase with disease severity [98, 137]. We find this fascinating, that both temporal variation in elastance is increased in disease and heterogeneity in impedance is increased in disease. This brings to light to an intriguing possibility, either they are independent, and the time-course of variability of elastance is an under recognized factor contributing to frequency dependence, or that there may be some mechanistic link between the development or increase in temporal

variation in elastance and the development or increase in heterogeneity within the airways.

These conclusions require that indeed elastance varies, at the frequency used to determine the impedance. However, this seems reasonable whether the time-varying behavior arises from breathing, and mechanics are determined from spontaneous breathing and measurement of transmural pressure and airway flow, or whether the time-varying behavior occurs during measurement of respiratory mechanics using mechanical ventilation such as the optimum ventilatory waveform (OVW), studies with voluntary apnea [28, 122] or paralysis [36, 40, 129-131]. Elastance would vary with volume-pressure swings that excite any nonlinearity in the respiratory system, such as the pressure volume relation, or periodic peripheral airway closure and reopening, or airflow limitation, which is an inherently nonlinear mechanism, as is well demonstrated in obstructive disease.

This phenomenon could also explain the frequency dependence in oscillatory studies of lung tissue strips. It is well established that the impedance of lung tissue strips has a strong inverse frequency dependence [140]. Knowing that nonlinearities cause a time-varying behavior, along with the fact that perturbations cause a small time-varying behavior in tissue elasticity, we hypothesize that the frequency dependence in tissue strips by perturbations is caused by time-varying behavior of the elastance. Bates et al [140] postulated that the striking $\frac{1}{\omega}$ frequency dependence of lung tissue resistance was related to the recruitment phenomenon arising from the elastic stress-strain curve of the collagen network. This recruitment/derecruitment behaviour is required for modeling the nonlinearity in the lung tissue, which by itself under oscillatory loading produces a time-varying stiffness. The time-frequency transfer function we have derived suggests that any respiratory system with nonlinearity in its elastic term would necessarily produce a frequency dependence in the real part. Here we show that the temporal variations in the elasticity can lead to this frequency dependent behaviour, therefore Bates's intuition may have been correct.

Hysteresivity is known to increase with increasing heterogeneity although Thorpe *et al* [25] and Bates *et al* [125] showed in a modeling study that this is up to a point, and

further or extreme heterogeneity will eventually reverse this and decrease η. The authors described the reason to why the change from increase to decrease in η is not observed in experimental studies to the sudden closure of airways before reaching the extreme heterogeneous conditions. Our results with increasing heterogeneity agrees with the increase in hysteresivity in a specific frequency range, however, we also show that time-variation, even without heterogeneity can produce an increase in η as well. This may be important, for cases with upper airway narrowing or for large amplitude ventilation without much heterogeneity. η may increase due to the increase in time variation of E_L, which may explain in part why in experimental studies η hasn't decreased in contrast to the modeling studies. This could be found in Figure 5.8 where a decrease in η due to heterogeneity at a certain frequency range could be compensated by an increase in time-varying. For example, assuming that the disease severity starts from a time invariant heterogeneous state (black line in Figure 5. 8 for $R_2 = 5R_1$) and deteriorates to a time-varying state with higher heterogeneity (grey line in Figure 5.8 for $R_2 = 10R_1$), η remains higher at all frequencies.

In summary we have extended the interpretation of the mechanics of the respiratory system using linear time-varying analysis methods to account for the time-varying behaviour of the parameters of the respiratory mechanics. We show that this can predict the inverse hyperbolic frequency dependence of the real part of the impedance and this largely arises from time-varying elastic behaviour. This result is important because frequency dependence of resistance is established to be directly related to the severity of disease providing a novel mechanism for this important behaviour. Furthermore, we found that Hanning windowing reduced the impact of variations in elastance on frequency dependence of Resistance. When variation in E is present, differences in windowing methodology could thus contribute to differences in the magnitude of frequency dependence reported in the literature. The windowing methodology may thus need to be standardized if frequency dependence of Rrs is to be used clinically.

5.5 APPENDIX. A

For a linear time-varying system of input $x(t)$ and output $y(t)$ we can represent the system with an ordinary differential equation below with time-varying parameters of a_n and b_n:

$$a_n(t)\frac{d^n y(t)}{dt^n} + \cdots + a_1(t)\frac{dy(t)}{dt} + a_0(t)y(t) = b_m(t)\frac{d^m x(t)}{dt^m} + \cdots + b_1(t)\frac{dx(t)}{dt} + b_0(t)x(t) \quad \text{(A 5.1)}$$

Zadeh [60] introduced the transfer function, $H(j\omega, t)$, as the response of the time-varying system, $h(t, \tau)$, to an everlasting exponential input $x(t) = e^{j\omega t}$:

$$H(j\omega, t) = \int_{-\infty}^{\infty} h(t, \tau)\, e^{-j\omega t}\, d\tau \quad \text{(A 5.2)}$$

Using equation (A 5.2) in equation (A 5.1), he came to the general solution of equation (A 5.3):

$$\alpha_n(t)\frac{d^n H(j\omega,t)}{dt^n} + \cdots + \alpha_1(t)\frac{dH(j\omega,t)}{dt} + \alpha_0(t)H(j\omega, t) = K(j\omega, t) \quad \text{(A 5.3)}$$

where $K(j\omega, t)$ and $L(j\omega, t)$ are respectively the numerator and the denominator of the impedance transfer function before applying the method and $\alpha_n(t) = \frac{1}{n!}\ \frac{\partial^n L(j\omega,t)}{\partial(j\omega)^n}$ with $n = 0, 1, \ldots$ as the approximation order.

Rewriting the equation of motion [equation (5.8)] in frequency-domain [equation (5.10)] with time-varying resistance and elastance gives:

$$j\omega . P(j\omega) = [R_L(t) . j\omega + E_L(t)] . Q(j\omega) \quad \text{(A 5.4)}$$

To solve for equation (A 5.4) using Zadeh's method we know that $L(j\omega, t) = j\omega$, therefore:

$$\alpha_1(t) = \frac{\partial(j\omega)}{\partial(j\omega)} = 1 \qquad \text{(A 5.5)}$$

and consequently $\alpha_2(t),\ \alpha_3(t), \dots, \alpha_n(t) = 0$. Therefore equation (A 5.6) is the differential equation of the time-varying single-compartment lung:

$$\frac{dZ}{dt} + (j\omega).Z = R_L(t).j\omega + E_L(t) \qquad \text{(A 5.6)}$$

where Z is used to represent $Z(j\omega, t)$. To solve the differential equation (A 5.6) we use a common approximation technique used in the Zadeh [60]. Rearrangement of (A.6) yields:

$$Z = \frac{R_L(t).j\omega + E_L(t)}{j\omega} - \frac{1}{j\omega}\frac{dZ}{dt} \qquad \text{(A 5.7)}$$

therefore,

$$Z_1 = \frac{R(t).j\omega + E(t)}{j\omega}$$

$$Z_2 = -\frac{1}{j\omega}\frac{dZ_1}{dt} \qquad \text{(A 5.8)}$$

Substituting Z_1 in Z_2 gives:

$$Z_2 = -\frac{(j\omega).\frac{d\left(R_L(t)\right)}{dt} + \frac{d\left(E_L(t)\right)}{dt}}{(j\omega)^2} \qquad \text{(A 5.9)}$$

Adding Z_1 and Z_2 provides the second order approximation to Z:

$$Z(j\omega,t)=\frac{R_L(t).j\omega+E_L(t)}{j\omega}-\frac{j\omega.\frac{d\left(R_L(t)\right)}{dt}+\frac{d\left(E_L(t)\right)}{dt}}{(j\omega)^2}=R_L(t)+\frac{\frac{d\left(E_L(t)\right)}{dt}}{(\omega)^2}+\frac{E_L(t)-\frac{d\left(R_L(t)\right)}{dt}}{j\omega}$$

(A 5.10)

It is important to mention that if inertance was included in equation (A 5.10), it's like E and R, it's derivative would also contribute, and like E_L, the inertance would contribute as a additional constant to the resistive part, however, because the inertance is very small, and likely its variation even smaller, it can be neglected, particularly in these low frequencies we explored here.

5.6 APPENDIX. B

Here we demonstrate the time varying impedance derived for the two compartment model. Using equation (5.11) for the impedance of each lobe equation (B 5.1) with index, n, in equation (5.12) and separating resistance and elastance yields:

$$Z_n=R_n(t)+\frac{\dot{E_n}(t)}{(\omega)^2}+\frac{E_n(t)-\dot{R_n}(t)}{j\omega} \qquad \text{(B 5.1)}$$

$$R_{\mathrm{TC}}=$$

$$R_C+\frac{\omega^2R_1R_2(R_1+R_2)+(\mathrm{El}_2^2R_1+\mathrm{El}_1^2R_2)}{\left(\dot{R_1}+\dot{R_2}-\mathrm{El}_1-\mathrm{El}_2\right)^2+\left(\frac{\dot{\mathrm{El}}_1}{\omega}+\frac{\dot{\mathrm{El}}_2}{\omega}+\omega(R_1+R_2)\right)^2}+$$

$$\dot{\mathrm{El}}_1\dot{\mathrm{El}}_2\left(\dot{\mathrm{El}}_1+\dot{\mathrm{El}}_2\right)+\omega^2\left(\dot{\mathrm{El}}_2\dot{R_1}^2+\dot{\mathrm{El}}_1\dot{R_2}^2\right)$$

$$-2\omega^2\left(\dot{\mathrm{El}}_2\dot{R_1}\mathrm{El}_1+\dot{\mathrm{El}}_1\dot{R_2}\mathrm{El}_2\right)+$$

$$\omega^2(\dot{\mathrm{El}}_2\mathrm{El}_1^2+\dot{\mathrm{El}}_1\mathrm{El}_2^2)+\omega^2(\dot{\mathrm{El}}_2^{\,2}R_1+\dot{\mathrm{El}}_1^{\,2}R_2)$$

$$+\omega^4\left(\dot{R_2}^2R_1+\dot{R_1}^2R_2\right)-2\omega^4\left(\dot{R_2}\mathrm{El}_2R_1+\dot{R_1}\mathrm{El}_1R_2\right)+$$

$$\frac{2\omega^2\dot{\mathrm{El}}_1\dot{\mathrm{El}}_2(R_1+R_2)+2\omega^4R_1R_2(\dot{\mathrm{El}}_1+\dot{\mathrm{El}}_2)+\omega^4(\dot{\mathrm{El}}_2R_1^2+\dot{\mathrm{El}}_1R_2^2)}{\omega^4\left(\left(\dot{R_1}+\dot{R_2}-\mathrm{El}_1-\mathrm{El}_2\right)^2+\left(\frac{\dot{\mathrm{El}}_1}{\omega}+\frac{\dot{\mathrm{El}}_2}{\omega}+\omega(R_1+R_2)\right)^2\right)}$$

(B 5.2)

$$E_{\mathrm{TC}} =$$

$$\frac{El_1El_2(El_1+El_2)+\omega^2\left(El_2\mathrm{R}_1^2+El_1\mathrm{R}_2^2\right)}{\left(\dot{R_1}+\dot{R_2}-\mathrm{El}_1-\mathrm{El}_2\right)^2+\left(\frac{\dot{\mathrm{El}_1}}{\omega}+\frac{\dot{\mathrm{El}_2}}{\omega}+\omega(R_1+R_2)\right)^2}+$$

$$-\omega^2\dot{\mathrm{R}_1}\dot{\mathrm{R}_2}\left(\dot{\mathrm{R}_1}+\dot{\mathrm{R}_2}\right)-\left(\dot{El_2}^2\dot{\mathrm{R}_1}+\dot{El_1}^2\dot{\mathrm{R}_2}\right)+2\omega^2\dot{\mathrm{R}_1}\dot{R_2}(\mathrm{El}_1+\mathrm{El}_2)$$
$$+\left(\dot{\mathrm{El}_2}^2\mathrm{El}_1+\dot{\mathrm{El}_1}^2\mathrm{El}_2\right)$$
$$+\omega^2\left(\dot{R_1}^2\mathrm{El}_2+\dot{R_2}^2\mathrm{El}_1\right)$$
$$-\omega^2\left(\dot{El_2}^2\dot{\mathrm{R}_1}+\dot{El_1}^2\dot{\mathrm{R}_2}\right)-2\omega^2El_1El_2\left(\dot{\mathrm{R}_1}+\dot{\mathrm{R}_2}\right)$$
$$+2\omega^2\left(\dot{El_1}\mathrm{El}_2R_1+\dot{El_2}\mathrm{El}_1R_2\right)$$
$$\frac{-2\omega^2\left(\dot{\mathrm{El}_2}\dot{R_1}\mathrm{R}_2+\dot{\mathrm{El}_1}\dot{R_2}\mathrm{R}_1\right)-\omega^4(\dot{\mathrm{R}_2}\mathrm{R}_1^2+\dot{\mathrm{R}_1}\mathrm{R}_2^2)}{\omega^2\left(\left(\dot{R_1}+\dot{R_2}-\mathrm{El}_1-\mathrm{El}_2\right)^2+\left(\frac{\dot{\mathrm{El}_1}}{\omega}+\frac{\dot{\mathrm{El}_2}}{\omega}+\omega(R_1+R_2)\right)^2\right)} \qquad \text{(B 5.3)}$$

5.7 APPENDIX. C

Salazar and Knowles [130] introduced their well-known pressure-volume relationship [equation (C 5.1)] from integrating [equation (C 5.2)]:

$$V = V_0(1 - e^{-KP}) \qquad \text{(C 5.1)}$$

$$\frac{dV}{dP} = K(V_0 - V) \qquad \text{(C 5.2)}$$

where K is a constant, P is pressure change, V is the actual volume change, and V_0 is the volume and total lung capacity (TLC). Knowing that $\frac{dV}{dP} = \frac{1}{E}$, we can calculate the derivative of elastance with respect to time using equation (C 5.2):

$$\dot{E} = \frac{\dot{V}}{K(V_0 - V)^2} \qquad \text{(C 5.3)}$$

Assuming that the FOT oscillations of pure sinusoids are applied ($V = V_{FOT}\sin(\omega t)$) we will have:

$$\dot{E} = \frac{\omega V_{FOT}\cos(\omega t)}{K(V_0 - V_{FOT}\sin(\omega t))^2} \qquad \text{(C 5.4)}$$

Chapter 6: Discussion

In this chapter, I first summarize the work presented in the thesis, then discuss the original findings and finally suggest future directions.

6.1 Summary

6.1.1 Airway Oscillometry Using Piezoelectric Actuator

Chapter 3 of this thesis presented the design and simulation of a new design for single frequency airwave oscillometry. This novel design used a piezoelectric bimorph actuator on resonance to create oscillations of air that is more commonly produced by electromagnetic actuators such as found in loudspeakers. To predict the performance in measuring the respiratory mechanics of human subjects, the dynamic model was simulated in SIMULINK, and included realistic respiratory impedance loads, and realistic breathing noise recorded from subjects. Model performance was also validated in a scaled prototype device. We found that while breathing noise substantially lowered SNR, the model could produce sufficient pressure and flows for acceptable SNR and accuracy. Also, the air-gap leak that is originated from the oscillating mesh and non-ideal mechanical insulation was modeled and a threshold resistance against the leak was found. Together the results of the simulations and the scaled prototype device indicated that this design is a feasible approach to develop an accurate lightweight, portable, single-frequency FOT device [108].

6.1.2 Accuracy Of Tracking Impedance Versus Time

Chapter 4 of this thesis focused on tracking impedance versus time while performing single frequency airwave oscillometry. This was motivated because it is increasingly clear that there exists important information contained in the breath-by-breath variations of impedance about the health of the lung. However, there was very little work evaluating the accuracy of estimating time-varying resistance and reactance

from pressure and flow data. In this chapter we analytically and computationally developed a time-frequency transfer function that revealed an increasing error with increasing breathing rate, then we evaluated the accuracy of STFT methods in tracking time-varying impedance in simulations of a sample population (children). As expected however, these errors were much higher than noise-free simulations. We also used the Goertzel algorithm to perform STFT improving algorithm efficiency. In a clinical sense our results emphasized on the existing knowledge that for accurate measurements of time-varying mechanics, subject's breathing rate has to stay low. Moreover, the time-frequency transfer function implied the influence of time-varying elastance on estimated resistance which became the inspiration to research presented in chapter 5.

6.1.3 Frequency Dependence Of Impedance And Time-Varying Impedance

It is established that the frequency dependence of resistance increases in disease as measured by either OS or OVW. On the other hand, other researchers have established in COPD that variations in reactance and therefore variations in elastance arising from within-breath flow limitation is an indication of disease [110]. The analytical formula for time-varying respiratory impedance from chapter 4 showed that these two camps of research might have more in common that was known previously. In this chapter we first analyzed the equation of motion of a single compartment respiratory system with a time-varying resistance and a time-varying elastance and proved that variations in elastance in fact do influence the frequency dependence of resistance. Then we used the same analytical formula from chapter 4 in simulations demonstrating the effect, and evaluating the magnitude of this effect using variations in impedance and mean impedance values typical for different disease models. Indeed the existence of this mechanism requires variations in elastance, however, this seems inevitably present as the time-varying behavior arises from breathing during OS or by induced ventilation waveform at the frequency that OVW is applied. Although this effect is much smaller in OS studies as they are smaller oscillations at higher frequencies, the implications on OVW studies specifically on animal would be significant and indistinguishable from the other

mechanisms associated with frequency dependence including tissue viscoelasticity and heterogeneity of the lung. This is important because frequency dependence of resistance is known to be correlated to the severity of disease.

An important question that arises from this finding is how much of the frequency dependence of resistance already seen in the literature is arising from time-varying elastance. Given the similarity between the constant phase model and the time-varying model that was shown in Eq. (15) of chapter 5, we can speculate that these three mechanisms might be interconnected. For example, nonlinearities in stress-strain relationships or the recruitment phenomena that are already linked to tissue viscoelasticity and heterogeneity can lead to causing variations in elastance and hence giving rise to frequency dependence of resistance. More importantly, from another point of view, if we think of lung as a heterogeneous system by nature and assume that the frequency dependence is already existent in the frequency spectrum of resistance, this gives rise to time-varying resistance and elastance.

Moreover, we found that increasing variations in mechanics also increases η. This is important because although the constant phase model is perhaps not the most appropriate to describe heterogeneity it nevertheless is able to account for altered mechanics due to heterogeneity, and researchers have linked the increase in heterogeneity or increase in disease severity with increase in η. However, modeling studies that include heterogeneity expect a decrease in η with high amounts of heterogeneity. We speculate that including the variations as another mechanism that correlates to disease severity can further explain increases and decreases in η.

6.3 Original Contributions Made

This list states the novel contributions made by this thesis.

1) I developed a novel model to simulate the mechanics of a novel piezoelectric actuator with realistic respiratory loads simulating different disease states in both adult and child subject populations. The model also included real recorded noise from several

subjects that was added to the simulation, scaling the noise cover a wide range of signal to noise ratios.

2) This model demonstrated that the use of a single frequency piezo-electric actuator driven OS device was a feasible approach, and could be used to measure respiratory mechanics.
3) I adapted Zadeh's method for continuous time-frequency analysis to develop an estimator of the error or bias that occurs due to time variation of the respiratory parameters assed using oscillometry. While this estimator was able to predict error at relatively slow respiration rates, it underestimated the true error that occurs during standard STFT, sequential windowed analysis of impedance with added noise.
4) I also estimated the accuracy of the STFT based approach for estimating respiratory impedance from time varying systems, using a model including realistic respiratory loads, and real recording breathing noise. This revealed that at high breathing rates, 0.4 Hz and above, errors in estimating impedance would exceed 10%.
5) I used the Goertzel algorithm to perform STFT based analysis of respiratory impedance that reduced the computational cost of transformation to frequency-domain when only a few frequencies are desired for the computation of impedance.
6) I showed using Zadeh's time-frequency method that although time-varying resistance can influence the estimation of elastance, this was negligible because the magnitude of the time derivative of resistance is much smaller than elastance.
7) I also showed in the time-domain (equation (8) in chapter 5) and time-frequency domain (equation (11) in chapter 5) that time-varying elastance influences the estimation of resistance and reveals a novel mechanism that can contribute to the well-established frequency dependence of resistance. This is important because the level of variations can be used to diagnoses the level of frequency dependence and hence the level of disease.
8) I provided a possible mechanism to why hysteresivity (η) from the constant phase model does not follow the dependence on heterogeneity predicted by heterogeneous respiratory impedance models.

6.4 Future Directions

This thesis produced multiple interesting findings and a very novel and surprising discovery regarding the origin of frequency dependence in respiratory mechanical systems. Also the thesis is not without limitations. These findings and limitations lead to possible future studies that I suggest for future work.

1) Chapter 3 proved that a piezoelectric cantilever can be successfully used as motor for OS; however, accuracy was sensitive to noise, leak and nonlinearity. Thus a future device must be made with the recommended amplitude and low leak as recommended. I would also recommend if possible to have as accurate as possible transducer measurement accuracy, and perhaps to explore optimizing the mesh to provide as stable and linear resistance. To achieve larger amplitude for even better SNR, the use of levers to amplify the oscillations may be considered if the SNR gain is worth the added mechanical complexity. Also, while I demonstrated feasibility over a wide range of breathing amplitudes, the actuator is possibly susceptible to larger transient breathing efforts as it is compliant. If this is too frequent or it's undesirable to remove these transients in post processing, using two actuators to stiffen the system could be done at minimal extra cost to reduce the vulnerability against the breathing load of the patient.
2) Chapter 4 showed that using STFT with multiple windows was a very accurate method for estimating average impedance despite time-variation of underlying impedance, however, it was not as accurate for tracking the variations of impedance, particularly if subjects breathed rapidly. While improvements in both signal analysis techniques, particularly in windowing as the results of chapter 5 can be explored with taking longer recording or repeating measurements where possible, it is also recommended in the case of rapid breathing to coach subjects to breathe slower where possible.
3) In chapter 4 I only investigated sinusoidally varying resistance and elastance. To be more realistic, it may be useful to develop a more complicated model with a broader

spectrum of resistance and elastance variation, using estimates from recorded temporal variation in impedance.

4) I also only modeled the typical child with mild to moderate asthma impedance with realistic added noise. It would be useful to include recorded noise from other patient populations, particularly COPD.
5) I developed an estimator of the error involved in estimating temporally varying respiratory impedance parameters based on the analytical method of Zadeh. This is a continuous analytical approach and does not include errors that arise from the STFT method with discrete sequential windows employed to track impedance in the literature. I demonstrated the estimator underestimated the true error. It is possible that an estimator that included the effects of windowing might be developed to help provide a more accurate and independent estimate of the error that may be incurred when using this method for tracking impedance variation.
6) To further generalize the study, the same method could be applied to multi-compartment models and other common respiratory system models to analyze the influence of time-varying impedance in estimation of models with greater numbers of parameters.
7) Similarly, in chapter 5, I only analyzed the single compartment model and a two-compartment model composed to the two single compartment models in parallel. This proved fairly complex analytically, and is not recommended for multi-compartment modelling. It may be possible to develop a Zadeh analysis for the effects of time variation within a multi-compartment model including the effects of variation of elastance and resistance that occurs with different phase as this is known to occur in the lung. How this might contribute to frequency dependence of resistance may be of interest.
8) Introducing time-varying elastance as another source of frequency dependence of resistance gives rise to the important question of: how much of the frequency dependence seen in the literature is due to this phenomenon, relative to tissue viscoelasticity and relative to multi-compartment heterogeneity. Experimental studies can be designed to measure the temporal variation of elastance, and with methods to assess heterogeneity to help elucidate the magnitude of the contribution.

9) The fact that temporal variation in elastance even in a single compartment model leads to frequency dependence of resistance, has some resemblance to the behavior in two compartment model as demonstrated by Otis that change in the reactive parameters (such as heterogeneity in elastance) leads to a change in the real part or the resistance and vice versa. While it may be as simple as that, the question occurs that how does the variation behavior in the elastance which is an energy storage element influence the energy dissipation? This type of coupling in a single compartment model leads to some fundamental questions on the nature of frequency dependence of resistance that may influence our understanding of tissue viscoelasticity and also heterogeneity. For example the nonlinearity in the respiratory system of flow limitation lead to the variable elastance used as a basis for modelling in this thesis, leading to frequency dependence of resistance. However lung tissue also demonstrates frequency dependence of resistance. Is there a similar mechanism at work there as well? Perhaps rather, or in addition to, distributed time constants that may be present in lung tissue mechanics, instead an underlying mechanism that may contribute is the variations in elastance as the oscillatory impedance is probed, perhaps via derecruitment-recruitment mechanisms, or fluidization and gelling behaviors as the tissue goes through both different levels of stretch, and different levels of stretch rate. These questions could be explored both through analytical and computation modelling approaches as well as experimental approaches.

REFERENCES

[1] DuBois, Arthur B., Stella Y. Botelho, and Julius H. Comroe Jr. "A new method for measuring airway resistance in man using a body plethysmograph: values in normal subjects and in patients with respiratory disease." *Journal of Clinical Investigation* 35, no. 3 (1956): 327.

[2] Oostveen, E., D. MacLeod, H. Lorino, R. Farre, Z. Hantos, K. Desager, and F. Marchal. "The forced oscillation technique in clinical practice: methodology, recommendations and future developments." *European Respiratory Journal* 22, no. 6 (2003): 1026-1041.

[3] Daróczy B and Hantos Z 1982 An improved forced oscillatory estimation of respiratory impedance *Int J Biomed Comput* 13 221-35

[4] Delavault E, Saumon G and Georges R 1980 Characterization and validation of forced input method for respiratory impedance measurement *Respir Physiol* 40 119-36

[5] Lándsér F J, Nagles J, Demedts M, Billiet L and van de Woestijne K P 1976 A new method to determine frequency characteristics of the respiratory system *J Appl Physiol* 41 101-6

[6] Michaelson E D, Grassman E D and Peters W R 1975 Pulmonary mechanics by spectral analysis of forced random noise *J Clin Invest* 56 1210-30

[7] N. B. Pride, “Forced oscillation techniques for measuring mechanical properties of the respiratory system.,” *Thorax*, vol. 47, no. 4, pp. 317–20, Apr. 1992.

[8] Schuessler, Thomas F., and Jason HT Bates. "A computer-controlled research ventilator for small animals: design and evaluation." *Biomedical Engineering, IEEE Transactions on* 42, no. 9 (1995): 860-866.

[9] Posada, Lucas. "PIEZOELECTRIC MULTILAYER BENDING ACTUATED OSCILLOMETRY PROTOTYPE." (2015).

[10] Farre R.,Navajas, D., and Rotger, M. M., (1987): 'Spectrum adapted excitation signals in measuring respiratory impedance', Bull. Eur. Physiopathol. Respirat., 23, suppl. 12, p. 324

[11] Suki B, Peslin R, Duvivier C and Farré R 1989 Lung impedance in healthy humans measured by forced oscillations from 0.01 to 0.1 Hz *J Appl Physiol (1985)* 67 1623-9

[12] Hall G L, Hantos Z, Peták F, Wildhaber J H, Tiller K, Burton P R and Sly P D 2000 Airway and respiratory tissue mechanics in normal infants *Am J Respir Crit Care Med* 162 1397-402

[13] Lutchen K R, Hantos Z, Peták F, Adamicza A and Suki B 1996 Airway inhomogeneities contribute to apparent lung tissue mechanics during constriction *J Appl Physiol* 80 1841-9

[14] Lutchen K R, Suki B, Zhang Q, Petak F, Daroczy B and Hantos Z 1994 Airway and tissue mechanics during physiological breathing and bronchoconstriction in dogs *J Appl Physiol* 77 373-85

[15] King G G, Downie S R, Verbanck S, Thorpe C W, Berend N, Salome C M and Thompson B 2005 Effects of methacholine on small airway function measured by forced oscillation technique and multiple breath nitrogen washout in normal subjects *Respir Physiol Neurobiol* 148 165-77

[16] Cavalcanti J V, Lopes A J, Jansen J M and Melo P L 2006 Detection of changes in respiratory mechanics due to increasing degrees of airway obstruction in asthma by the forced oscillation technique *Respir Med* 100 2207-19

[17] Cavalcanti J V, Lopes A J, Jansen J M and de Melo P L 2006 Using the forced oscillation technique to evaluate bronchodilator response in healthy volunteers and in asthma patients presenting a verified positive response *J Bras Pneumol* 32 91-8

[18] Van Noord J A, Smeets J, Clément J, Van de Woestijne K P and Demedts M 1994 Assessment of reversibility of airflow obstruction. *Am J Respir Crit Care Med* 150 551-4

[19] Van Noord J A, Clément J, Van de Woestijne K P and Demedts M 1991 Total respiratory resistance and reactance in patients with asthma, chronic bronchitis, and emphysema *Am Rev Respir Dis* 143 922-7

[20] Clément J, Làndsér F J and Van de Woestijne K P 1983 Total resistance and reactance in patients with respiratory complaints with and without airways obstruction. *Chest* 83 215-20

[21] Downie S R, Salome C M, Verbanck S, Thompson B R, Berend N and King G G 2013 Effect of methacholine on peripheral lung mechanics and ventilation heterogeneity in asthma *J Appl Physiol (1985)* 114 770-7

[22] Kjeldgaard J M, Hyde R W, Speers D M and Reichert W W 1976 Frequency dependence of total respiratory resistance in early airway disease *Am Rev Respir Dis* 114 501-8

[23] Hantos Z, DarÃ³czy B, Suki B and Nagy S 1987 Low-frequency respiratory mechanical impedance in the rat. p 36

[24] Lutchen K R and Gillis H 1997 Relationship between heterogeneous changes in airway morphometry and lung resistance and elastance *J Appl Physiol* 83 1192-201

[25] Thorpe C W and Bates J H 1997 Effect of stochastic heterogeneity on lung impedance during acute bronchoconstriction: a model analysis *J Appl Physiol* 82 1616-25

[26] Otis A B, McKerrow C B, Bartlett R A, Mead J, McIlroy M B, Selver-Stone N J and Radford E P, Jr. 1956 Mechanical factors in distribution of pulmonary ventilation *J Appl Physiol* 8 427-43

[27] Mead J 1969 Contribution of compliance of airways to frequency-dependent behavior of lungs *J Appl Physiol* 26 670-3

[28] Kaczka D W, Ingenito E P, Suki B and Lutchen K R 1997 Partitioning airway and lung tissue resistances in humans: effects of bronchoconstriction. *J Appl Physiol* 82 1531-41

[29] Kaczka D W, Ingenito E P, Israel E and Lutchen K R 1999 Airway and lung tissue mechanics in asthma. Effects of albuterol. *Am J Respir Crit Care Med* 159 169-78

[30] Gillis H L and Lutchen K R 1999 How heterogeneous bronchoconstriction affects ventilation distribution in human lungs: a morphometric model *Ann Biomed Eng* 27 14-22

[31] Lutchen K R, Greenstein J L and Suki B 1996 How inhomogeneities and airway walls affect frequency dependence and separation of airway and tissue properties *J Appl Physiol (1985)* 80 1696-707

[32] Mount L E 1955 The ventilation flow-resistance and compliance of rat lungs *J Physiol* 127 157-67

[33] Bates J H, Decramer M, Zin W A, Harf A, Milic-Emili J and Chang H K 1986 Respiratory resistance with histamine challenge by single-breath and forced oscillation methods *J Appl Physiol* 61 873-80

[34] Bates J H, Ludwig M S, Sly P D, Brown K, Martin J G and Fredberg J J 1988 Interrupter resistance elucidated by alveolar pressure measurement in open-chest normal dogs *J Appl Physiol* 65 408-14

[35] Bates J H, Abe T, Romero P V and Sato J 1989 Measurement of alveolar pressure in closed-chest dogs during flow interruption *J Appl Physiol* 67 488-92

[36] Hantos Z, Daróczy B, Suki B, Nagy S and Fredberg J J 1992 Input impedance and peripheral inhomogeneity of dog lungs *J Appl Physiol* 72 168-78

[37] Jason H.T. Bates, “Lung Mechanics: an Inverse Modeling Approach”, Cambridge University Press, 2009.

[38] Hirai T, McKeown K A, Gomes R F and Bates J H 1999 Effects of lung volume on lung and chest wall mechanics in rats *J Appl Physiol* 86 16-21

[39] Hantos Z, Adamicza A, Govaerts E and Daróczy B 1992 Mechanical impedances of lungs and chest wall in the cat *J Appl Physiol* 73 427-33

[40] Gomes R F, Shen X, Ramchandani R, Tepper R S and Bates J H 2000 Comparative respiratory system mechanics in rodents *J Appl Physiol* 89 908-16

[41] Wagers S, Lundblad L K, Ekman M, Irvin C G and Bates J H 2004 The allergic mouse model of asthma: normal smooth muscle in an abnormal lung? *J Appl Physiol* 96 2019-27

[42] Malmberg P, Larsson K, Sundblad B M and Zhiping W 1993 Importance of the time interval between FEV1 measurements in a methacholine provocation test *Eur Respir J* 6 680-6

[43] Kapsali T, Permutt S, Laube B, Scichilone N and Togias A 2000 Potent bronchoprotective effect of deep inspiration and its absence in asthma *J Appl Physiol* 89 711-20

[44] Allen G and Bates J H 2004 Dynamic mechanical consequences of deep inflation in mice depend on type and degree of lung injury *J Appl Physiol* 96 293-300

[45] Takubo Y, Guerassimov A, Ghezzo H, Triantafillopoulos A, Bates J H, Hoidal J R and Cosio M G 2002 Alpha1-antitrypsin determines the pattern of emphysema and function in tobacco smoke-exposed mice: parallels with human disease *Am J Respir Crit Care Med* 166 1596-603

[46] Tomioka S, Bates J H and Irvin C G 2002 Airway and tissue mechanics in a murine model of asthma: alveolar capsule vs. forced oscillations *J Appl Physiol* 93 263-70

[47] Suki B, Yuan H, Zhang Q and Lutchen K R 1997 Partitioning of lung tissue response and inhomogeneous airway constriction at the airway opening *J Appl Physiol* 82 1349-59

[48] Kaczka D W, Hager D N, Hawley M L and Simon B A 2005 Quantifying mechanical heterogeneity in canine acute lung injury: impact of mean airway pressure *Anesthesiology* 103 306-17

[49] Kaczka D W, Brown R H and Mitzner W 2009 Assessment of heterogeneous airway constriction in dogs: a structure-function analysis *J Appl Physiol* 106 520-30

[50] Kaczka D W, Lutchen K R and Hantos Z 2011 Emergent behavior of regional heterogeneity in the lung and its effects on respiratory impedance *J Appl Physiol (1985)* 110 1473-81

[51] Bates, J. H. T., G. N. Maksym, D. Navajas, and B. Suki. "Lung tissue rheology and 1/f noise." *Annals of biomedical engineering* 22, no. 6 (1994): 674-681.

[52] Maksym, Geoffrey N., Robert E. Kearney, and Jason HT Bates. "Nonparametric block-structured modeling of lung tissue strip mechanics." *Annals of biomedical engineering* 26, no. 2 (1998): 242-252.

[53] Lutchen K R, Yang K, Kaczka D W and Suki B 1993 Optimal ventilation waveforms for estimating low-frequency respiratory impedance *J Appl Physiol* 75 478-88

[54] Kaczka D W, Ingenito E P and Lutchen K R 1999 Technique to determine inspiratory impedance during mechanical ventilation: implications for flow limited patients *Ann Biomed Eng* 27 340-55

[55] Bhatawadekar, Swati. "Airway Impedance, Heterogeneity and Variability in Adult Asthma." (2015).

[56] Masoli M, Fabian D, Holt S, Beasley R and Program G I f A G 2004 The global burden of asthma: executive summary of the GINA Dissemination Committee report *Allergy* 59 469-78

[57] Grimby G, Takishima T, Graham W, Macklem P and Mead J 1968 Frequency dependence of flow resistance in patients with obstructive lung disease *J Clin Invest* 47 1455-65

[58] Lauzon, A. M., and J. H. T. Bates. "Estimation of time-varying respiratory mechanical parameters by recursive least squares." *J Appl Physiol* 71, no. 3 (1991): 1159-1165.

[59] Bhatawadekar, Swati A., Del Leary, Y. Chen, J. Ohishi, P. Hernandez, T. Brown, C. McParland, and Geoff N. Maksym. "A study of artifacts and their removal during forced oscillation of the respiratory system." *Annals of biomedical engineering* 41, no. 5 (2013): 990-1002.

[60] Zadeh, Lotfi A. "Frequency analysis of variable networks." *Proceedings of the IRE* 38, no. 3 (1950): 291-299.

[61] Sanchez, B., Ebrahim Louarroudi, R. Bragos, and Rik Pintelon. "Harmonic impedance spectra identification from time-varying bioimpedance: theory and validation." *Physiological measurement* 34, no. 10 (2013): 1217.

[62] Dellaca, Raffaele L., Alessandro Gobbi, Miriam Pastena, Antonio Pedotti, and Bartolomè Celli. "Home monitoring of within-breath respiratory mechanics by a simple and automatic forced oscillation technique device." *Physiological measurement* 31, no. 4 (2010): N11.

[63] Lorino, H., C. Mariette, M. Karouia, and A. M. Lorino. "Influence of signal processing on estimation of respiratory impedance." *Journal of Applied Physiology* 74 (1993): 215-215.

[64] Ionescu, Clara M., and Robin De Keyser. "Relations between fractional-order model parameters and lung pathology in chronic obstructive pulmonary disease." *Biomedical Engineering, IEEE Transactions on* 56, no. 4 (2009): 978-987.

[65] Tranter, William, K. Shanmugan, Theodore Rappaport, and Kurt Kosbar.*Principles of communication systems simulation with wireless applications*. Prentice Hall Press, 2003. Page 502

[66] Pintelon R, Louarroudi E and Lataire J 2012 Detection and quantification of the influence of time variation in frequency response function measurements using arbitrary excitations IEEE Trans. Instrum. Meas. 61 3387–95

[67] Sanchez, B., E. Louarroudi, E. Jorge, J. Cinca, R. Bragos, and R. Pintelon. "A new measuring and identification approach for time-varying bioimpedance using multisine electrical impedance spectroscopy." *Physiological measurement* 34, no. 3 (2013): 339.

[68] Pintelon, Rik, Ebrahim Louarroudi, and John Lataire. "Time-Variant Frequency Response Function Measurements on Weakly Nonlinear, Arbitrarily Time-Varying Systems Excited by Periodic Inputs."

[69] Piskorowski, Jacek, and Tomasz Barcinski. "Dynamic compensation of load cell response: A time-varying approach." *Mechanical Systems and Signal Processing* 22, no. 7 (2008): 1694-1704.

[70] Shih, Li Y., Casper W. Barnes, and Leonard A. Ferrari. "Estimate of attenuation coefficient for ultrasonic tissue characterization using time-varying state-space model." *Ultrasonic imaging* 10, no. 2 (1988): 90-109.

[71] Erfani, Shervin, Majid Ahmadi, and Nima Bayan. "Two-dimensional analog signal processing and its implications on circuit theory." *Analog Integrated Circuits and Signal Processing* (2015): 1-10.

[72] Zhu, Yan, Guoyong Shi, Frank Lee, and Andy Tai. "Symbolic time-varying root-locus analysis for oscillator design." In *New Circuits and Systems Conference (NEWCAS), 2012 IEEE 10th International*, pp. 165-168. IEEE, 2012.

[73] Louarroudi, E., J. Lataire, and R. Pintelon. "Nonparametric estimation of the instantaneous transfer function of linear periodically time-varying systems excited by arbitrary signals." In *Instrumentation and Measurement Technology Conference (I2MTC), 2012 IEEE International*, pp. 1435-1440. IEEE, 2012.

[74] Min, B. G., W. Welkowitz, and S. Fich. "Frequency analysis of time-varying elastance model of the left ventricle." *Bulletin of mathematical biology* 42, no. 2 (1980): 173-180.

[75] T. Morita, “Miniature piezoelectric motors”, *Sensors and Actuators A* 103, pp. 291-300. 2003.

[76] Uchino, K., K. Kato and M. Tohda, "Ultrasonic Linear Motors Using a. Multilayered Piezoelectric Actuator" *Ferroelectrics* 87, 331-334. 1988.

[77] Qing-Ming Wang, Xiao-hong Du, Baomin Xu, and L. Eric Cross, “Electromechanical Coupling and Output Efficiency of Piezoelectric Bending Actuators” *IEEE Transactions on Ultrasonics, Ferroelectrics, and Frequency Control*, Vol. 46, pp. 638-646. 1999.

[78] Moskalik, Andrew. "Piezoelectric actuation: state of the art." (2001).

[79] Lumentut, M. F., and I. M. Howard. "Analytical and experimental comparisons of electromechanical vibration response of a piezoelectric bimorph beam for power harvesting." Mechanical Systems and Signal Processing 36, no. 1 (2013): 66-86.

[80] Shi, Huaduo, Jianguo Chen, Guoxi Liu, Wenlei Xiao, and Shuxiang Dong. "A piezoelectric pseudo-bimorph actuator." *Applied Physics Letters* 102, no. 24 (2013): 242904.

[81] Chattaraj, Nilanjan, and Ranjan Ganguli. "Multiobjective optimization of piezoelectric bimorph actuator with rigid extension." In *SPIE Smart Structures and Materials+ Nondestructive Evaluation and Health Monitoring*, pp. 94311V-94311V. International Society for Optics and Photonics, 2015.

[82] Kang, Jeonggoo, Jongsuh Lee, Heewon Kim, Kwangsu Cho, Semyung Wang, and Jeha Ryu. "Smooth vibrotactile flow generation using two piezoelectric actuators." *Haptics, IEEE Transactions on* 5, no. 1 (2012): 21-32.

[83] Qing-Ming Wang, Xiao-hong Du, Baomin Xu, and L. Eric Cross, "Electromechanical Coupling and Output Efficiency of Piezoelectric Bending Actuators" *IEEE Transactions on Ultrasonics, Ferroelectrics, and Frequency Control*, Vol. 46, pp. 638-646. 1999.

[84] Motoo, Kohei, N. A. O. Y. A. Toda, Toshio Fukuda, F. U. M. I. H. I. T. O. Arai, Koichi Kikuta, Shin-ichi Hirano, and Takayuki Matsuno. "Tailor-made multilayer piezoelectric actuator having large displacements and forces produced from lead-free piezoelectric ceramics." In *Micro-NanoMechatronics and Human Science, 2006 International Symposium on*, pp. 1-6. IEEE, 2006.

[85] Smits, Jan G., Susan I. Dalke, and Thomas K. Cooney. "The constituent equations of piezoelectric bimorphs." *Sensors and Actuators A: Physical* 28, no. 1 (1991): 41-61.

[86] Mason WP (1948) Electromechanical transducers and wave filters. D Van Nostrand, New York

[87] Redwood M (1961) Transient performance of a piezoelectric transducer. J Acoust Soc Am 33:527–536

[88] Kirmholtz R, Leedom DA, Mathaei GL (1970) New equivalent circuit for elementary piezoelectric transducers. Electron Lett 6:398–399

[89] Cady, W.G. (1922) The piezo-electric resonator. In: Proceedings of the Institute of Radio Engineers, Vol. 10, pp. 83–114

[90] Van Dyke, K.S. (1925) The electric network equivalents of a piezoelectric resonator. In: Physical Review. American Institute of Physics. Vol. 25, 895A

[91] Dubois AB, Brody AW, Lewis DH, Burgess BF Jr. (1956) Oscillation mechanics of lungs and chest in man. *J. Appl. Physiol*. 8:587–94.

[92] Dellacà RL, Pompilio PP, Walker PP, Duffy N, Pedotti A, Calverley PM. (2009) Effect of bronchodilation on expiratory flow limitation and resting lung mechanics in COPD. *Eur. Respir. J.* 33(6): 1329–37.

[93] H.-M. Cheng, M.T. Ewe, R. Bashir, G.T.-C. Chiu. (2001) Modeling and control of piezoelectric cantilever beam micro-mirror and micro-laser arrays to reduce image banding in electro photographic processes. *J.Micromech. Microeng*. pp. 11487–498.

[94] J. Goli, J. G. Smits, and A. Ballato. (1995) Dynamic bimorph matrix of end-loaded bimorphs. *IEEE Int. Freq. Contr. Symp*, pp. 794–797.

[95] Brown, N., Xuan, W., Salome, C., Berend, N., Hunter, M., Musk, A., James, A., King, G. (2010) Reference equations for respiratory system resistance and reactance in adults. *Respiratory physiology & neurobiology.* 172(3), 162-8.

[96] Navajas D, Alcaraz J, Peslin R, Roca J, Farre R. (2000) Evaluation of a method for assessing respiratory mechanics during noninvasive ventilation" *Eur Respir J*, 16:704-709.

[97] Van Den Bergh A, Kerrebijn K. (1985) Forced oscillation technique. Reference values for resistance and reactance over a frequency spectrum of 2–26 Hz in healthy children aged 2.3–12.5 years. *Bull Eur Physiopathol Respir* 21(2):171-8. 1985.

[98] Lall CA, Cheng N, Hernandez P, Pianosi PT, Dali Z, Abouzied A, Maksym GN. (2007) Airway resistance variability and response to bronchodilator in children with asthma. *Eur Respir J*, 30: 260 –268.

[99] Inman, D. (2001) Engineering vibration. Upper Saddle River. *N.J: Prentice Hall*.

[100] Rohrer, R. (1915) Der stroemungswiderstand in den menschlichen atemwegen und der einfluss der unregelmaessigen verzweigung des bronchialsystems auf den atmungsverlauf in verschiedenen lungenbezirken. *Arch. Ges. Physiol*. 162:225–229.

[101] A. Bouhuys, B. Jonson. (1967) Alveolar pressure, air flow rate, and lung inflation in man. *J. Appl. Physiol*. 22: 1086-l 100.

[102] Barbini, P., Cevenini, G. and Avanzolni, G. (2003) Nonlinear mechanisms determining expiratory flow limitation in mechanical ventilation: a model-based interpretation. *Ann. Biomed. Eng*. 31. 908-916.

[103] Schweitzer C, Chone C, Marchal F. (2003) Influence of data filtering on reliability ofrespiratory impedance and derived parameters in children. *Pediatr Pulmonol*, 36:502–508.

[104] Kaczka, David W., George M. Barnas, Bela Suki, and Kenneth R. Lutchen. "Assessment of time-domain analyses for estimation of low-frequency respiratory mechanical properties and impedance spectra." *Annals of biomedical engineering* 23, no. 2 (1995): 135-151.

[105] Dellacà, Raffaele L., Emanuela Zannin, Peter Kostic, Marie Andersson Olerud, Pasquale P. Pompilio, Goran Hedenstierna, Antonio Pedotti, and Peter Frykholm. "Optimisation of positive end-expiratory pressure by forced oscillation technique in a lavage model of acute lung injury." *Intensive care medicine* 37, no. 6 (2011): 1021-1030.

[106] Oppenheim, Alan V., Alan S. Willsky, and Syed Hamid Nawab. *Signals and systems*. Vol. 2. Englewood Cliffs, NJ: Prentice-Hall, 1983.

[107] Allen, Jont B., and L. A. W. R. E. N. C. E. Rabiner. "A unified approach to short-time Fourier analysis and synthesis." *Proceedings of the IEEE* 65, no. 11 (1977): 1558-1564.

[108] Alamdari, Hamed Hanafi, Lucas Posada, Swati A. Bhatawadekar, Jeremy A. Brown, and Geoffrey N. Maksym. "A resonance-mode piezoelectric device for measurement of respiratory mechanics." *Journal of Biomedical Science and Engineering* 6, no. 11 (2013): 1062.

[109] Farré, R., M. Rotger, and D. Navajas. "Time-domain digital filter to improve signal-to-noise ratio in respiratory impedance measurements." *Medical and Biological Engineering and Computing* 29, no. 1 (1991): 18-24.

[110] Dellaca, R. L., P. Santus, A. Aliverti, N. Stevenson, S. Centanni, P. T. Macklem, A. Pedotti, and P. M. A. Calverley. "Detection of expiratory flow limitation in COPD using the forced oscillation technique." *European Respiratory Journal*23, no. 2 (2004): 232-240.

[111] Thamrin, Cindy, Catherine L. Gangell, Kanokporn Udomittipong, Merci MH Kusel, Hilary Patterson, Takayoshi Fukushima, André Schultz, Graham L. Hall, Stephen M. Stick, and Peter D. Sly. "Assessment of bronchodilator responsiveness in preschool children using forced oscillations." *Thorax* 62, no. 9 (2007): 814-819.

[112] Robinson, Paul D., Martin Turner, Nathan J. Brown, Cheryl Salome, Norbert Berend, Guy B. Marks, and Greg G. King. "Procedures to improve the repeatability of forced oscillation measurements in school-aged children."*Respiratory physiology & neurobiology* 177, no. 2 (2011): 199-206.

[113] Timmins, Sophie C., Chantale Diba, Cindy Thamrin, Norbert Berend, Cheryl M. Salome, and Gregory G. King. "The feasibility of home monitoring of impedance with the forced oscillation technique in chronic obstructive pulmonary disease subjects." *Physiological measurement* 34, no. 1 (2013): 67.

[114] Dellaca, Raffaele, Bob Romano, Joe Garuccio, Cherian John, Ramesh Thimmiah, Melvin Saludes, and Charles Cain. "Automatic tailoring of positive end-expiratory pressure (PEEP) by forced oscillation technique (FOT) during non-invasive ventilation: Effects of posture and exertion in COPD." *European Respiratory Journal* 40, no. Suppl 56 (2012): P2063.

[115] Peslin, R., J. Felicio da Silva, F. Chabot, and C. Duvivier. "Respiratory mechanics studied by multiple linear regression in unsedated ventilated patients." *European Respiratory Journal* 5, no. 7 (1992): 871-878.

[116] Avanzolini, G., and Paolo Barbini. "A versatile identification method applied to analysis of respiratory mechanics." *Biomedical Engineering, IEEE Transactions on* 7 (1984): 520-526.

[117] Avanzolini, Guido, Paolo Barbini, Angelo Cappello, Gabriele Cevenini, and Lorenzo Chiari. "A new approach for tracking respiratory mechanical parameters in real-time." *Annals of biomedical engineering* 25, no. 1 (1997): 154-163.

[118] Nirav, Daphtary. "LUNG IMPEDANCE MEASUREMENTS USING TRACKED BREATHING." PhD diss., 2010.

[119] Farré, R., J. Rigau, J. M. Montserrat, E. Ballester, and D. Navajas. "Evaluation of a simplified oscillation technique for assessing airway obstruction in sleep apnoea." *European Respiratory Journal* 17, no. 3 (2001): 456-461.

[120] Kim, Jae-Hyung, Jun-Gu Kim, Young-Hyok Ji, Yong-Chae Jung, and Chung-Yuen Won. "An islanding detection method for a grid-connected system based on the goertzel algorithm." *Power Electronics, IEEE Transactions on* 26, no. 4 (2011): 1049-1055.

[121] Bates, J. H. T., F. Shardonofsky, and D. E. Stewart. The low-frequency dependence of respiratory system resistance and elastance in normal dogs. Respiration physiology. 78, no. 3 369-382, 1989.

[122] Hantos, Z., B. Daroczy, B. Suki, G. Galgoczy, and T. Csendes. Forced oscillatory impedance of the respiratory system at low frequencies. Journal of Applied Physiology. 60, no. 1, 123-132, 1986.

[123] Leary, Del, Swati A. Bhatawadekar, Grace Parraga, and Geoffrey N. Maksym. Modeling stochastic and spatial heterogeneity in a human airway tree to determine variation in respiratory system resistance. Journal of applied physiology. 112, no. 1, 167-175, 2012.

[124] Hirai, T., and J. H. Bates. Effects of deep inspiration on bronchoconstriction in the rat. Respir. Physiol. 127:201–215, 2001.

[125] Bates, Jason HT, and Gilman B. Allen. The estimation of lung mechanics parameters in the presence of pathology: a theoretical analysis. Annals of biomedical engineering. 34, no. 3, 384-392, 2006.

[126] Que, Cheng-Li, C. M. Kenyon, R. Olivenstein, Peter T. Macklem, and Geoffrey N. Maksym. Homeokinesis and short-term variability of human airway caliber. Journal of Applied Physiology. 91, no. 3, 1131-1141, 2001.

[127] Shirai, Toshihiro, Kazutaka Mori, Masashi Mikamo, Yuichiro Shishido, Takefumi Akita, Satoru Morita, Kazuhiro Asada, Masato Fujii, Takafumi Suda, and Kingo Chida. Usefulness of colored 3D imaging of respiratory impedance in asthma. Allergy, asthma & immunology research. 5, no. 5, 322-328, 2013.

[128] Mori, Kazutaka, Toshihiro Shirai, Masashi Mikamo, Yuichiro Shishido, Takefumi Akita, Satoru Morita, Kazuhiro Asada, Masato Fujii, Takafumi Suda, and Kingo Chida. Colored 3-dimensional analyses of respiratory resistance and reactance in COPD and asthma. COPD: Journal of Chronic Obstructive Pulmonary Disease. 8, no. 6, 456-463, 2011.

[129] Navajas, Daniel, R. A. M. O. N. Farre, J. A. U. M. E. Canet, M. Rotger, and J. Sanchis. Respiratory input impedance in anesthetized paralyzed patients. Journal of Applied Physiology. 69, no. 4, 1372-1379, 1990.

[130] Peták, Ferenc, Zoltán Hantos, Ágnes Adamicza, Tibor Asztalos, and Peter D. Sly. Methacholine-induced bronchoconstriction in rats: effects of intravenous vs. aerosol delivery. Journal of Applied Physiology. 82, no. 5, 1479-1487, 1997.

[131] Sly, Peter D., Rachel A. Collins, Cindy Thamrin, Debra J. Turner, and Zoltan Hantos. Volume dependence of airway and tissue impedances in mice. Journal of applied physiology. 94, no. 4, 1460-1466, 2003.

[132] Salazar, Eduardo, and John H. Knowles. An analysis of pressure-volume characteristics of the lungs. Journal of applied physiology. 19, no. 1: 97-104, 1998.

[133] Lutchen, Kenneth R., Andrew Jensen, Haytham Atileh, David W. Kaczka, Elliot Israel, Bela Suki, and Edward P. Ingenito. Airway constriction pattern is a central component of asthma severity: the role of deep inspirations. American Journal of Respiratory and Critical Care Medicine. 164, no. 2: 207-215, 2001.

[134] Samee, Saba, Talissa Altes, Patrick Powers, Eduard E. de Lange, Jack Knight-Scott, Gary Rakes, John P. Mugler III et al. Imaging the lungs in asthmatic patients by using hyperpolarized helium-3 magnetic resonance: assessment of response to methacholine and exercise challenge. Journal of Allergy and Clinical Immunology. 111, no. 6, 1205-1211, 2003.

[135] Venegas, Jose G., Tilo Winkler, Guido Musch, Marcos F. Vidal Melo, Dominick Layfield, Nora Tgavalekos, Alan J. Fischman, Ronald J. Callahan, Giacomo Bellani, and R. Scott Harris. Self-organized patchiness in asthma as a prelude to catastrophic shifts. Nature 434, no. 7034: 777-782, 2005.

[136] Bhatawadekar, Swati A., Del Leary, and Geoffrey N. Maksym. Modelling resistance and reactance with heterogeneous airway narrowing in mild to severe asthma. Canadian Journal of Physiology and Pharmacology ja.

[137] Abstract: C.A. Lall, P. Hernandez, P. Pianosi, and G.N. Maksym, Respiratory System Reactance: a sensitive indicator of bronchodilator effect in children with asthma. *Proc. Amer. Thoracic Soc.* San Diego. 2:A775, 2005.

[138] Ma, Baoshun, and Kenneth R. Lutchen. An anatomically based hybrid computational model of the human lung and its application to low frequency oscillatory mechanics. Annals of biomedical engineering. 34, no. 11: 1691-1704, 2006.

[139] Tgavalekos, Nora T., J. G. Venegas, B. Suki, and K. R. Lutchen. Relation between structure, function, and imaging in a three-dimensional model of the lung. Annals of biomedical engineering. 31, no. 4: 363-373, 2003.

[140] Bates, Jason HT, and Charles G. Irvin. Time dependence of recruitment and derecruitment in the lung: a theoretical model. Journal of Applied Physiology. 93, no. 2 : 705-713, 2002.

Appendix

ERSJ Permission: October 8, 2015

Detection of expiratory flow limitation in COPD using the forced oscillation technique

R.L. Dellacà, P. Santus, A. Aliverti, N. Stevenson, S. Centanni, P.T. Macklem, A. Pedotti, P.M.A. Calverley

European Respiratory Journal Feb 2004, 23 (2) 232-240; DOI: 10.1183/09031936.04.00046804

Material: Figure 3

Acknowledgement Wording: Reproduced with permission of the European Respiratory Society ©. *European Respiratory Journal Feb 2004, 23 (2) 232-240; DOI: 10.1183/09031936.04.00046804*

Permission is granted for the material stated above to be reproduced for your thesis in accordance with ERS copyright policy – see below

Notes, Terms & Conditions (*where applicable*)

"Green" Open Access and Author Archiving: Authors who do not wish to pay for the ERJ Open option will still have their manuscripts made free to access via the ERJ online archive following the journal's 18-month embargo period; after this embargo period, authors also have licence to deposit their manuscripts in an institutional (or other) repository for public archiving, provided the following requirements are met:

1) The final, peer-reviewed, author-submitted version that was accepted for publication is used (before copy-editing and publication).

2) A permanent link is provided to the version of the article published in the ERJ, through the dx.doi.org platform. For example, if your manuscript has the DOI 10.1183/09031936.00123412, then the link you provide must be dx.doi.org/10.1183/09031936.00123412

3) The repository on which the manuscript is deposited is not used for systematic distribution or commercial sales purposes.
4) The following required archiving statement appears on the title page of the archived manuscript: “This is an author-submitted, peer-reviewed version of a manuscript that has been accepted for publication in the European Respiratory Journal, prior to copy-editing, formatting and typesetting. This version of the manuscript may not be duplicated or reproduced without prior permission from the copyright owner, the European Respiratory Society. The publisher is not responsible or liable for any errors or omissions in this version of the manuscript or in any version derived from it by any other parties. The final, copy-edited, published article, which is the version of record, is available without a subscription 18 months after the date of issue publication.”

Authors of articles published under one of the Creative Commons licences (this includes all articles in ERJ Open Research, European Respiratory Review and Breathe) retain further rights to share, reuse or adapt their manuscript. The extent of these rights depends on the specific Creative Commons licence used. Please consult the relevant section of the online instructions for authors.

Kind regards,
Kay